SCIENCE PRODUCTS SESSION SUMMARY

Chairs: Steven Klosko and Gerhard Beutler

The 15th International Laser Ranging Workshop held in Canberra, Australia in October 2006 provided an overview of the state of SLR technologies, campaign activities, and science products. The Science Products Sessions began the meeting and consisted of 16 papers. These presentations demonstrated that satellite laser ranging continues to provide an important resource for satellite orbit determination, verification and validation of active remote sensing systems, and for producing science products that are needed to support a wide range of space geodesy and geodynamic investigations.

A theme of the meeting was the continued contribution of SLR to the progress being made in studying the Earth's system in four dimensions. At the same time, the SLR techniques are being used to both directly provide precision orbits and calibrate precise orbit positioning provided by other tracking systems. And by being a dynamic as opposed to reduced dynamic technique, SLR investigators have contributed significant insight into the intricate force modeling needed to produce cm-level orbit accuracy. All of these topics were discussed during the Science Products Session of the Workshop.

The first set of presentations of the session focused on the orbit determination capabilities of SLR. While GPS analyses benefit from continuous 3-D tracking, which allows "reduced" dynamic orbital techniques, SLR satellites are only observed and directly tracked for a small percentage of the time. Thereby precision orbit determination for SLR requires a high level of sophisticated conservative and non-conservative force modeling.

R. Noomen (1) gave a presentation demonstrating the state of the art in modeling the thermal imbalance and radiative forces acting on the LAGEOS 1 and 2 satellites. These satellites, given their specific design and highly stable orbits, provide an excellent laboratory to study very subtle thermal and drag-like effects acting on these orbits. The thermal perturbations acting on these satellites evolve over time as the satellite spin rate slows and the satellite experiences larger levels of thermal imbalance. R. Noomen presented results obtained at the Delft Technical University of the detailed modeling they have undertaken for the pair of LAGEOS satellites to determine the spin orientation and spin rates for the LAGEOS satellites. In the analysis they account for the complete regime of the spin behavior of the LAGEOS satellites as well as a complete description of the satellites' material composition. This has allowed them to greatly improve the orbit accuracy and fit to the SLR data while reducing the need for empirical correction parameters. SLR provides important and in many cases key independent validation capabilities for a variety of orbit applications. Herein, SLR is complementing GPS and measurements being acquired by these missions to validate orbit accuracy, detect manoeuvres, and provide a back up, fail safe orbit determination capability. Papers given by Urschl (2,5), Govind (4), and Deleflie (3) focused on SLR orbit determination applications that are being applied to study the orbits of GPS-35 and GIOVE-A.

Dedicated SLR satellite missions continue to provide unique long wavelength gravity and decadal time histories of site motions to help establish the geophysical context for many phenomena, a robust reference frame to report these changes within, and place constraints on the geophysical models themselves. Kurt Lambeck (6) gave a paper on the status and future plans for the geodetic network and geospatial modeling framework

within Australia. Australia is moving towards a highly integrated GPS, VLBI, and SLR geodetic reference and geophysical monitoring system. Currently there are two widely e-w separated SLR stations (Yarragadee and Mt Stromlo). Kurt discussed the possibility of deploying a third station in the north central part of the country co-located with VLBI near Katherine.

Contributions are coming from SLR to monitor and better understand long wavelength changes in the Earth's gravity field. Mass flux within the Earth's system over large spatial scales can be observed through the orbit changes they induce on well tracked SLR satellites. The return of the Earth to isostatic equilibrium since the time of the most recent Ice Age is a major source of nearly secular long wavelength gravity field changes. To understand the glacial mass flux apart from the total mass flux dominant over high latitude regions, detailed understanding of the Glacial Isostatic Adjustment (GIA) processes are needed. Dick Peltier of the University of Toronto gave a paper on recent refinements he has instituted to improve GIA modeling (7). Frank Lemoine (8) gave a talk on the long time history of gravity changes obtained from SLR for the longest wavelengths in the field and how they relate to GRACE. To understand contemporary ice sheet mass balance and its contribution to sea level rise, both the high latitude gravity changes and their decoupling from GIA processes are needed.

As knowledge of the long wavelength gravity field has improved, especially with advances coming from the GRACE Mission, further improvements have been made in deriving a constraint on the Lens Thirring effect. Erricos Pavlis (9) of the University of Maryland gave a paper on an improved estimate of the Lens Thirring term. This team has measured the value of this term to approximately 1% of its expected value as predicted by General Relativity. The experiment reported by Ciufolini and Pavlis was based on the long term behavior of the argument of the ascending node of the LAGEOS 1 and 2 satellites. The Lens Thirring predicted "frame-dragging" is seen as an unmodeled node signal for the LAGEOS pair. By evaluating more than eleven years of these data, these authors were able to isolate Lens Thirring from zonal gravity field error sources.

There were a set of papers focused on the reference frame, SLR contributions to the International Terrestrial Reference Frame (ITRF) and www-based tools for comparing time series from different experiments and technologies. D. Delefilie (10) of GRGS gave a presentation on a www-based tool for comparing geodetic times series. D. Coulot (11) of IGN presented a paper on different approaches to accommodate the "least squares mean effect", that is, the effect in a least squares environment of the variation of solved for parameters when a model is imposed on their behavior. H. Mueller of GFZ gave two papers (12 and 16). In the first, he discussed various experiments ongoing to compare SLR solutions using different processes and these results to VLBI and GPS. In the 2nd paper, the authors evaluated the contribution of SLR to the ITRF and presented a comparison of SLR solutions being produced at GFZ with those of IGN. Of high interest in this paper, in contrast to results described below, the GFZ Group is not seeing a scale difference from 2001 onward with their SLR solution and VLBI.

A contrasting paper was given by Z. Altamimi (15) of IGN on the construction and results he derived in computing the ITRF 2005 solution. Therein, this author found a greater than 1 ppb scale difference between SLR and VLBI, and this scale difference seemingly got progressively larger from 2001 onward. Zuheir went into considerable

detail about the use of local survey ties to bring SLR, GPS, and VLBI into a common frame.

The contrast between the IGN and GFZ results with regard to SLR scale, and the decision to use the scale provided by VLBI in the final ITRF 2005 realization caused a great deal of discussion, splinter groups, and involvement of the Analysis Centers in an attempt to better understand, resolve, and develop a strategy for utilizing the ITRF in future SLR analyses.

Also given during this portion of the session were papers by R. Govind (13) who discussed geocenter solutions he has obtained from SLR. This was followed by a paper by D. Gambis (14) of GRGS who presented results for the determination of EOP and Earth rotation using both SLR and LLR and the changing balance of contributions from all technologies over time in the combination solutions produced by IERS.

References:

[1] Andres, J. and R. Noomen, Enhanced modeling of the non-gravitational forces acting on LAGEOS.

[2] Urschl, C., G. Beutler, W. Gurtner, U. Hugentobler, S. Schaer, Calibrating GNSS orbits with SLR tracking.

[3] Deleflie, F., S. Melachroinos, F. Perosanz, O. Laurain, P. Exertier, GIOVE-A and GPS-35 satellite orbits: analysis of dynamical propoerties based on SLR-only tracking.

[4] Govind, R., GIOVE-A using Satellite Laser Ranging Data.

[5] Urschl, C., G. Beutler, W. Gurtner, U. Hugentobler, M. Ploner, Orbit determination for GIOVE-A using SLR tracking.

[6] Lambeck, K., Satellite Laser Ranging in the National Collaborative Research Infrastructure Proposal for Geospatial R&D in Australia.

[7] Lemoine, F., S. Klosko, C. Cox, T. Johnson, Time-variable gravity from SLR and DORIS tracking

[8] Peltier, W., Global glacial isostatic adjustment: target field for Space Geodesy.

[9] Pavlis, E., I. Ciufolini, R. Konig, Recent results from SLR experiments in fundamental physics.

[10] Deleflie, F., A “web-service” to compare geodetic time series.

[11] Coulot, D. Ph. Berio, A. Pollet, Least-squares mean effect: application to the analysis of SLR time series.

[12] Mueller, H., D. Angermann, M. Kruegel, Some aspects concerning the SLR part of ITRF2005.

[13] Govind, R., Determination of the temporal variations of the Earth’s centre of mass from a multi-year SLR data.

[14] Gambis, D., R. Biancale, Contribution of Satellite and Lunar Laser Ranging to Earth orientation monitoring.

[15] Altamimi, Z., Station positioning and the ITRF.

[16] Koenig, R. H. Mueller, Station coordinates, earth rotation parameters, and low degree harmonics from SLR with GGOS-D.

Enhanced modelling of the non-gravitational forces acting on LAGEOS

J.I. Andrés[1], R. Noomen[1]

1. Delft University of Technology, Kluyverweg 1, 2629 HS Delft, The Netherlands.

Contact: j.i.andres@tudelft.nl, r.noomen@tudelft.nl

Abstract

LAGEOS-I and LAGEOS-II orbit Earth since 1976 and 1992 respectively. With 426 Corner Cube Reflectors (CCRs) embedded in a spherical surface and a very low area-to-mass ratio, the LAGEOS satellites are among the best tools for global space geodetic research. By means of SLR observations, geophysical phenomena such as variations of the Terrestrial Reference Frame (TRF) origin w.r.t. the geocenter, global scale, low-degree gravity field terms, Earth Orientation Parameters (EOPs) and plate tectonic motions can be accurately measured, their accuracy directly dependent on that of the ground laser instrumentation and the accuracy of the orbit determination.

Intensive orbital analyses yielded a decrease in the semi-major axis of the orbit of LAGEOS-I, at a rate of 1.3 mm/d, shortly after launch; a similar decay has been observed for LAGEOS-II. Various physical processes (or a combination of them) have been proposed as possible causes for this acceleration: radiation pressure from celestial bodies (Earth and Sun) mismodeling, thermal thrust (re-radiation from the satellite itself), together with eclipse dependencies of the (re-)radiation, and ionospheric drag (neutral and charged particles). This decay can be modeled by an empirical along-track acceleration with a mean value of about -3.4 pm/s^2. The modeling efforts done so far have given a partially successful explanation of the non-gravitational perturbations acting on LAGEOS. However, a clear signal is still present in the calculations, due to a lack of precise modeling of the (unique) physical truth.

This study has concentrated on an accurate modeling of the major factors which could be responsible of the unexplained signal: the geometrical and optical properties, the rotational dynamics of the spacecraft, and poorly modeled forces. Accurate results have been obtained for the rotational dynamics thus eliminating one of the largest uncertainties still present. In parallel, finite element modeling has permitted a detailed characterization of the various elements of the spacecraft, together with an accurate description of their (time-dependent) geometry w.r.t. radiation sources. This has yielded a numerical answer for the thermal accelerations for all possible spinning regimes. Uncertainties in some physical parameters have been dealt within a sensitivity analysis.

Introduction

Although the technique of Satellite Laser Ranging (SLR) dates back more than 40 years [Marshall *et al.*, 1995], it is still one of the main techniques to be used for studying certain elements of System Earth. In particular, global aspects of the terrestrial reference frame, such as origin and scale, are uniquely determined by this technique by virtue of its direct and unambiguous method of observation: the travel time measurements of a pulse of light from a ground station to a satellite and back are typically measurable with high precision, and the various elements that play a role in

converting these 2-way travel times into a 1-way range observation (*e.g.* satellite signature, atmospheric refraction, station delay, etcetera) can be modeled with an accuracy of various mm typically [Otsubo and Appleby, 2005]. To arrive at the best possible solutions for such global parameters, it is mandatory to model the orbit of the satellites as accurately as possible. Typically, the cannonball satellites LAGEOS-1 and LAGEOS-2 (launched in May 1976 and October 1992, respectively) are used for this purpose by virtue of their attractive area-to-mass ratio, making them relatively insensitive to (intrinsically complex to model) surface forces.

In spite of the attractive design of these spacecraft, high-precision orbit determination currently necessitates the estimation of so-called empirical accelerations (typically, in various directions w.r.t. an orbit-referenced frame and with different character – constant or sinusoidal with orbital period). This is a clear indication of the limitations of current analysis models to represent "physical truth" correctly. An illustration of this is given in Figure 1, which shows the residuals of the constant along-track acceleration as observed/estimated for the satellite LAGEOS-1, *i.e.* bi-weekly solutions of such a parameter after subtraction of best known physical mechanisms to explain the acceleration (in reality, the accelerations show a mean value of -3.4 pm/s^2, which can be addressed to a variety of surface forces). The plot clearly illustrates that there is a signal in the residuals at the level of several pm/s^2, which needs a physical explanation in order to advance the contributions of LAGEOS–type missions to geophysical studies further. Candidates for the residuals shown here are (1) thermal radiation exerted by the satellite itself, (2) direct radiation forces, (3) charged and neutral particle drag, and others; of course shortcomings in the modeling of any of these individually, and/or a combination of effects can play a role here. This paper will focus on the so-called thermal forces: minute forces that are introduced by the emission of thermal energy by surface elements of a satellite.

First, a model for the rotational behavior of the satellites will be presented. Previous investigations by other authors show that a proper understanding and description of this aspect is crucial for a good modeling of the thermal behavior. The thermal behavior of the satellites will be the next topic of discussion, and a multi-node model of each satellite will be developed and used to simulate actual temperatures. Then, the temperature distribution will be used to compute contributions to thermal forces as exerted by individual surface elements, resulting in a total acceleration. This acceleration will be used in a first-order assessment of its orbital effect. The paper will end with conclusions and recommendations.

Rotational dynamics

Compared to the orbital motion of the spacecraft, the rotational dynamics of LAGEOS-1 and -2 can be considered as a neglected element of the mission: observations of the attitude and spin rate are few, and models of the rotational behavior are hardly available. One of the reasons for this is the absence of any need for such information: the rotation dynamics plays a subtle role in the orbital behavior of the vehicles, which only come into play when the requirements on orbital accuracies arrive at the level of a single cm and below. A recently developed description of the spin behavior of the LAGEOS pair is given in [Andrés *et al.*, 2004].

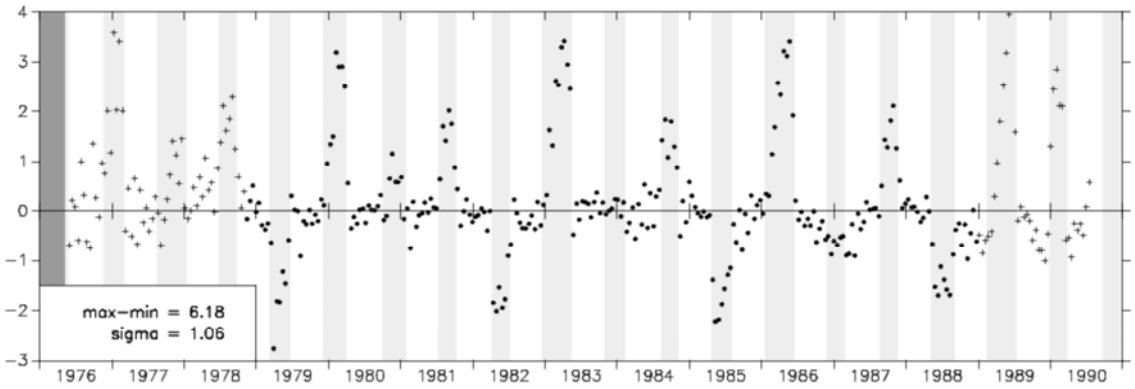

Figure 1. *Residuals of the along-track accelerations as observed for LAGEOS-1, for the time period 1976-1990. Grey areas indicate the periods when the satellite experienced an umbra while orbiting the Earth [Scharroo et al., 1991].*

The LAGEOS Spin Axis Model (LOSSAM) that is developed in this reference is based on a straightforward integration of Euler's equation:

$$\frac{d\vec{L}}{dt} = \vec{M}_{magn} + \vec{M}_{grav} + \vec{M}_{offset} + \vec{M}_{reflec}$$

Here, the external torques represent the influence of the Earth's magnetic field, gravity, a possible difference between the center-of-pressure w.r.t. the center-of-mass, and a possible difference in effective reflectivity between the northern and southern hemisphere of the satellites, respectively. LOSSAM has been obtained after confrontation of the theoretical model as described by the previous equation with independent observations on spin-axis orientation and spin rate taken by a variety of stations and institutes: (*i*) University of Maryland, USA, (*ii*) the laser station in Herstmonceux, UK (owned by the Natural Environment Research Council, NERC), (*iii*) the laser station in Matera, Italy (owned by the Agenzia Spaziale de Italia, ASI) and (*iv*) Lincoln Laboratory [Sullivan, 1980]. Figures 2 and 3 show the behavior of the spin axis orientation of LAGEOS-1 and -2 according to LOSSAM, respectively (spin rate results are withheld here). The plots also show the independent observations that were used in the derivation of the model, and the level of fit. Clearly visible is that LAGEOS-1 is in a different rotational regime currently than LAGEOS-2: the spin-axis orientation of the former satellite follows a more irregular pattern, which is due to a slowing down from a rotational period of 10.5 s at launch (1976) to about 6000 s now (Figure 2). LAGEOS-2 is still spinning with a period of about 360 s currently. Also visible is the fact that the set of observations on the spin axis that is available for LAGEOS-1 is quite restricted: the last ones were taken at the end of 1996, and effectively one cannot do but make predictions of the current behavior of the satellite; the absence of recent observations is directly related to the fact that the rotation of LAGEOS-1 has almost come to a standstill, which makes it extremely difficult to actually apply currently practiced observation techniques on spin axis orientation and rotation rate. For LAGEOS-2, the situation is much better (cf. Figure 3). The reader is referred to [Andrés *et al.*, 2004] for more details.

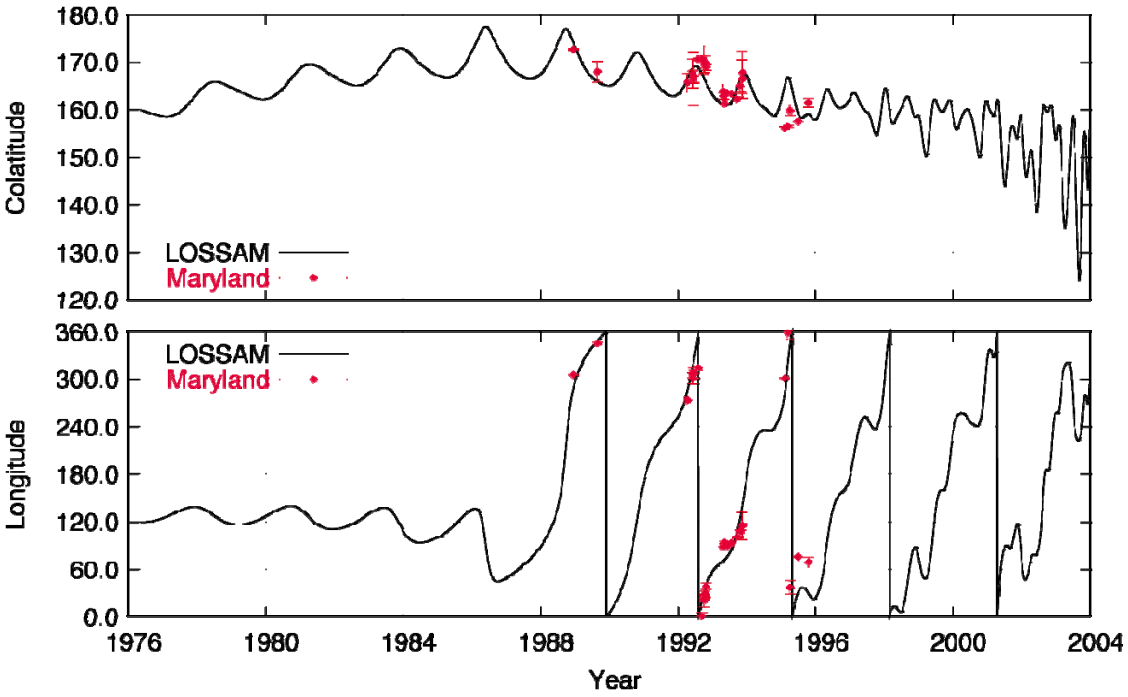

Figure 2. *The LOSSAM spin orientation behavior of LAGEOS-1 as a function of time, as described by the longitude and co-latitude w.r.t. the J2000 reference frame. The red symbols represent the independent observations that were used to derive this model [Andrés et al., 2004].*

Thermal model

Thermal forces, *i.e.* forces that are generated somehow by either direct or reflected radiation, are known to play an important role in the explanation of the observed decay of the semi-major axis of the LAGEOS pair and, directly related to this, of the solutions for the empirical accelerations; many studies have been done into the effects of direct solar radiation (Yarkovsky effect), albedo radiation, earth infrared radiation, the effect of eclipses (Yarkovsky-Schach effect), etcetera (*e.g.* [Rubincam, 1982], [Anselmo *et al.*, 1983], [Barlier *et al.*, 1986], [Rubincam, 1987a], [Rubincam, 1987b], [Afonso *et al.*, 1989], [Rubincam, 1990], [Martin and Rubincam, 1996], [Slabinski, 1997] and [Vokrouhlický and Métris, 2004]). However, none of these investigations has led to a full description and complete understanding of the actual phenomena that influence the orbital behavior of the LAGEOS satellites; if only because simplifications had to be made in order to arrive at first-order estimates of the effects. Clearly, in view of the slow rotation of LAGEOS-1 and a similar trend for LAGEOS-2, the necessity for a more detailed modeling of the satellite and its interaction with various elements in its environment has arisen. As mentioned in the introduction, this paper addresses one of those elements: the thermal interaction with the various radiation sources, and the resulting accelerations. A detailed discussion of procedures, models and results is given in [Andrés *et al.*, 2006].

To model the interaction in detail, making allowance for potential differences in its reaction to various sources of energy, the satellite model needs to be split up into a number of different components. In recognition of the various mechanisms that are effectively responsible for heat transfer (*i.e.* radiation and conduction; any other can be shown to be insignificant [Andrés *et al.*, 2006]) and the differences in thermal and mechanical properties of the various construction elements, a finite-element model of each LAGEOS satellite has been created, with 2133 elements in total: the inner core

(core and stud), two hemispheres, and 426 retroreflector assemblies each consisting of 5 elements: a retainer ring, an upper ring, a corner-cube reflector, a set of ring posts, and a lower ring.

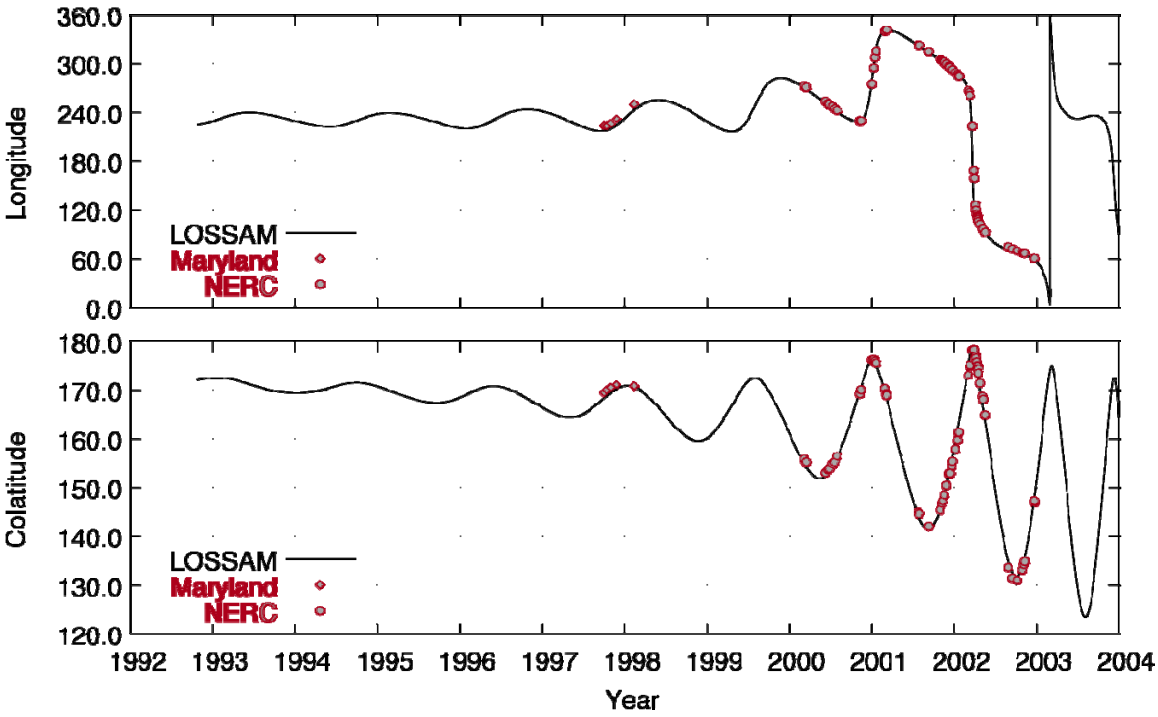

Figure 3. *The LOSSAM spin orientation behavior of LAGEOS-2 as a function of time, as described by the longitude and co-latitude w.r.t. the J2000 reference frame. The red symbols represent the independent observations that were used to derive this model [Andrés et al., 2004].*

For each LAGEOS element *i*, the following (abstract) heat equation can be written:

$$H_i \frac{\partial T_i}{\partial t} = Q_{in} - Q_{out}$$

For more details, see [Andrés *et al.*, 2006]. In combination with cm-level accurate solutions for the orbital motion of the satellites (obtained with GEODYN [Pavlis *et al.*, 1998], the positions of sources of radiative energy (Sun, Earth), models for these radiative flows, models for the thermal and mechanical properties of the spacecraft components, and the LOSSAM model for the rotational behavior of the spacecraft [Andrés *et al.*, 2004] this equation can be integrated over time for each element to yield the thermal behavior of each individual element. This has been done for both satellites from the date of launch onwards, with a step-size of 60 s, and taking care that allowance is made for aspects like shadowing, aliasing (when the rotational period and the integration step size are integer multiples) and rotationally averaged radiation input. An illustration of the result is given in Figure 4, which shows the temperature distribution of the various elements of LAGEOS-1 and -2 for the (arbitrary) epoch January 1, 2002, respectively. The plots clearly show the different temperatures of the Germanium reflectors (3 out of 4 are visible in each plot; the thermal absorption and emission coefficients are very different from the quantities for the 422 Silicium reflectors), and, in a similar fashion, the different temperatures for

the retainer rings. In the case of LAGEOS-1 (Figure 4, left), the Sun is more-or-less located over the satellites equator, resulting in a similar temperature for the northern and the southern hemispheres. In the case of LAGEOS-2 (Figure 4, right), the Sun is at an apparent latitude of about 45°, with a higher temperature for the northern hemisphere as a consequence.

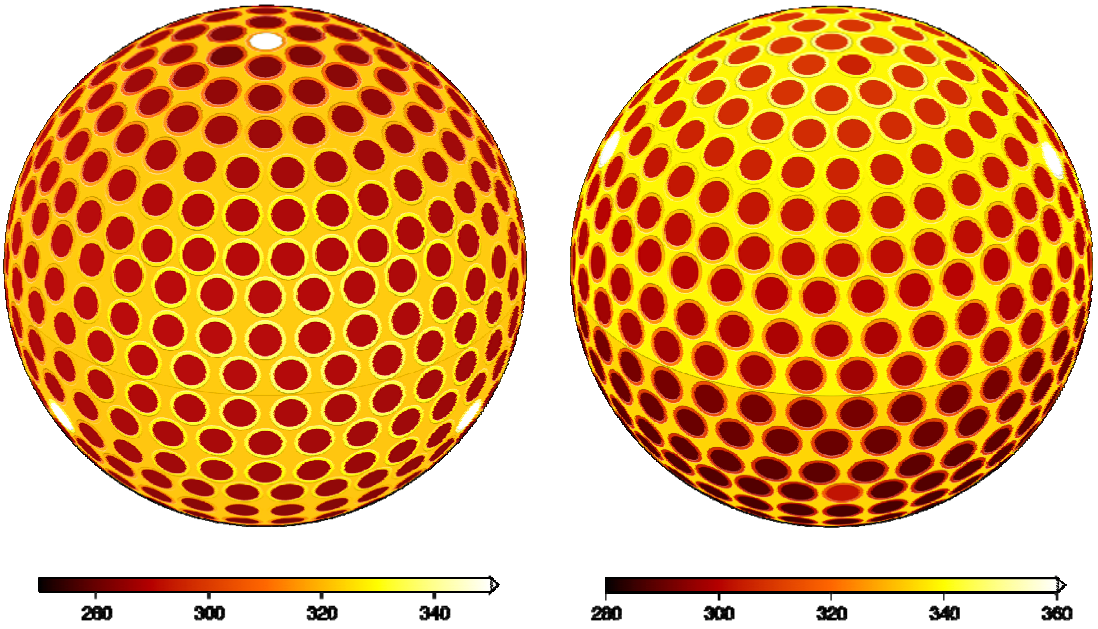

Figure 4. *Temperature distribution on January 1, 2002, for LAGEOS-1 and -2, respectively. All values are in Kelvin [Andrés et al., 2006].*

As an illustration, Figure 5 shows the long-term temperature behavior for a number of elements of LAGEOS-1; a similar behavior has been derived for LAGEOS-2 (not included here; cf. [Andrés *et al.*, 2006]). Figure 5(a) shows the temperatures for representative retainer rings and a Silicium CCR in the northern hemisphere. By virtue of its thermal properties, the CCR has an average temperature which is some 20 K lower than that of the retainer rings. All elements show a variation with time, which is correlated with the occurrence of solar eclipses (indicated by grey bands) and the position of the Sun (the main source of energy) w.r.t. the satellite spin axis; in the case of reflector assembly 89, which is located at a (satellite-fixed) co-latitude of about 58°, temperature variations are relatively humble, but after about 10 years in orbit the attitude of the spacecraft starts to develop into an erratic behavior w.r.t. λ and the spin rate drops off, resulting in extreme temperature variations for the retainer ring located at the satellite's north pole. A similar observation can be made for the retainer rings and the reflectors located in the southern hemisphere of the satellite (Figure 5(b)): the CCRs are typically cooler, show less variation, and big excursions of up to 60 K are visible for the retainer rings closer to the pole (in this case the south pole of the satellite). Figure 5(c), finally, very clearly illustrates the sensitivity of the Germanium CCRs to the actual lighting conditions: the 3 Ge CCRs that are located at co-latitude 121°, show a temperature variation of about 50 K (already large when compared to the behavior of the Si CCRs, cf. Figure 5(a)), but the situation appears to change dramatically for the CCR located at the very north pole of LAGEOS-1: temperature variations of up to 300 K are observed here.

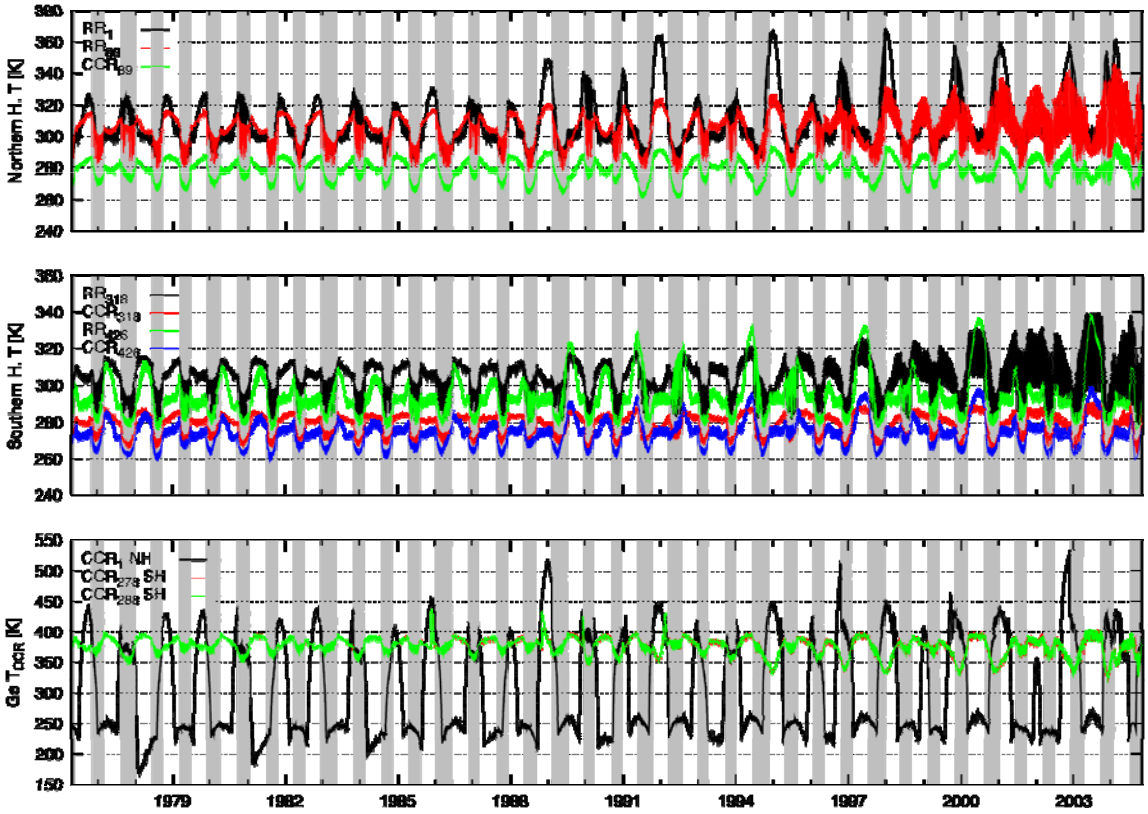

Figure 5. *Temperature behavior of several retainer rings and CCRs for LAGEOS-1 since launch [Andrés et al., 2006].*

Accelerations

Having arrived at a time-series of temperatures for the 2133 elements of each LAGEOS finite-element model, it is possible to derive values for the force that each element exerts (cf. [Slabinski, 1997]):

$$d\vec{F}_i \;=\; -\frac{2}{3}\,\frac{\varepsilon_i\;\sigma\;T_i^{\,4}}{c}\;dA_i\;\vec{n}_i$$

Integration of all contributions from all surface elements (clearly, internal elements do not contribute) yields the net thermal acceleration that each satellite experiences. An illustration of that is given in Figure 6: accelerations in the radial, along-track and cross-track directions for one day for LAGEOS-1 and LAGEOS-2, respectively; the right-hand side of the plots zooms in for a particular orbit during that day. It is clearly visible that for both satellites, radial and along-track accelerations of up to 50 pm/s^2 can be obtained (the two follow one another by virtue of the rotation of the orbital, satellite-related reference frame); much larger than the average value of about -3.4 pm/s^2 that is seen in the empirical (constant) accelerations. Since the cross-track orientation of the orbit remains more-or-less constant during one day, this component shows much less of a variation (but can have a very significant value). The plots indicate that an irregular behavior occurs in particular during times of eclipse; in such a situation, the cause for an uneven heating of the satellite disappears (ignoring any

influence form the Earth, that is) and the net acceleration tends to develop towards zero.

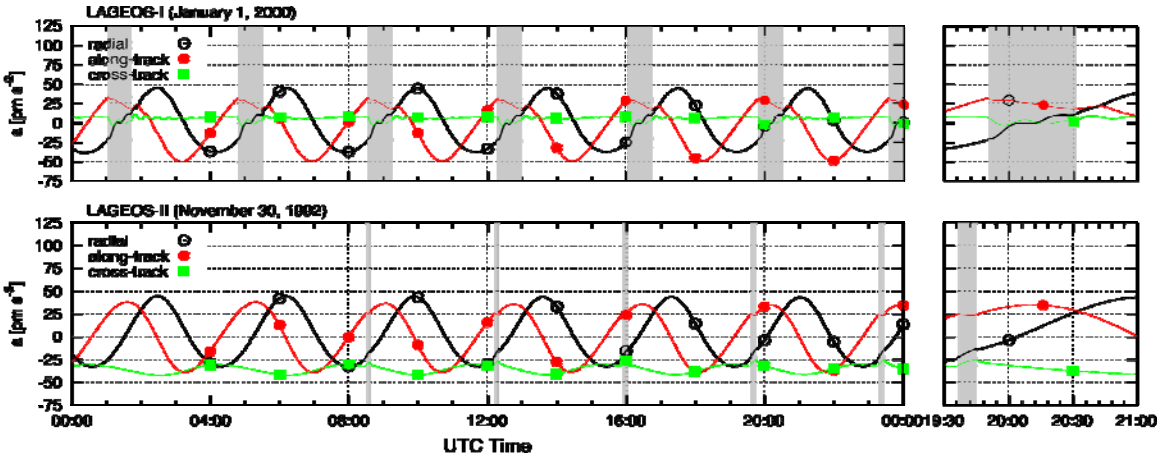

Figure 6. *Net thermal accelerations for (top) LAGEOS-1 on January 1, 2000, and (bottom) LAGEOS-2 on November 30, 1992. The grey bands indicate the exact periods when the satellites are in eclipse [Andrés et al., 2006].*

Extending the presentation to the full lifetime of the satellites (so far), Figure 7 shows the development of the net accelerations as well as the orientation of the Sun in a satellite frame, for each LAGEOS version. Again, the grey bands indicate when eclipses occur (somewhere in the orbit). Starting the discussion with LAGEOS-2 (Figure 7(b)), the long-term behavior is in line with what was shown in Figure 6 already: radial and along-track components interchange by virtue of the definition of the orbital frame, and the variation of the cross-track component is slower. All LAGEOS-2 components have values that go up to about 50 pm/s^2. In the situation that the Sun is located in the equatorial; plane of the satellite (i.e. $\beta_{\text{Sun-SA}}$ is equal to 90°), all 3 components of the net acceleration are effectively zero (by virtue of the rapid rotation of LAGEOS-2). As for LAGEOS-1, a similar story holds (Figure 7(a)), albeit that the relations are a bit more difficult to observe because of the longer time-span covered since launch. Also visible are the larger values for the net accelerations after about 1990, which is due to the specific rotational behavior of the spacecraft (with consequences for the temperature of particular elements of the satellite; cf. Figure 5). Although not included here explicitly, it can be shown that the model for the rotational behavior of the satellites plays a crucial role: net accelerations computed with the LOSSAM model (which is regarded as the state-of-the-art representation of the actual rotational behavior) differ by an amount of about 25 pm/s^2 with the results that would have been obtained with a more traditional (*i.e.* constant) model for the spin axis [Andrés *et al.*, 2006].

Orbit computations

As a very first test of the actual usefulness of the results, two types of orbital computations have been done for LAGEOS-2 only (the choice of this satellite is arbitrary). First, weekly orbital fits have been computed using a model that does not include any external acceleration, and in which the solar radiation pressure force scaling parameter C_R is estimated only (in addition to the state-vector at epoch). Second, similar computations have been done but now with inclusion of the thermal

accelerations as derived by the procedures sketched above (and keeping them fixed at their nominal values). Computations were done for the period October 1993 until

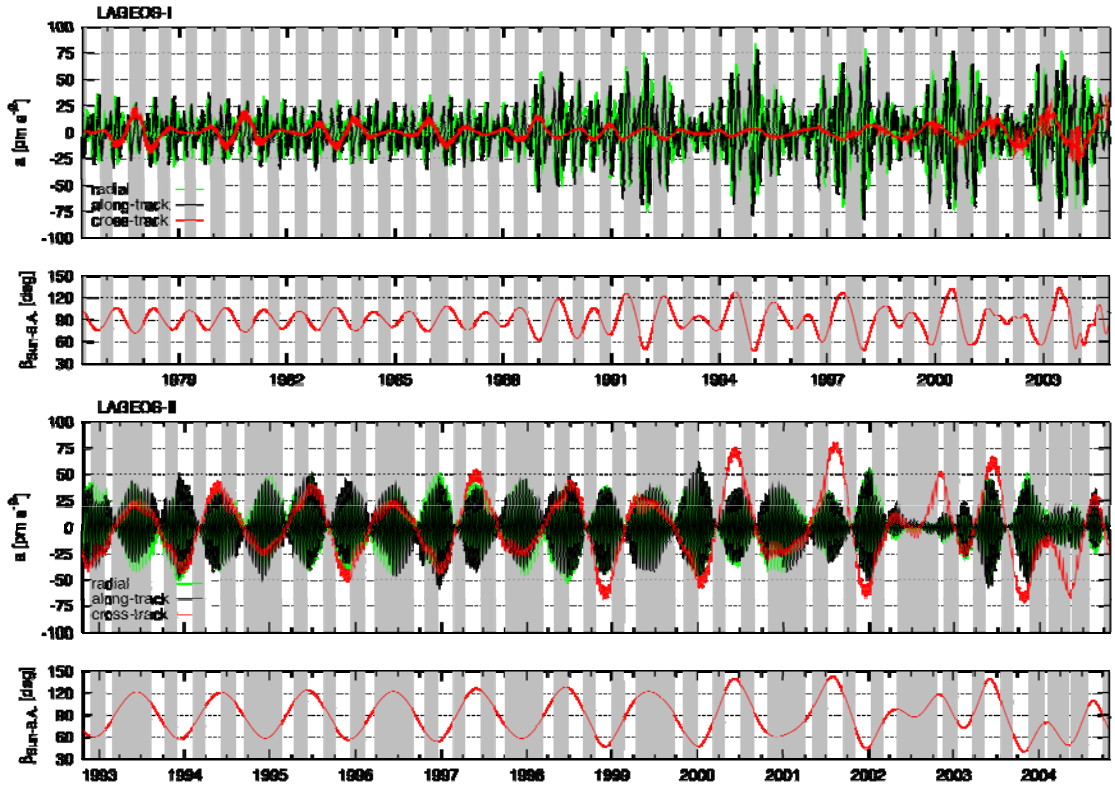

Figure 7. *Net thermal accelerations and solar co-latitude (i.e. position w.r.t. the satellite north pole) for (top) LAGEOS-1, and (bottom) LAGEOS-2. The grey bands indicate the exact periods when the satellites are in eclipse [Andrés et al., 2006].*

December 1994. It should be emphasized here that no effort was done to fine-tune these results, nor to include other (necessary) elements to represent the orbital dynamics of the spacecraft. This explains the relatively high values for the rms-of-fit, which is shown in Figure 8 (typically, one would obtain fits in the order of better than 30 mm (for this period, that is), at the expense of solving for a collection of empirical accelerations; this was explicitly not the purpose of the current test). Figure 8 shows that the use of the thermal accelerations does lead to significant reductions in the quality of the orbit: the fit reduces from a range of 2.5-7.5 cm to a range of 2-4 cm, whereas the stability of the radiation scaling parameter C_R (a physical parameter, which should be constant rather than time-dependent – ignoring adjustments to the space environment during the first months in orbit [Ries *et al.*, 1997] indeed improves as well. The results shown here are very first results; further fine-tune of the computational model will hopefully result in the situation where the (estimation of) empirical accelerations can be discontinued altogether, without any loss of quality of the orbital solution nor of the derived parameters (origin, scale, station coordinates and such); preferably even an improvement of the latter products can be obtained.

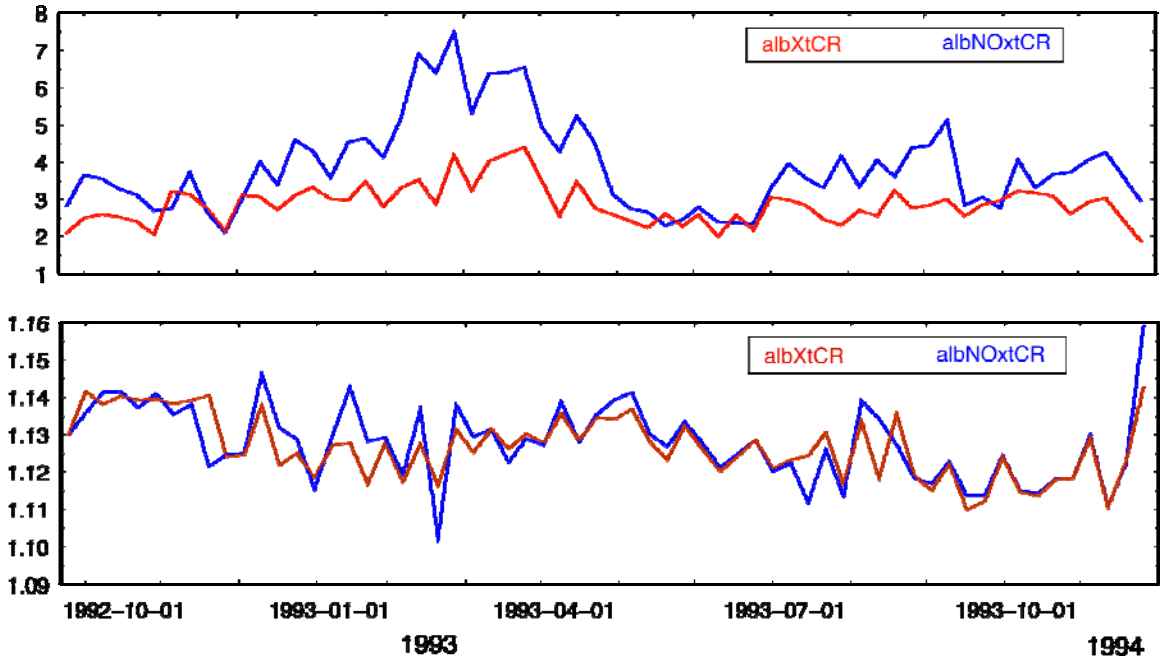

Figure 8. *Rms-of-fit (in cm) and solutions for the solar radiation scaling parameter C_R as a function of time for LAGEOS-2, with and without inclusion of the nominal thermal accelerations as shown in Figure 7.*

Conclusions and recommendations

Based on a detailed finite-element representation of the pair of LAGEOS satellites, and in combination with LOSSAM, the state-of-the-art model for the rotational behavior of each satellite, it has been possible to derive a highly accurate and unprecedented model for the thermal behavior of 2133 different components of each satellite: LOSTHERM. The temperatures appear to show a strong correlation with geometry w.r.t. the Sun as the main source of influx of energy. Also, temperature variations of up to several hundreds of Kelvin are observed by virtue of the sensitivity of particular spacecraft components to irradiation (absorption and emission coefficients). The instantaneous temperature distribution of the outer components in particular can be integrated to yield the net thermal acceleration. These accelerations have magnitudes of up to 75 pm/s^2, much larger than the average value that is typically obtained from orbital computations. The results clearly shows that the rotational behavior of the satellites plays a decisive role in the actual values of these accelerations, and underlines the neccessity of including such formulations in the most demanding orbital computations. It also underpins the need for continuation of independent observations of the rotational behavior of LAGEOS-2, and an answer to the challenge of doing similar things for LAGEOS-1.

References

[1] Afonso, G., F. Barlier, M. Carpino, P. Farinella, F. Mignard, A. Milani and A.M. Nobili, Orbital effects of LAGEOS seasons and eclipses, Ann. Geophys., 7(5), 501-514, 1989.

[2] Andrés, J.I., G. Bianco, D. Currie, R. Noomen and T. Otsubo, The spin axis behavior of the LAGEOS satellites. J. Geophys. Res., 109, B06403, doi:10.1029/2003JB002692, 2004.

[3] Andrés, J.I., R. Noomen and S. Vecellio None, Numerical simulation of the LAGEOS thermal behavior and thermal accelerations, J. Geophys. Res., 111, B09406, doi:10.1029/2005JB003928, 2006.

[4] Anselmo, L., P. Farinella, F. Mignard, A. Milani and A.M. Nobili, Effects of the Earth reflected sunlight on the orbit of the LAGEOS satellite, Astron. Astrophys., 117, 3-8, 1983.

[5] Barlier, F., M. Carpino, P. Farinella, F. Mignard, A. Milani and A. Nobili, Non-gravitational perturbations on the semimajor axis of LAGEOS, Ann. Geophys., Ser. A, 4, 193-210, 1986.

[6] Farinella, P., D. Vokrouhlický and F. Barlier, The rotation of LAGEOS and its long-term semimajor axis decay, J. Geophys. Res., 101(B8), 17,861-17,892, 1996.

[7] Marshall, J.A., S.M. Klosko and J.C. Ries, Dynamics of SLR tracked satellites, Reviews of Geophysics, 33(S1), 353-360, 1995.

[8] Martin, C.F., and D.P. Rubincam, Effects of Earth albedo on the LAGEOS-1 satellite, J. Geophys. Res., 101(B2), 3215-3226, 1996.

[9] Otsubo, T., and G. Appleby, Centre-of-Mass Correction Issues: Towards mm-Ranging Accuracy, in: Garate, J., J.M. Davila, C. Noll and M. Pearlman (eds.), Proceedings 14th International Laser Ranging Workshop, San Fernando, Spain, June 2004, Boletin ROA No. 5, Ministerio de Defensa, Real Instituto y Observatorio de la Armada en San Fernando, Spain, 467-472, 2005.

[10] Pavlis, D.E. et al., GEODYN-II systems description, NASA Goddard Space Flight Center, Greenbelt, Maryland, USA, 1998.

[11] Ries, J.C., R.J. Eanes, G. Métris and D. Vokrouhlicky, Anomalous variations in the LAGEOS and LAGEOS-2 eccentricity, presented at the AGU Fall Meeting, San Diego, California, USA, 1997.

[12] Rubincam, D.P., On the secular decrease in the semimajor axis of LAGEOS' orbit, Celestial Mech., 26, 361-382, 1982.

[13] Rubincam, D.P., LAGEOS orbit decay due to infrared radiation from Earth, J. Geophys. Res., 92(B2), 1287-1294, 1987a.

[14] Rubincam, D.P., Earth anisotropic reflection and the orbit of LAGEOS, J. Geophys. Res., 92(B11), 11,662-11,668, 1987b.

[15] Rubincam, D.P., Drag on the LAGEOS satellite, J. Geophys. Res., 95(B4), 4881-4886, 1990.

[16] Scharroo, R., K.F. Wakker, B.A.C. Ambrosius and R. Noomen, On the along-track acceleration of the LAGEOS satellite, J. Geophys. Res., 96(B1), 729-740, 1991.

[17] Sullivan, L.J., Infrared coherent radar, Proc. Soc. Photo Opt. Instrum. Eng., 227(148), 1980.

[18] Vokrouhlický, D., and G. Métris, LAGEOS asymmetric reflectivity and corner cube reflectors, J. Geophys. Res., 109, B10401, doi:10.1029/2003JB002921, 2004

Calibrating GNSS orbits with SLR tracking data

C. Urschl[1], G. Beutler[1], W. Gurtner[1], U. Hugentobler[2], S. Schaer[3]

1. Astronomical Institute, University of Bern, Switzerland
2. Institute of Astronomical and Physical Geodesy, Technical University of Munich, Germany
3. Federal Office of Topography, swisstopo, Wabern, Switzerland

Contact: claudia.urschl@aiub.unibe.ch

Abstract

SLR tracking data allow for a completely independent validation of GNSS orbits that are derived from microwave data. SLR validation results show mean range residuals of several centimeters for both, GPS and GLONASS satellites, as well as significant seasonal variations for the two GPS satellites that are equipped with retroreflector arrays. It was, however, not clear whether these systematic effects could be assigned to orbit modeling deficiencies or to SLR tracking biases. We present new SLR validation results, which point to serious GPS orbit modeling problems. Moreover, we address the question, whether it would make sense to perform a combined analysis of microwave and SLR data for GNSS orbit determination. With the available low number of SLR observations no significant improvement of the orbit accuracy is found. An a priori variance-covariance analysis shows an improvement of the situation, if continuous SLR tracking data of already a very small number of globally distributed SLR sites were available.

1. Introduction

The International Laser Ranging Service (ILRS) provides Satellite Laser Ranging (SLR) tracking data of Global Navigation Satellite Systems (GNSS, at present consisting of GPS and GLONASS). Two GPS satellites that are equipped with laser retrorereflector arrays (LRAs), and a subset of three GLONASS satellites (all GLONASS satellites carry LRAs) are tracked by SLR.

SLR data allow for an independent validation of GNSS orbits that are derived from microwave data. In Section 2 we present recent SLR validation results, covering about four years of SLR data.

SLR observations may contribute to the GNSS orbit determination in a combined analysis of microwave and SLR observations. The possible improvement of the orbit accuracy is demonstrated on the basis of an a priori variance-covariance analysis in Section 3.

The main results of this work were already presented at the COSPAR 36th Scientific Assembly in Beijing. As this analysis is of a particular interest for the ILRS community, we will briefly introduce and sum up the most important results. We refer to (Urschl et al., 2007) for a detailed discussion.

2. GNSS orbit validation using SLR

For orbit validation we compare the SLR range measurements with the ranges derived from GNSS orbits. We used SLR normal points provided by the ILRS (Pearlman et al., 2002), and final orbits of CODE (Center for Orbit Determination in Europe). CODE is one of the analysis centers of the International GNSS Service (IGS) generating daily orbit solutions for all active GNSS satellites. The orbit determination is based on GNSS microwave observation provided by the IGS (Dow et al., 2005).

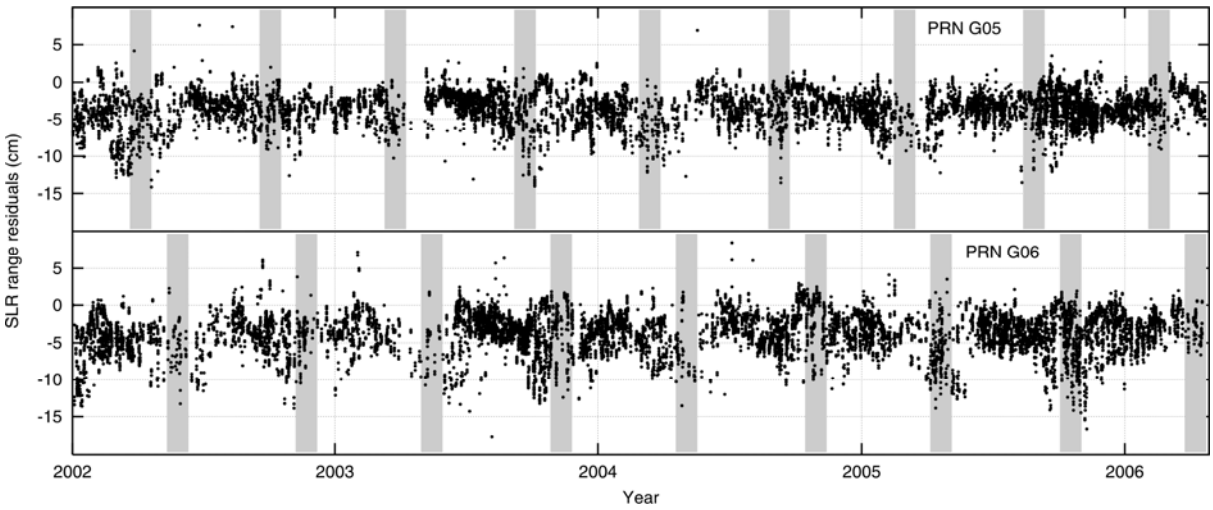

Figure 1. *SLR range residuals in cm for GPS satellites PRN G05 and G06, derived from CODE final orbits. The shaded areas indicate eclipse seasons*

The resulting range residuals indicate the GNSS orbit accuracy, but mainly in radial direction due to the observation geometry. SLR data of about four years starting 2002 were used for the range residual analysis.

Figure 1 shows the range residuals for the two GPS satellites. A standard deviation of the range residuals of 2 cm and 5 cm was estimated for the GPS and GLONASS satellites, respectively. The GPS orbits have a better accuracy compared to the GLONASS orbits due to the much denser GPS microwave tracking network. The GPS range residuals show a mean bias of about –3 to –4 cm. This bias is already known from previous studies, but its origin still remains unexplained. A wrong value for the retroreflector offset, giving the distance from the LRA's center to the satellite's center of mass, could be a possible explanation. It is interesting to note that there is no significant mean bias for the GLONASS satellites.

As part of the analysis, systematic variations were found in the SLR residuals of the GPS satellites, correlated to eclipsing seasons and with amplitudes of up to 10 cm. The largest residuals occur when the satellite is observed within the Earth's shadow during eclipsing seasons (indicated with shaded areas in Figure 1).

We could attribute the periodic signature to orbit modeling problems by displaying the range residuals in the (β,u)-coordinate system. β is the Elevation of the Sun above the orbital plane, and u is the argument of latitude of the satellite with respect to the argument of latitude of the Sun.

Figure 2 shows the range residuals in the (β,u)-system. The residuals are color-coded according to their values. The dependency of the range residuals on the satellite's position within the orbital plane is visible, and rules out SLR tracking biases. The pattern is rather caused by the microwave analysis, indicating attitude or orbit modelling problems.

3. Combined analysis of microwave and SLR data for GNSS orbit determination

Beside the validation purpose, SLR data can be used for GNSS orbit determination in a combined analysis together with microwave observations. But does this make sense in terms of orbit improvement? To answer this question an a priori variance-covariance analysis is performed.

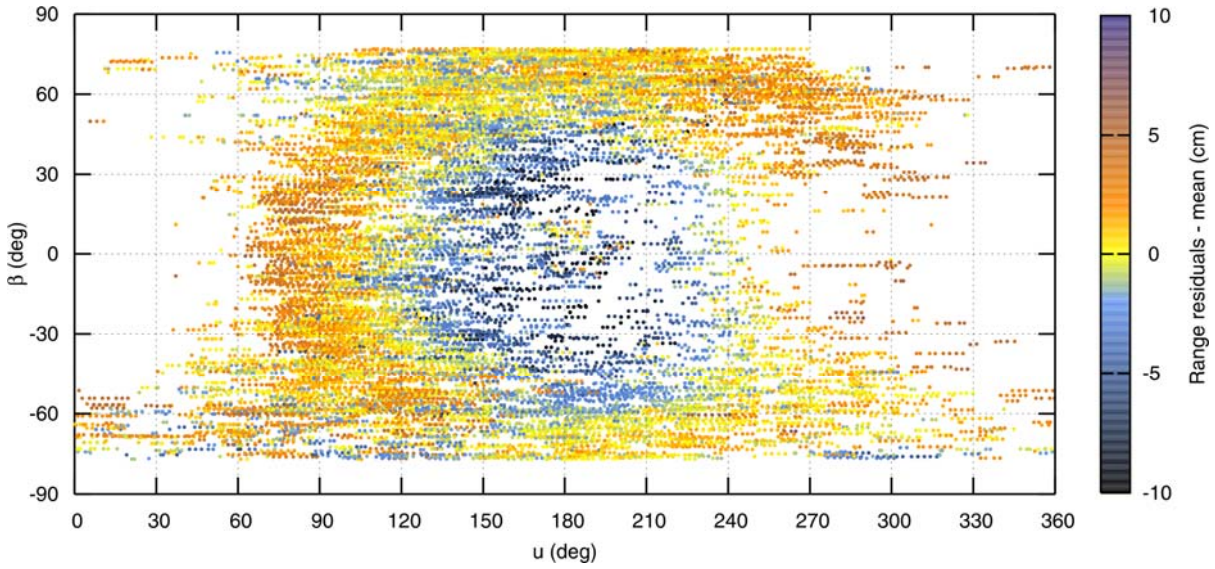

Figure 2. *Color-coded SLR range residuals in cm minus mean value for the GPS satellites PRN05 and PRN06, derived from CODE final orbits*

We used microwave phase observations of about 150 IGS sites and SLR data of 13 ILRS sites. For the variance-covariance analyses only the number, the temporal distribution, and an error model of the observations are needed. The a priori formal errors of the orbit components can be derived from the covariance matrices.

Several experiments were performed using different SLR observation weights. In the first experiment the SLR observation weight is set to zero by setting the a priori sigma of the SLR observations σ_{SLR} to infinity. Thus, the first experiment corresponds to a pure microwave solution. In the second experiment σ_{SLR} is set to 1 cm, similar to that of the microwave observations. In the third experiment the weight of SLR is increased by setting σ_{SLR} to 1 mm.

We compare the a priori formal errors of the orbital parameters of the different experiments. The a priori formal errors only decrease with very strong SLR observation weights (σ_{SLR} = 1 mm) and only around epochs, where SLR observations are available. When using real SLR observations, no significant improvement of the orbit accuracy was found, as SLR tracking data of GNSS satellites are very sparse and not well distributed.

But the situation changes, if SLR data would cover the entire satellite arc. Evenly distributed SLR observations have been simulated with an accuracy of 5 mm, equally spaced at 15 min interval, for altogether four globally distributed SLR tracking sites. SLR data of four sites can cover as much as 90% of a GNSS satellite arc. The a priori formal errors of the orbit parameters decrease significantly for SLR observations with 1 cm accuracy, and even more for SLR observations with increased weighting.

Two additional experiments have been performed using SLR data of only two or three SLR sites. With the data of two sites about 50% of a GNSS satellite arc can be covered, with three sites about 75%. The a priori formal errors in radial orbit component decrease by about 20% including additional SLR data of two sites into orbit determination. The formal error decreases even more if data of three sites are used. Data of the fourth site leads to no further improvement.

For the GLONASS satellites the a priori formal errors of the radial orbit component decrease by about 50%. The impact of additional SLR data on GLONASS orbit determination is larger than for GPS satellites as the number of GLONASS microwave observations is much smaller.

4. Conclusion

The quality of GNSS orbits can be validated using SLR observations of GNSS satellites. An orbit accuracy of about 2 cm and 5 cm was estimated for the GPS and GLONASS orbits, respectively, from a 4-year time series of range residuals covering 2002-2006. A mean bias of –3 to –4 cm for the GPS satellite orbits remains still unexplained. Periodic variations of the GPS range residuals were found, which are highly correlated with eclipsing seasons. We could demonstrate that these variations are not caused by SLR tracking data, but due to deficiencies in the GNSS orbit modeling. An improved solar radiation pressure model might solve the problem. Radiation pressure caused by Earth albedo was not considered in the GNSS orbit determination, but it may have a non-negligible effect on the orbit. Attitude modeling problems might also cause similar periodic variations in the range residuals. Further studies will follow to understand the source of the systematic residual pattern.

The combined analysis of microwave and SLR observations could improve GNSS orbit determination, assuming that the SLR observations are evenly distributed over the entire arc. Already a small network of three globally distributed SLR sites tracking the GNSS satellites continuously may contribute significantly to GNSS orbit improvement.References

References

[1] Dow, J.M., R.E. Neilan, G. Gendt, et al.: “The International GPS Service (IGS): Celebrating the 10th anniversary and looking to the next decade”, Adv. Space Res., 36(6),pp. 320-326, 2005.

[2] Pearlman, M.R., J.J. Degnan, J.M. Bosworth: “The International Laser Ranging Service”, Adv. Space Res., 30(2), pp. 135-143, 2002.

[3] Urschl, C. , G. Beutler, W. Gurtner, U. Hugentobler, S. Schaer: “Contribution of SLR tracking data to GNSS orbit determination”, Adv. Space Res., in press.

GIOVE-A and GPS-35/36 orbit determination and analysis of dynamical properties based on SLR-only tracking data

Stavros A. Melachroinos[1], Felix Perosanz[1,3], Florent Deleflie[2], Richard Biancale1[1,3], Olivier Laurain[2], Pierre Exertier[2]

1. Groupe de Recherche en Géodésie Spatiale/LDTP-UMR5562
2. Groupe de Recherche en Géodésie Spatiale-OCA/GEMINI, Grasse, France
3. Centre National d'Etudes Spatiales, 18 avenue Edouard Belin, 31400 Toulouse, France

Contact: stavros@calc-gen3-ci.cst.cnes.fr

Abstract

SLR tracking data provided by the ILRS (International Laser Ranging Service) network are used to compute orbits of radio-navigation satellites equipped with laser retroreflectors : GPS-35 and GPS-36 for the American GPS constellation, and the first European GIOVE-A (Galileo In-Orbit Validation Element) satellite, launched in December 2005. The equations of motion are computed through an exhaustive dynamical model and is propagated with the two orbit determination softwares of the French GRGS (Groupe de Recherche de Géodésie Spatiale) group: GINS (for high frequency analyses), and CODIOR (for secular orbital elements analyses).

For each of these satellites, a set of SLR (Satellite Laser Ranging) data is processed and the results of the post-fit residuals analysis are shown. The orbit validation for GIOVE-A is based on overlaps between 2-day, 10-day and 30-day arcs calculated with the GINS software. The resulting 3D rms and radial residuals are the primary criteria for the internal accuracy of SLR orbits and may indicate possible dynamical perturbations such as orbit or attitude control manoeuvres. For GPS-35/36 satellites we compare two 10-day arcs to the precise IGS (International Global Navigation Satellite Systems Service) sp3 microwave final orbits. An offset of 2-3 cm in the radial direction appears between the two solutions and may reflect the effect of the non-homogeneity of the SLR tracking network. "Mean observed elements" are also provided.

***Keywords**: GNSS, GIOVE-A, Satellite Laser Ranging, Solar radiation pressure modeling, mean orbital elements*

1. Introduction

GIOVE-A is the first satellite of the future GALILEO global navigation system. It has been developed by Surrey Satellite Technology Ltd and the ESA (*European Space Agency*) . It was launched from Baikonur Cosmodrome on 28 December 2005 and placed into a MEO (*Medium Earth Orbit*) with a semi major axis of 29600 km, an inclination of 56° and an eccentricity of 0.002**.** GIOVE-A is equipped with a LRR (*Laser Retro Reflector*) array having 76 corner cubes with a diameter of 27 mm each (*ESA-EUING-TN/10206*), which provides 40 % more return energy than GPS-35/36 LRR arrays (ILRS). The final constellation of Galileo will consist of 27 operational spacecrafts equipped with such identical LRR arrays. After the launch of GIOVE-A, ESA has requested ILRS an SLR campaign support during spring and summer 2006

(http://www.esa.int). The purpose of these campaigns is to provide data for the characterization of the satellite's on-board clock

The first of theses campaigns has taken place between 22 May and 24 July 2006, with the participation of 13 globally distributed SLR stations. This paper presents the results of the GIOVE-A orbit determination for this period. The orbit validation is based on overlaps of fitted SLR-only orbits of 2-day, 10-day and 30-day duration arcs.

The ILRS community is also actively tracking the only two GPS (*Global Positioning System*) satellites which have LRR arrays on-board, designated GPS-35 and GPS-36. The GPS satellites are equipped with LRR arrays of 32 corner cubes arranged in a flat panel of 19x29 cm (*Degnan and Pavlis, 1994; ILRS, 2004; Urschl et al., 2005*)**.** The altitude of GPS 35 and 36 is that of 20,195 km and 20,030 km respectively, with a 0.000 and 0.006 eccentricity and a 54 ° inclination for both.

In this study we are using 10 days of SLR data, for the two GPS satellites, in the period of 6th till 16th of June 2006. In this period most of the SLR stations where pointing to the GIOVE-A satellite and the SLR tracking data for the two GPS satellites have always been sparse. In this investigation the challenge consists in discovering the achievable orbit accuracy with sparse tracking data for the two GPS satellites. The analysis of SLR orbits of both GPS satellites is based on overlaps wrt the precise IGSsp3 orbits and the examination of difference residuals in the radial, normal and along-track direction. Transformation parameters between the fitted SLR arcs and the IGSsp3 orbits are adjusted.

Moreover, a propagation of the mean equations of motion, accounting for only the long periodic effects acting on the GIOVE-A orbit, has been led. This study provides the values of the mean observed elements, giving a mean value of each orbital parameter, and of the angles in particular (ascending node, argument of perigee, mean anomaly) for the 10-day arc.

The paper is organized such as follows. The analysis of the SLR-orbit estimation strategy and the solar radiation pressure modeling is outlined in Section 2. Section 3 describes the data set being used for GIOVE-A and GPS-35 and GPS-36 satellites. Section 4 analyses the results of the GIOVE-A internal orbit overlaps. Section 5 makes the analysis of the differences of the estimated SLR orbits of GPS-35/36 wrt IGSsp3 final microwave orbits for the period in question. Section 6 is dedicated to the analysis of GIOVE-A and GPS-35/36 orbit mean elements. Section 7 derives the necessary conclusions and summarizes the results.

2. SLR orbit estimation strategy

Our motivation to process the GIOVE-A and GPS-35/36 satellite SLR data on the period of June 2006 is two-fold: firstly we want to evaluate the implementation of the new box-and-wing SRP (Solar Radiation Pressure) model of GIOVE-A in our software GINS 6.1, and secondly to test the performances of SLR-only orbit determination for these 3 GNSS (Global Navigation Satellite System) satellites.

Our estimation strategy is based on a weighted least squares scheme. The present analysis is made by the orbit determination and analysis software package GINS 6.1 developed by the CNES (Centre National d'Etudes Spatiales) geodetic team of. In table (1) the ad-hoc models and estimated parameters are summarized.

The attitude model used for all three s/c is illustrated in Fig. 1. and corresponds to the following coordinate frame :

- The **Y-axis** points along the solar panels
- The **D-axis** points towards the sun
- The **X-axis** completes the system

For GIOVE-A and GPS-35/36 we have implemented a box and wing solar radiation pressure model including respectively 8 and 19 surfaces with a-priori reflectivity and specularity coefficients

GINS 6.1 soft. package	***GPS 35/36***	***GIOVE-A***
Datum definition	ITRF 2000, EOPC04	ITRF 2000, EOPC04
Tidal displacements	IERS03	IERS03
Gravity field	EIGEN_GL04S(20x20)	EIGEN_GL04S(20x20)
Atmospheric loading Ocean loading	ECMWF FES2004 (K2 cor.)	ECMWF FES2004 (K2 cor.)
Troposphere	Marini-Murray	Marini-Murray
Solar Radiation Pressure	Box-and-wing	Box-and-wing
Albedo and infra-red	Analytical model (10°x10°)	Analytical model (10°x10°)
Satellite's retro-reflector offsets	x=-0.863, y=0.524, z=-0.658	x=0.828, y=0.655, z=-0.688
Attitude model	X, Y, D	X, Y, D
Numerical integration	Cowell 8th order, step size 180s	Cowell 8th order, step size180s
Parameter adjustment	6 orbital parameters, 1 SRP coeff., 1 Y-bias, 1 X, D per revolution (cos, sin)	6 orbital parameters, 1 SRP coeff., 1 Y-bias, 1 X, D per-revolution (cos, sin)

Table 1. *SLR-only orbit processing parameters for GPS-35/36 and GIOVE-A*

We have processed a set of 2-day, 10-day and 30-day arcs for the GIOVE-A satellite and two 10-day arcs for the GPS-35/36 satellites. Depending on the length of each arc, we include 1 per revolution terms for 2-day arcs (with constraints) and 5 per revolution terms (1 every 2d) for 10-day arcs in X, D directions. An additional acceleration along the s/c's Y-axis, the so-called Y-bias, is also adjusted.

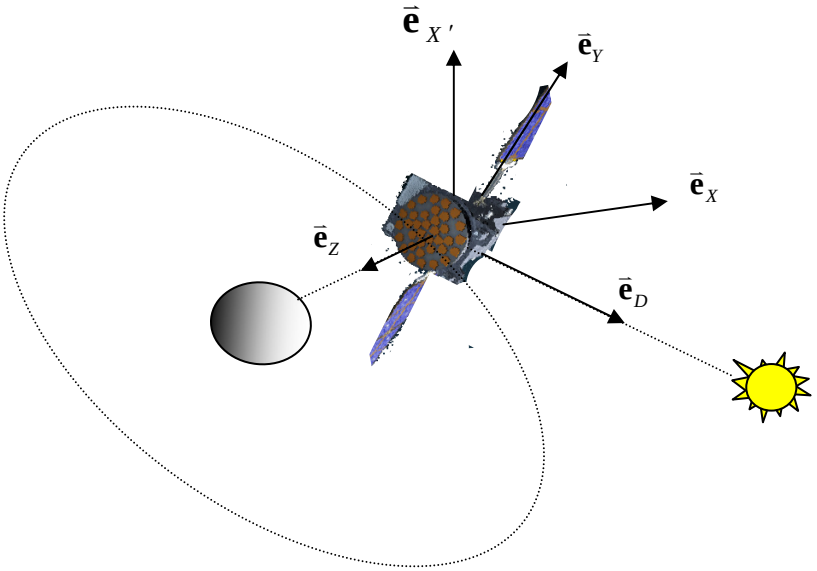

***Fig. 1**. The GIOVE-A and GPS-35/36 attitude model*

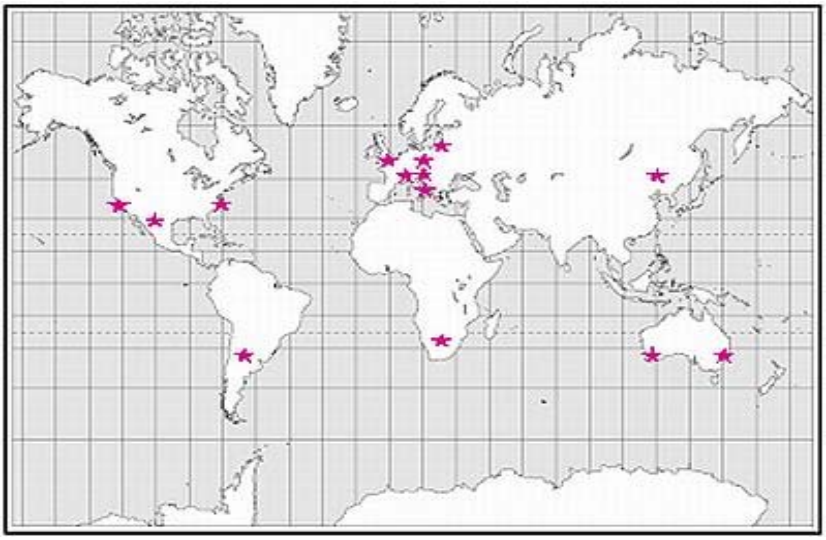

***Fig. 2.** The 13 SLR network stations distributed globally (ESA courtesy)*

3. Data set

Fourteen laser ranging stations (Fig. 2) participated in a campaign to track ESA's GIOVE-A satellite during spring and summer of 2006, providing invaluable data for the characterization of the satellite's on-board clock. The campaign was coordinated by ILRS and the GIOVE Processing Centre at ESA-ESTEC.

See www.esa.int/esaNA/SEM8QOKKKSE_index_2.html .

GIOVE-A satellite data from June to August 2006 used in this study have been processed. Figure 2 illustrates the distribution of the SLR tracking network. The total number of normal SLR points for this period arises up to 2311.

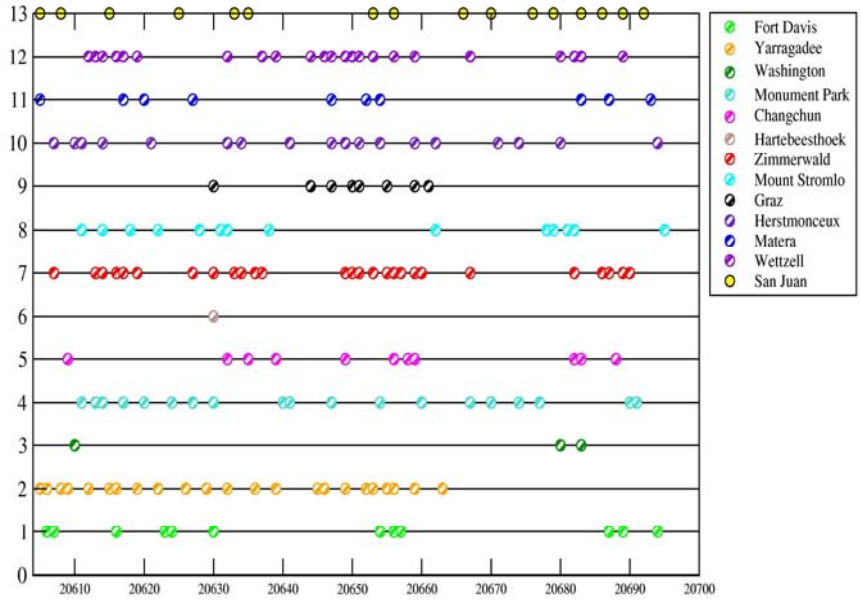

Fig. 3. *3 months (in Julian days 1950) of GIOVE-A SLR data from global tracking stations*

For GPS-35/36 we processed data from the period of June 2006 corresponding to a set of 306 and 402 normal points respectively. For the same period the amount of normal points for GIOVE-A is 900.

4. Orbit analysis of GIOVE-A

In this section we are examining:

- 1-day overlapping SLR-only sessions for GIOVE-A, from JULD50 (Julian day 1950) 20612 (2006/06/05) till JULD50 20623 (2006/06/19),
- a 10-day arc (2006/06/01.5-2006/06/11.5) over a 30-day arc (2006/06/01.5-2006/06/30.5)
- the overlaps with a 90-day arc expanding over the whole period of 3 months.

The illustration of the overlapping strategy is shown in Fig. 4.

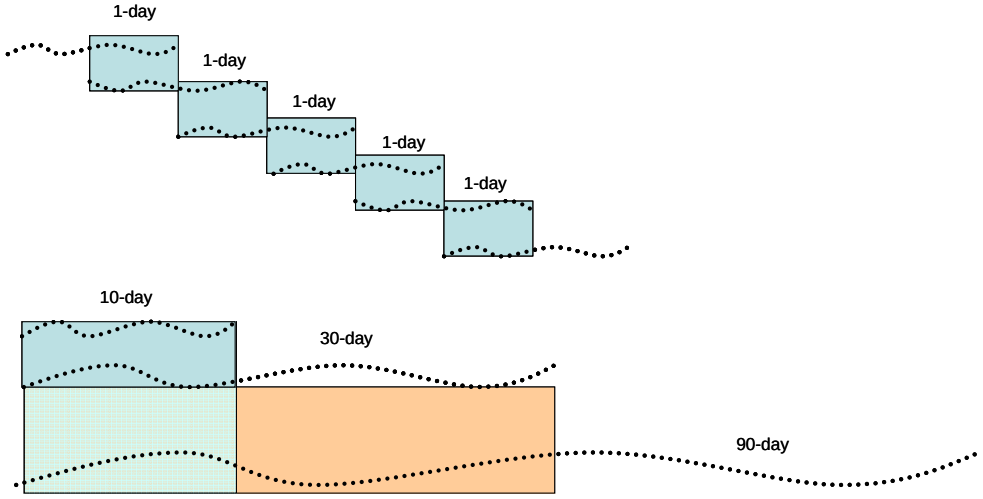

Fig. 4*. The overlapping periods of successive SLR arcs*

The evaluation criteria of the estimated orbit used are the root mean square misfit (RMS) (Eq. 1) and standard deviation (SD) of overlapping periods of successive arcs. An orbit overlap is defined by the comparison of the satellite's position vector between the common time-span of the two successive orbits (e.g. 1-day overlaps over 2 successive 2-day arcs).

$$rms_{misfit} = \sqrt{\frac{\left(\mathbf{x}^{arc1} - \mathbf{x}^{arc2}\right)}{n}}$$
$$rms_{3D} = \sqrt{rms^2_{Radial} + rms^2_{Along} + rms^2_{Cross}} \qquad (1)$$

Figure 5 shows the statistical results of the overlapping period of 2-day successive arcs.

For the arcs between JULD50 20611 (2006/06/08) and JULD50 20613 (2006/06/10), there is a significant change in the estimated accelerations, as well in the overlap mean difference and RMS. This implies that a dynamic perturbation like a manoeuvre occurred. In addition, a degradation of the mean difference of the SLR residuals appears at JJULD50 20620 (2006/06/16). This effect could be related to a reduction in the number of tracking stations for that epoch especially in the southern hemisphere.

The overlapping mean difference for the 2-day arcs is 43 cm in the Radial direction. Without accounting for the possible manoeuvre period it falls down to 14 cm. The same effect can be seen on the residual SD which decreases from 1.41 m to 32 cm for both 2 cases respectively.

Table 2 shows the orbit overlap misfit between a 10-day and a 30-day arc for the

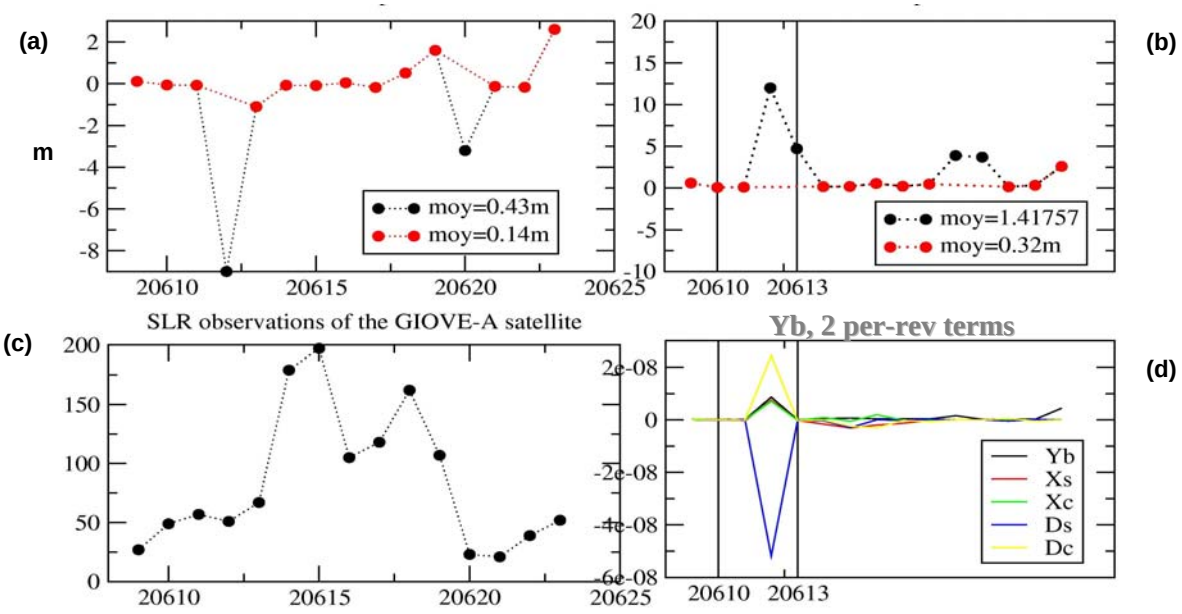

Fig. 5 *statistical results of the overlapping period of 2-day successive arcs: In (a) and (b) are illustrated the mean difference and the RMS misfit in the radial direction respectively. In black are the mean values (in m) including the perturbation days and in red are the mean values without the perturbation days. In (c) is the number of observations for every day and in (d) is the values of the empirical accelerations. Y-b is the Y bias, Xs and Xc are the sin and cos revolution terms in X direction, Dc and Ds are the sin and cos revolution terms in D direction. The perturbation has a stronger influence in the D direction revolution terms.*

period JULD50 20605 (2006/06/01) to 20615 (2006/06/11). The RMS of the satellite positions projected in the radial, normal and tangential directions are respectively 8cm, 45cm and 37cm.

The SLR residuals of a 10-day, 30-day and a 90-day arc are given figure 6 and lead to the same conclusions about the perturbations dates. All arcs agree in the residual level. Outliers up to 8m, verify the existence of dynamical perturbation event and appear in all arcs.

GIOVE-A RMS Misfits (cm)

Earth Along (Tangential)	45.64
Earth Normal	37.46
Earth Radial	8.96

Table 2*. GIOVE-A 10-day orbit overlaps from 2006/06/01.5 to 2006/06/11.5 over a 30-day arc from 2006/06/01.5 – 2006/06/30.5*

5. Orbit analysis of GPS 35/36

One 10-day SLR-only arc has been computed for GPS-35/ 36. The SLR data set spans from JULD50 20610 (2006/06/06) to 20620 (2006/06/16). As already mentioned, this period corresponds to a SLR campaign giving the priority to GIOVE-A tracking. This validation method has been very well known in the last 10 years and many studies, like Pavlis(1995), Appleby and Otsubo (2000), Hujsak et al. (1998) have investigated the undergoing problems of SLR sparse tracking orbit determination.

Tables 3(a) and 3(b) compare the adjusted orbits to the IGSsp3 final precise orbits in terms of position differences in the radial, normal and tangential directions. The RMS is at the level of 3 cm in radial, 47 cm in cross-track and 23 cm in along-track direction for GPS-35.

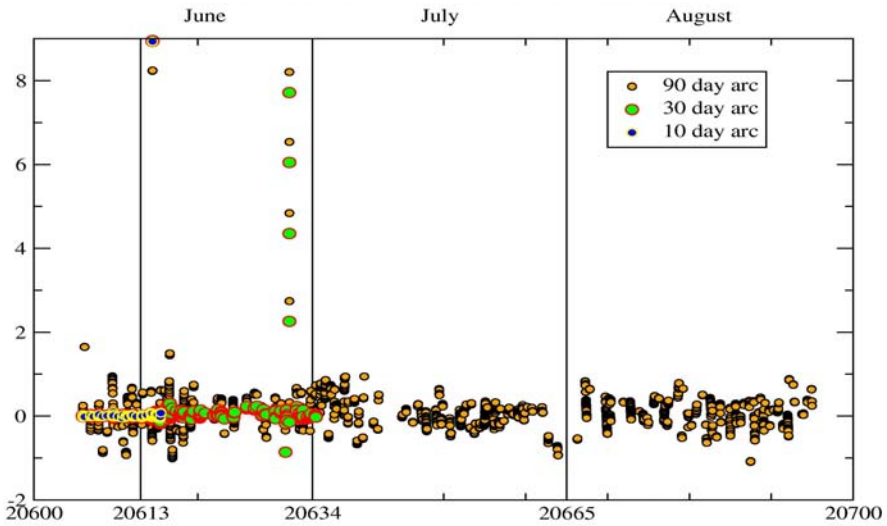

. ***Fig. 6:*** *SLR residuals for the 10-day, 30-day and 90-day arcs from the 1st of June*

GPS-35 RMS Misfits (cm)

Earth Along (Tangential)	23.81
Earth Normal	47.25
Earth Radial	3.24

Table 3 (a). *GPS-35 10-day SLR arc overlap wrt IGSsp3 final orbits*

GPS-36 RMS Misfits (cm)

Earth Along (Tangential)	9.55
Earth Normal	25.75
Earth Radial	2.03

Table 3 (b). *GPS-36 10-day SLR arc overlap wrt. IGSsp3 final orbits*

For the case of GPS-36 the level of agreement in comparison with the IGSsp3 radiometric orbits, is respectively in the radial, along-track, cross-track directions: 2-9-25 cm. Obviously, for GPS-35 and GPS-36, this result reflects the poor geographical distribution of SLR tracking stations. When one station in the southern hemisphere tracks GPS-36, for the same period, the factor of disagreement wrt IGSsp3 orbits drops down by a factor of 2.

Tx	-7.8 +/- 9.
Ty	-.4 +/- .9
Tz	**59.8 +/- 9.**
S (ppb)	$.620124 \times 10^{-9}$ +/- $.375 \times 10^{-9}$
S (m)	**16.5 +/- 10**
Rx	-.3 +/- .1
Ry	.01 +/- .1
Rz	**-2.4 +/- .1**

Table 4 (a). *Helmert transformation wrt. the IGS microwave orbits for GPS-35 JJULD 20610-20620 in mm*

In order to further quantify any RF (Reference Frame) systematic differences, we applied a 7-parameter Helmert transformation between SLR-only orbits and IGSsp3 solutions. Table 4 (a) and 4 (b) summarize the statistics from this comparison.

Both translation coefficients in Z for GPS 35/36 are significative with 60 mm (± 10 mm) and 45 mm (± 5 mm) respectively. This offset may reflect systematic problems

in either or both types of orbit as a result of non-homogeneity of SLR tracking stations in the global networks. In addition there is a factor of 8 in scale differences for GPS 35 and GPS 36 wrt the RF defined by IGSsp3 orbit. This statement is probably related to the poor number of southern tracking SLR tracking stations.

Tx	2.2 +/- 5.3
Ty	. 8 +/- 5.3
Tz	**45.3 +/- 5.3**
S (ppb)	$.712820 \times 10^{-10} +/- .2 \times 10^{-9}$
S (m)	**1.9 +/- 5.**
Rx	-.3 +/- .05
Ry	.04 +/- .05
Rz	**-1.4 +/- .05**

Table 4 (b). *Helmert transformation wrt. the IGS microwave orbits for GPS-36 JJULD 20610-20620 in mm*

Furthermore, the overall agreement of SLR-only orbits with sparse data wrt. the radiometric IGSsp3 final orbits, is 2 to 3 cm radially. The consistency of the RF arises up to 6-4 cm in translation along the z-axis.

6. Mean observed elements

A complementary study has been led to give the value of the mean elements of the orbits of GIOVE-A, GPS-35 and GPS-36, namely : the mean semi-major axis, the mean eccentricity and inclination for the metric variables (those providing the computation of secular effects induced on the angles), the mean ascending node, mean perigee and mean “mean anomaly”. Such an approach leads up to an evaluation of the long term validity of gravitational and non gravitational models, and requires a data processing strategy where short periodic effects are removed from the osculating orbit, on each orbital element. This filtering approach has been carried out following the analytic part of the method, developed in (Exertier, 1990).The formulation of (Kaula, 1966) has been used to express the short period acting on the semi major axis, inclination, ascending node, and the one developed in (Deleflie, 2006) for the components of the eccentricity vector, because the investigated orbits are nearly circular.

Figures 7, 8, 9 show the temporal evolution of the mean metric elements of the GIOVE-A, GPS-35 and GPS-36 orbits, respectively. Table 5 gathers up some of these main elements, and Table 6 the main dynamic characteristics of these orbits which can be deduced from this study.

7. Conclusion and perspectives

The capability to estimate SLR-only orbits for GIOVE-A s/c has been implemented and evaluated in the GINS 6.1 CNES/GRGS software. The generated orbits are internally accurate to the level of 5-10 cm radially. This is the case when we are taking into account longer arc periods where orbit dynamics can absorb uniformly in the least square process a possible un-mapped perturbation such as s/c manoeuvres. Unknown manoeuvres are a critical issue for the s/c orbit determination.

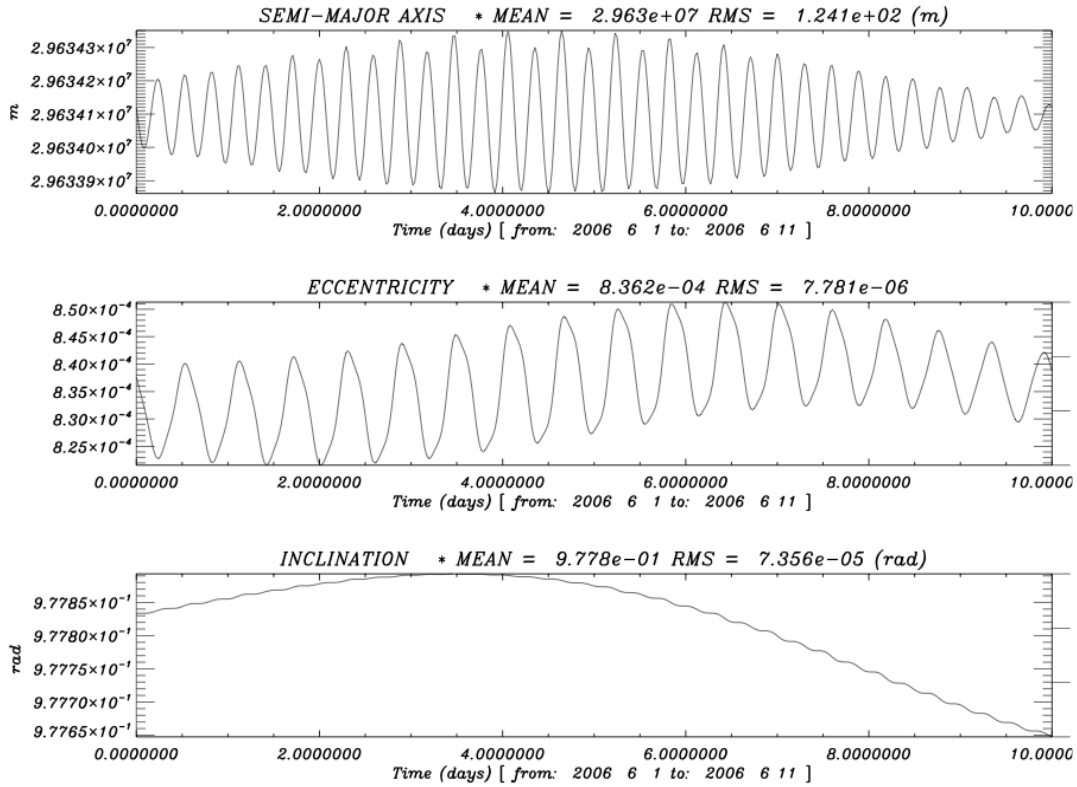

Fig 7. *Temporal evolution of the mean metric elements of the GIOVE-A orbit, from 2006, 1st of June to 2006, 11th of June*

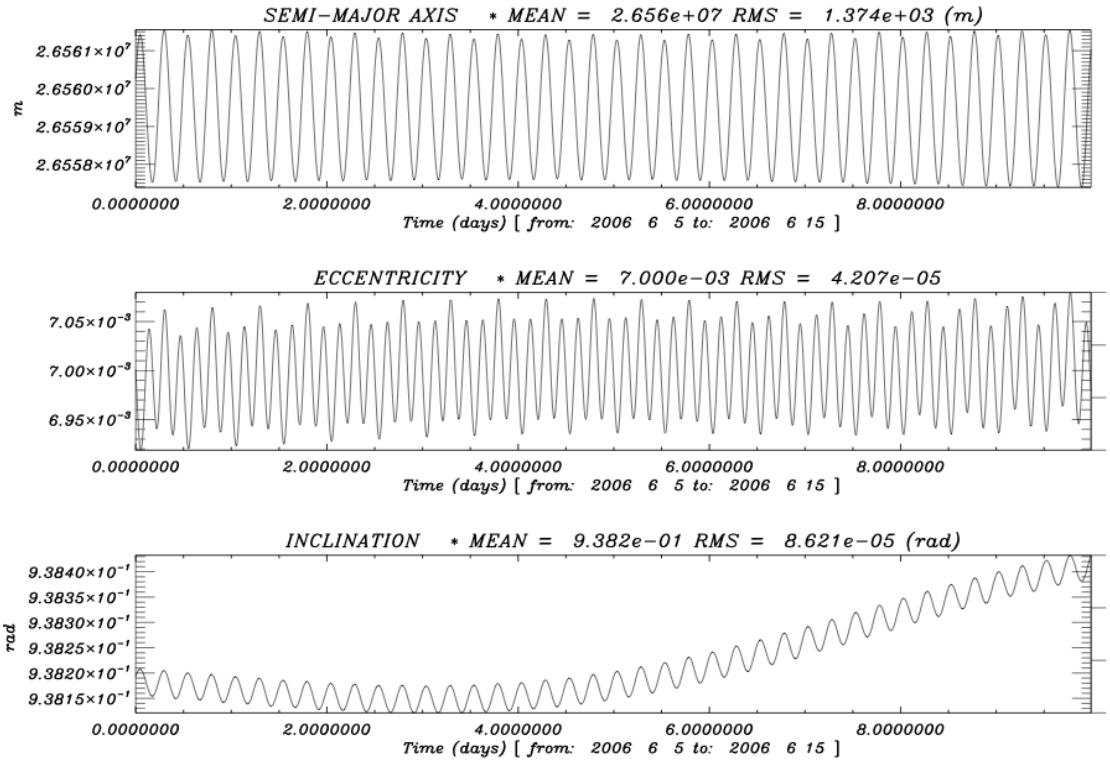

Fig 8. *Temporal evolution of the mean metric elements of the GPS-35 orbit, from 2006, 6th of June to 2006, 15th of June*

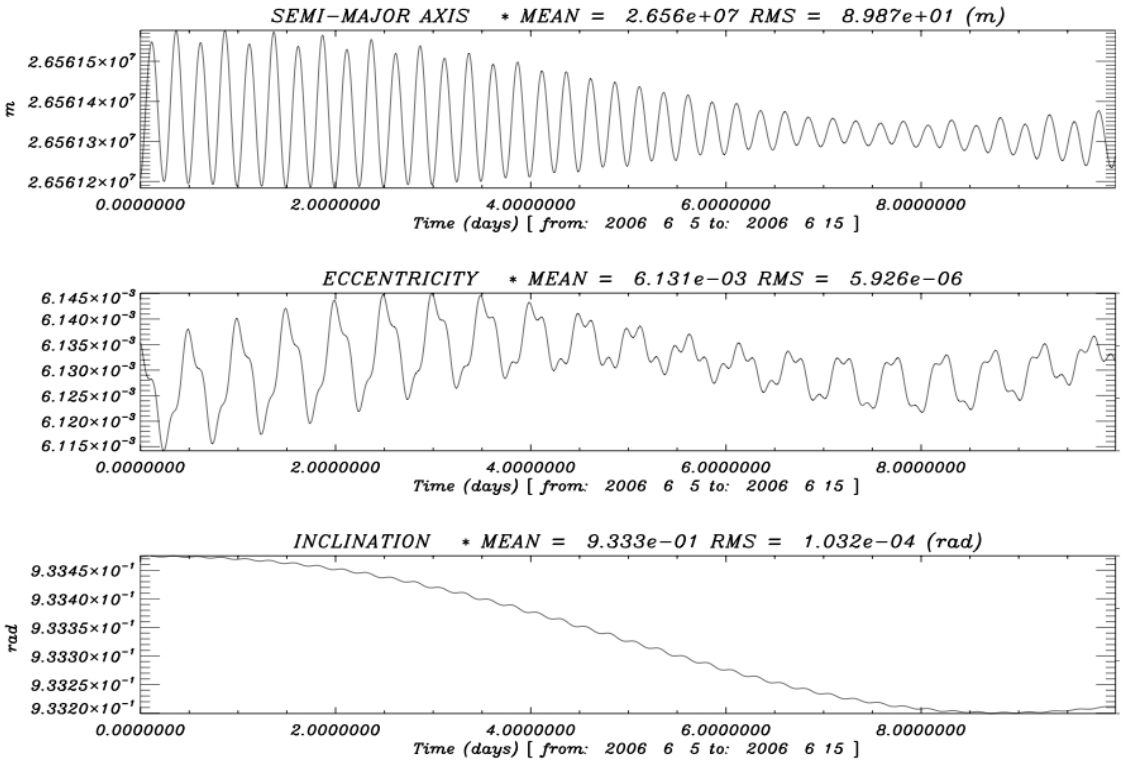

***Fig 9**. Temporal evolution of the mean metric elements of the GPS-36 orbit, from 2006, 6th of June to 2006 15th of June*

By comparing the results for the 90-day, 30-day, 10-day and 2-day orbits we believe that 2-day orbits are the most appropriate for further orbit dynamics investigation. Another critical aspect in the orbit determination of GIOVE-A s/c is the solar radiation pressure model (SRP). We are using an analytical box-and-wing SRP model with approximate specularity and reflectivity coefficients.

	Epoch. (Julian Days 1950)	Semimajor Axis *(m)*	Eccentricity	Inclination °	Ascending node *(rad)*	Argument of perigee *(rad)*	Mean anomaly *(rad)*
GIOVE-A	20605,5	0.29634118E+08	0.83763674E-03	56.025730°	0.32550034E+01	0.57163824E+01	0.11332092E+01
	20615,5	0.29634120E+08	0.83869966E-03	56.015079°	0.32504105E+01	0.57263379E+01	0.12404609E+01
GPS-35	20609,5	0.26560245E+08	0.70009131E-02	53.754485°	0.24052494E+01	0.10521913E+01	0.19530670E+01
	20619,5	0.26561274E+08	0.69619513E-02	53.768426°	0.23981146E+01	0.10572299E+01	0.23138993E+01
GPS-36	20609,5	0.26561208E+08	0.61354695E-02	53.484095°	0.35019663E+01	0.44620688E+01	0.31748379E+01
	20619,5	0.26561276E+08	0.61312841E-02	53.469107°	0.34948338E+01	0.44640863E+01	0.35254203E+01

***Table 5.** Mean observed elements for three orbits, deduced from an analytical filtering of the short periodic terms inside the osculating orbit adjusted on SLR-data.*

	Secular effectsd induced on			riod of revolution of			Altitude of	
	Asc. Node *(rad/s)*	Perigee *(rad/s)*	Mean anomaly *(rad/s)*	Asc. Node *(day)*	Perigee *(day)*	Mean anomaly *(min)*	Perigee *(km)*	Apogee *(km)*
GIOVE-A	-0.520220E-08	0.261182E-08	0.123762E-03	13979	27843	846	23231	23280
GPS-35	-0.807674E-08	0.510770E-08	0.145861E-03	9003	14238	718	19995	20367
GPS-36	-0.812694E-08	0.525981E-08	0.145852E-03	8948	13826	718	20020	20345

Table 6. *Main characteristics of motion.*

A further improvement would be the adjustment of these coefficients in at least one year period time by making use, as well, of the most accurate radiometric observations in L1 and E5. Though an empirical model like those used by CODE orbit analysis center and implemented in the Bernese GPS software, would be further investigated

For GPS 35/36 the presented comparison to the IGSsp3 final orbits for the two 10-day arcs shows a high quality of SLR-only orbits derived with sparse data. RMS residuals are of the order of 2-3 cm radially, 5-10 cm in along and 25-40 cm in cross-track. The systematic patterns of the translation and scale parameters of the RF demonstrate the dependencies in the geographic distribution of the SLR network.

Finally, only two s/c of the GPS constellation are equipped with LRR arrays for orbit validation and the end of their life time could be within the next year. Nevertheless Europe's satellite navigation system Galileo will offer this valuable opportunity of independent orbit validation procedures since all s/c of the constellation will be equipped with LRR arrays.

References

[1] Appleby, G., Otsubo, T. Comparison of SLR measurements and orbits with GLONASS and GPS microwave orbits, in : Proceedings of the 12th International Workshop on Laser Ranging, Matera Italy, 13-17 November 2000

[2] C. Urschl, W. Gurtner, U. Hugentobler, S. Schaer, G. Beutler, Validation of GNSS orbits using SLR observations, Advances in Space Research 36 (2005) 412 – 417

[3] Degnan, J.J., Pavlis, E.C., Laser ranging to GPS satellites with centimeter accuracy. GPS World 62-70, 1994

[4] Deleflie, F., Métris, G., Exertier, P., An analytical solution of the lagrange equations valid also for very low eccentricities. Influence of a central potential, Celest. Mech. 94, 1, 105-134, 2006

[5] European Space Agency, Specifications of Galileo and GSTB-V2 space segment properties relevant for satellite laser ranging, ESA-EUING-TN/10206, Technical note, 2005

[6] Exertier, P., Precise determination of mean orbital elements from osculating elements , by semi-analytical filtering, -V 15, pp 115-123, 1990

[7] Hujsak, R. S., Gilbreath, G. C., Sequential Orbit Determination for GPS-35 and GPS-36 using SLR data from NRL@SOR " SPIE Proceedings, 3380 (32), April 1998

[8] International Laser Ranging Service, GIOVE-A, http://ilrs.gsfc.nasa.gov

[9] Kaula, W. M., Theory of Satellite Geodesy. Blaisdell publ. Co., New York, 1996

[10] Pavlis, E.C, Comparison of GPS S/C orbits determined from GPS and SLR tracking data, Adv. Space Res. Vol. 16, No. 12, pp (12)55-(12)58, 1995

Orbit Determination and Analysis of Giove-A using SLR Tracking Data.

Ramesh Govind[1]

1. Geoscience Australia, Canberra, Australia

Abstract

Using the early available SLR data since its launch, precise orbit determination of the GIOVE-A satellite was undertaken in weekly arcs. A description of the contributing data set, the computation process and the initial results of the orbit quality are presented. From these solutions, the inferred data quality from the individual stations is summarised. Using one estimate of the state vector from these solutions, a spectral analysis of the orbit perturbations due to the Earth's gravity field is shown.

Orbit determination for GIOVE-A using SLR tracking data

C. Urschl[1], G. Beutler[1], W. Gurtner[1], U. Hugentobler[2], M. Ploner[1]

1. Astronomical Institute, University of Bern, Switzerland
2. Institute of Astronomical and Physical Geodesy, Technical University of Munich, Germany

Contact: claudia.urschl@aiub.unibe.ch

Abstract

The first European navigation test bed satellite GIOVE-A was launched on 28 December 2005. SLR observations of GIOVE-A, collected from the ILRS tracking network, are available since 21 May 2006. SLR data are primarily needed for the validation of the microwave-based orbit. As no microwave tracking data are available until now, the orbit determination based on SLR data is of high interest. We present GIOVE-A orbit determination results based on SLR-only data. In addition, the contribution of SLR data to the microwave-based orbit determination is demonstrated.

For the SLR-based orbit determination of GIOVE-A SLR data of the first GIOVE-A SLR tracking campaign were used. Orbits with different arc lengths were determined, as well as orbit predictions. Orbit overlaps were derived to assess the orbit quality. SLR-based orbits of 9-days arc length were determined with an accuracy of about 10 cm in radial orbit component, and about 0.5 m and 1 m in along-track and out-of-plane components.

The microwave-based GIOVE-A orbits as well as the first Galileo orbits in the In Orbit Validation (IOV) phase will rely on microwave tracking data of a very limited number of stations. Therefore, SLR would give an important contribution to the orbit determination through a combined analysis of microwave and SLR data. The possible improvement of the orbit accuracy including SLR observations is demonstrated on the basis of an a priori variance-covariance analysis. For this purpose SLR range measurements and simulated microwave data of GIOVE-A are used.

1. Introduction

Galileo, the European global navigation satellite system (GNSS), is presently being developed. The first of two "Galileo In-Orbit Validation Element" test satellites, GIOVE-A (GSTB/V2A), was successfully launched on 28 December 2005. It carries a retroreflector array and can thus be observed by Satellite Laser Ranging (SLR). For evaluating the characterization of the on-board atomic clocks a first SLR tracking campaign on GIOVE-A was initiated. Between 22 May and 24 July 2006, 14 globally distributed SLR stations participated in the campaign.

As no microwave tracking data are available for scientific use, the orbit determination based on SLR is of high interest. In Section 2, we present first results of the GIOVE-A orbit determination using SLR data of the tracking campaign. Different orbit solutions with varying arc-length were determined. In order to assess the orbit quality, orbit overlaps were computed and compared with each other. In addition, orbit predictions were generated and evaluated by comparing the predicted orbits with the orbits derived from real tracking data.

Orbit determination of GIOVE-A (and the first Galileo satellites as well) based on microwave observations will rely on data of a very limited number of microwave tracking receivers in the beginning. In view of this situation, SLR data would give an

important contribution for precise orbit determination. SLR data may significantly improve the orbit estimates used in addition to the microwave data in a combined analysis. Section 3 shows results of an a priori variance-covariance analysis, demonstrating the possible positive impact of additional SLR data on GIOVE-A orbit determination. For this purpose, simulated microwave data and real SLR data from the tracking campaign were used.

2. GIOVE-A orbit determination using SLR observations

In this Section, we present first GIOVE-A orbit determination results based on SLR data only. SLR data collected during the first GIOVE-A SLR tracking campaign lasting nine weeks (May 22 – July 24, 2006) were used. The SLR data are provided by the International Laser Ranging Service (ILRS) (Pearlman et al., 2002). The triangles in Figure 1 indicate the geographical location of the 11 SLR sites that were included in our analysis. Note that we did not use SLR measurements of San Juan (located in South America), as no official terrestrial reference frame coordinates have been available at the time of analysis.

The temporal distribution of the SLR tracking data is shown in Figure 2. Each line represents 24 hours of a particular day. SLR observation epochs are indicated with a bar. The varying data coverage is clearly visible. Thus, the quality of the orbits derived from these data will vary, depending on the available SLR data.

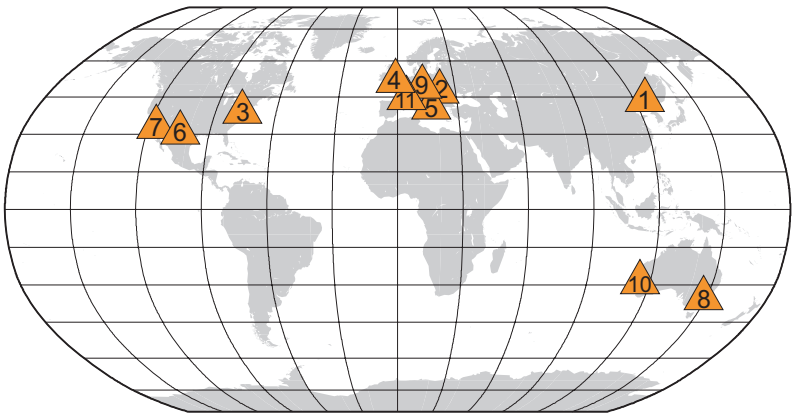

1 Changchun
2 Graz
3 Greenbelt
4 Herstmonceux
5 Matera
6 McDonald
7 Monument Peak
8 Mount Stromlo
9 Wettzell
10 Yarragadee
11 Zimmerwald

Figure 1. *Geographical location of the 11 SLR sites used for orbit determination*

In each orbit determination process six osculating elements and nine dynamical orbit parameters were estimated. The dynamical parameters represent solar radiation pressure (SRP) parameters defined in the SRP frame (D,Y,X). The SRP frame origin corresponds to the satellite's center of mass. The D-axis points towards the Sun, the Y-axis points along the solar panel axis, and the X-axis completes the right-handed system. The nine estimated SRP parameters are three constant acceleration (in D,Y, and, X direction) as well as six once per orbit revolution sinusoidal accelerations (sine and cosine in D, Y, and X direction).

Different orbits solutions were prepared using arc-lengths of n-days (n = 5, 7, 9, 11, 14) in order to estimate the arc-length that leads to the best possible orbit quality. The Bernese GPS Software Version 5.0 (Hugentobler et al., 2005) was used for the parameter estimation.

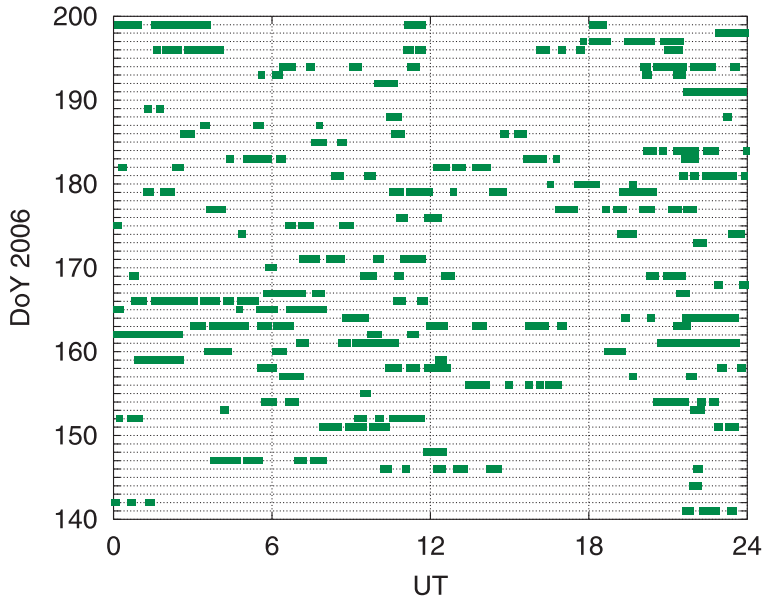

Figure 2. *SLR data coverage of the GIOVE-A SLR tracking campaign*

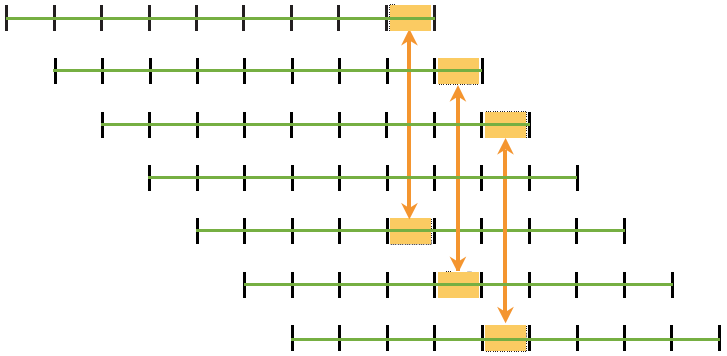

Figure 3. *Sketch illustrating the generation of orbit overlaps for 9-day arcs; orbit overlap is the orbit difference between last and central day*

For each solution we generated between 32 and 50 n-day arcs within the 60 days interval of the SLR tracking campaign of GIOVE-A. Consecutive n-day arcs are shifted by one day each. Thus, overlapping orbits can be generated. The resulting orbit differences (referred to as orbit overlaps in the following) indicate the orbit quality. Small overlaps indicate a good quality, whereas large overlaps indicate a bad quality of the determined orbit. We assume that the central part of an arc is best defined and that the boundary parts of an arc are worst defined. The overlap analysis concept is to compare the last day of an arc with the corresponding central day of another arc of the same arc-length, as illustrated in Figure 3. In the sketch each line represents a 9-day arc, day boundaries are indicated. The arrows show the orbital parts that are compared with each other.

Figure 4 shows the orbit overlaps of the GIOVE-A 9-day arcs. This arc length of 9 days has proved to be the best one, as the overlaps of the other orbit solutions with arc lengths of 5, 7, 11, or 14 days are larger. The orbit overlaps vary significantly, as the orbit quality is highly correlated with the number and temporal distribution of the SLR observations. Arcs with less or badly distributed observations are determined worse. Satellite maneuvers might also cause problems, if they are not considered in the orbit model. The radial orbit overlaps (top chart in Figure 4) show values of up to 10 cm. The radial component is best defined, as the SLR ranges represent observations mainly in radial direction. Orbit overlaps in along-track and out-of-plane components vary up to

1 m and 2 m, respectively. For arcs with a good temporal distribution of SLR data the orbit overlaps are smaller with values up to 0.5 m in along-track and 1 m in out-of-plane component. The formal errors of the satellite positions in the orbit system (radial, along-track, out-of-plane) show corresponding magnitudes similar to the overlap values.

Figure 5 displays the range residuals derived from the 9-day arc solution. The standard deviation of the residuals is about 2 cm, which is within the range of the accuracy of the SLR observations. SLR observations are assumed to be accurate at the 1-2 cm level.

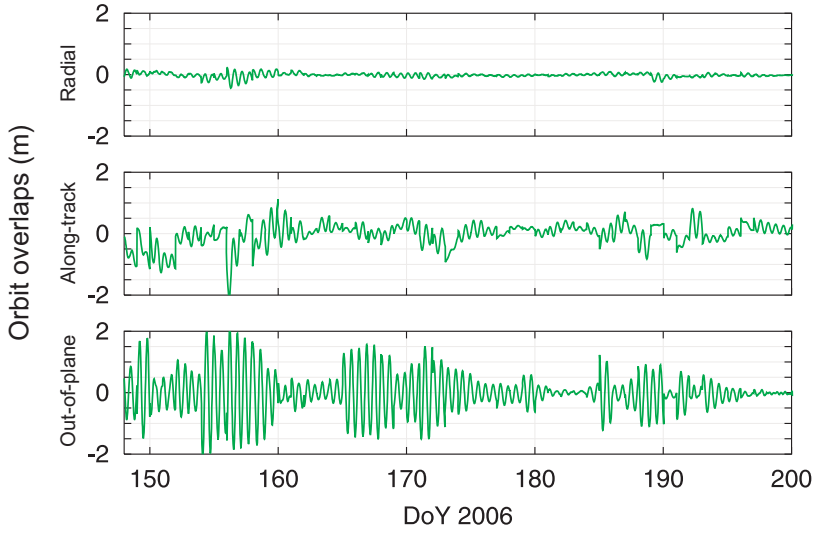

Figure 4. *Orbit overlaps of SLR-based 9-day arcs of GIOVE-A; orbit overlaps are the orbit differences between the central days and the last days of the corresponding 9-day arcs*

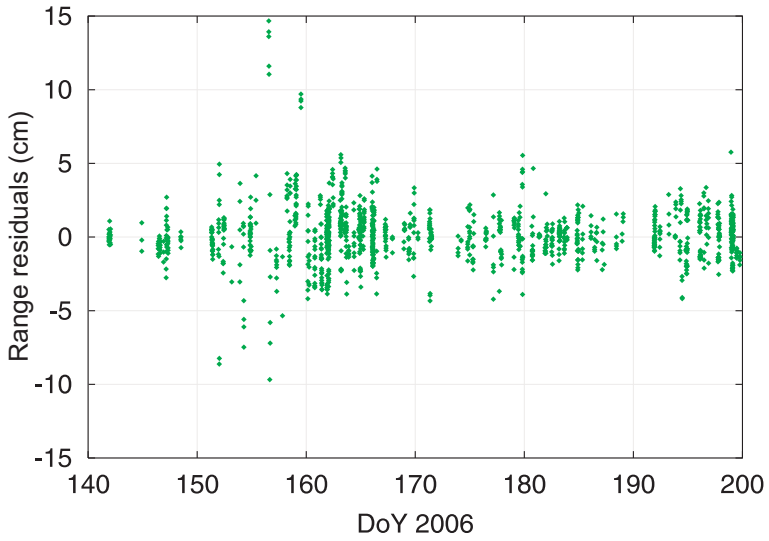

Figure 5. *Range residuals derived from SLR-based 9-day arcs of GIOVE-A*

In addition to the SLR-based 9-day arcs, we computed consecutive 5-day orbit predictions. For the overlap computation, each predicted day is compared with the corresponding central day of the orbit part covered by SLR observations, as illustrated in Figure 6. Thus, for each 9-day arc overlaps of the five prediction days are generated.

Figure 7 shows the orbit overlaps for all prediction days of all orbital arcs. The predictions are getting worse in time due to the accumulated orbit errors. The computed prediction overlaps are dominated by the along-track error of the orbital arc, as this

error increases exponential in time. The overlaps indicate a potential orbit accuracy of about 20-30 m after 5 days of prediction.

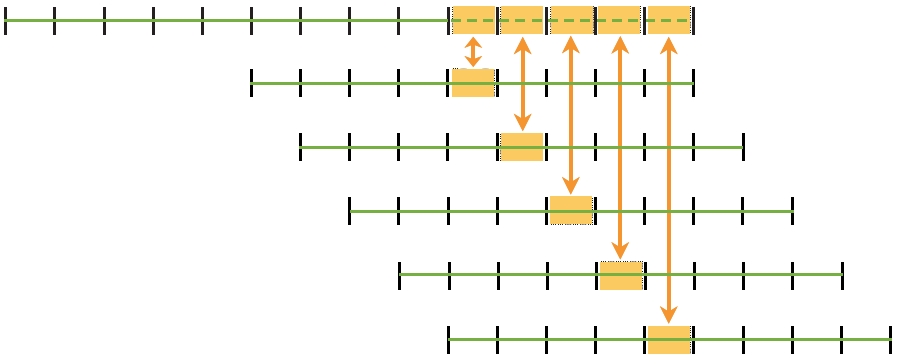

Figure 6. *Sketch illustrating the generation of orbit overlaps for 9-day arcs with 5 day predictions; orbit overlap is the orbit difference between each prediction day and the corresponding central day of the orbit part covered by SLR observations*

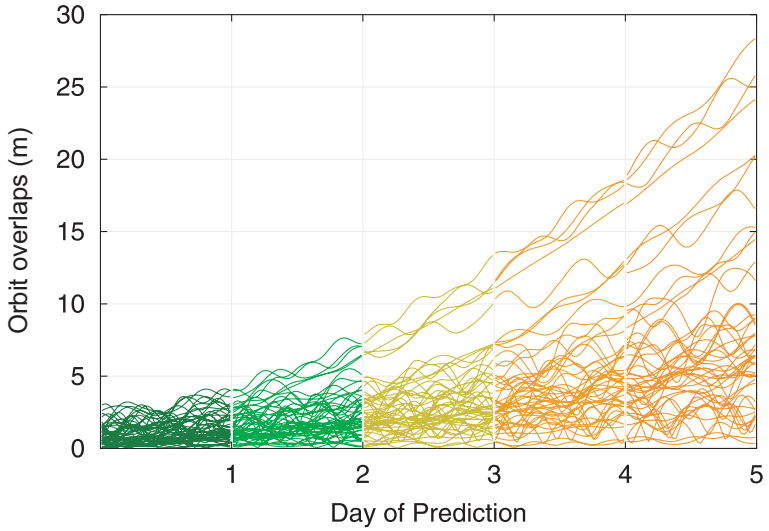

Figure 7. *Orbit overlaps of 5-day predictions based on GIOVE-A 9-day arcs; orbit overlaps are the orbit differences between the prediction days and the central days of the corresponding 9-day arcs*

3. Combined analysis of SLR and microwave observation for GIOVE-A orbit determination

This Section demonstrates the possible contribution of SLR to GIOVE-A orbit determination through a combined analysis of microwave and SLR data. As no microwave tracking data of GIOVE-A were available at the time of our analyses, we performed an a priori variance-covariance analysis. For such an analysis the observations are not needed, rather the number and temporal distribution and the assumed a priori error of the observations. Note that model deficiencies are not considered here.

Microwave phase observations were simulated for 13 GIOVE-A tracking sites, which are chosen similar to the proposed sites of the first Galileo tracking network. Their global distribution is indicated with circles in Figure 8. In addition we used the SLR true observations of the SLR sites represented with triangles.

The microwave phase observations are sampled with 30 s and have an accuracy of 1 mm. Observation equations were set up for microwave phase zero difference observations and SLR normal points. Satellite clocks, ambiguities, and orbit parameters were included in the parameter estimation. Other parameters, as station coordinates,

receiver clocks, tropospheric zenith path delays, and Earth orientation parameters are assumed to be known accurately, as for example from a global analysis of GPS and GLONASS data.

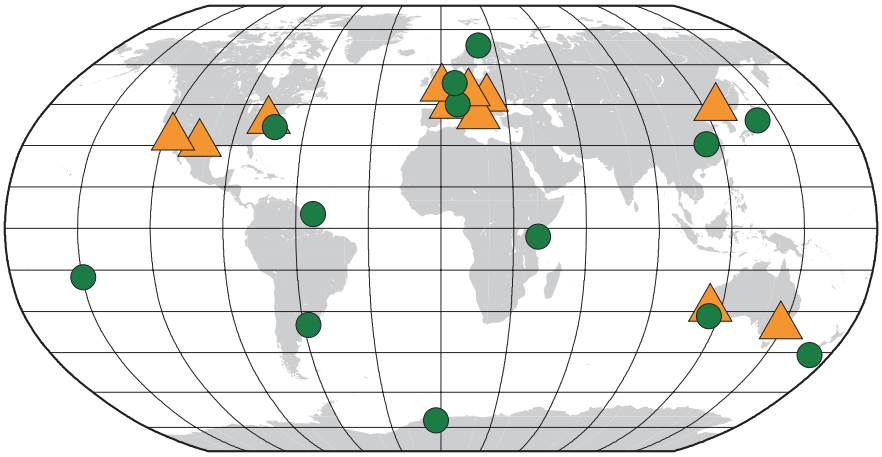

Figure 8. *GIOVE-A tracking sites (circles) and SLR tracking sites (triangles)*

The *a priori* variance-covariance matrix is derived from the obtained normal equation system. The *a priori* formal errors of the orbit parameters are then computed from the variance-covariance matrix. We used the same orbit parameters as in Section 2, i.e. six osculating elements and nine solar radiation pressure parameters in D,Y,X- direction. In summary 57 orbital arcs of 3 days length were determined, shifted by one day each.

To assess the impact of additional SLR observation on GIOVE-A orbit determination, we performed three different analysis with different SLR observation weight scenarios. The first solution corresponds to a pure microwave solution. The SLR observation weight is set to zero by setting the a priori sigma σ_{SLR} to infinity. In the second case, σ_{SLR} is set to 1cm. In the third case, the SLR observation weight is increased (with σ_{SLR} = 1 mm), and corresponds to the microwave observation weight.

We calculate the a priori formal errors of the satellite position in the inertial system from the *a priori* formal orbit errors by applying the law of error propagation. Figure 9 shows the *a priori* formal errors of the satellite position in radial, along-track, and out-of plane component for the three different solutions of a GIOVE-A 3-day arc. The absolute error values must be considered to be much too optimistic, as the error scales with the number of observations. We used 30 s sampled microwave data, but did neglect any temporal correlations between consecutive observations. A sampling rate of 180 s should rather be used for further studies.

The introduced parameters (e.g., station coordinates, troposphere parameters), which are assumed to be known from the GPS/GLONASS analysis, are not error free. Neglecting the formal errors of the introduced parameters, and of temporal correlations between observations causes too optimistic formal errors. However, in this analysis we are not interested in the absolute values of the formal orbit errors, but rather in the relative difference of the formal orbit errors between the three solutions. We may from this assess the impact of additional SLR observations on GIOVE-A (or Galileo) orbit determination in terms of orbit improvement.

The major impact of additional SLR data on the resulting orbit accuracy is given in the radial orbit component. A possible improvement of the radial orbit accuracy of about 60-80% may be feasible, depending on the SLR weight and the number and distribution of SLR observations. The formal orbit error in along-track and out-of-plane components

decreases with strong SLR weights, only. A good temporal distribution of the SLR observations over the entire arc is always necessary. Otherwise, if e.g. SLR observations are only available at the beginning of an orbital arc, the orbital errors as well as the orbit positions will show periodic variations.

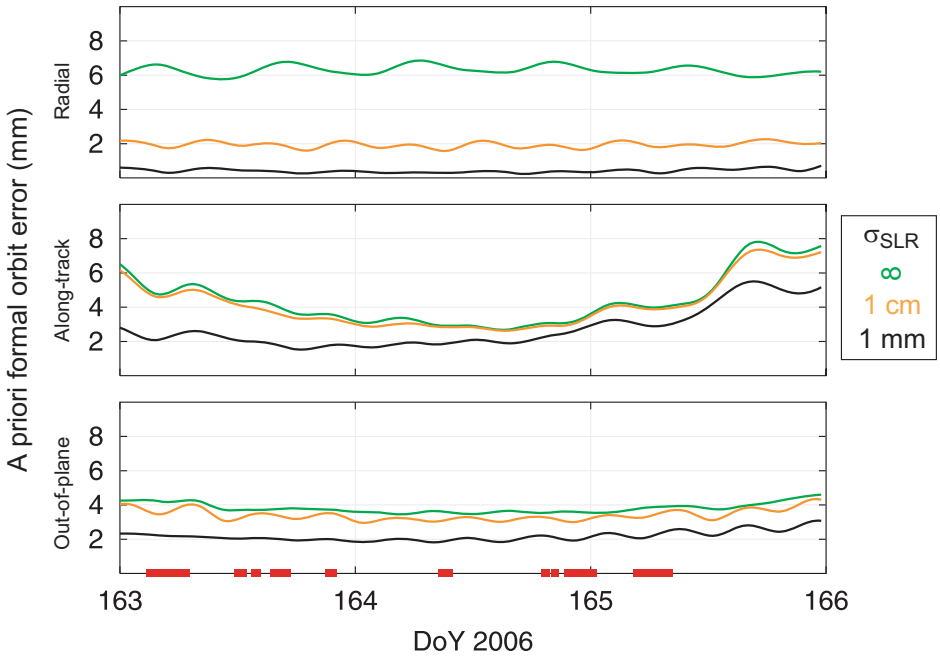

Figure 9. *A priori formal orbit errors in the inertial system; the three lines indicate the different orbit solutions using different a priori sigmas σ_{SLR} for the SLR observations; the bars on the horizontal axis indicate the SLR observation epochs*

4. Summary

We presented GIOVE-A orbit determination results based on SLR observations of the first GIOVE-A SLR tracking campaign. Orbits of several arc-length were determined and compared with each other. Nine-day arcs proofed to provide the best possible orbits with the used orbit model. No a priori solar radiation pressure model was introduced in the orbit determination, but constant accelerations and once-per orbit revolution accelerations were estimated. The orbit accuracy of a 9-day arc is about 10 cm, 0.5 m, and 1 m in radial, along-track, and out-of-plane component, unless the observation coverage of the orbit is poor. If SLR observations are very sparse and not well distributed over the entire arc, the orbit quality decreases. Orbit predictions are at the 20-30 m accuracy level after five days.

The impact of SLR observations used in addition to microwave observations for precise orbit determination of GIOVE-A was demonstrated. An a priori variance-covariance analysis shows a significant orbit improvement mainly in radial direction of about 60%, if additional and well distributed SLR observations are used. This can be addressed to the very low number of microwave tracking sites for the upcoming Galileo system in the very beginning of the system implementation.

References

[1] Pearlman, M.R., J.J. Degnan, J.M. Bosworth: “The International Laser Ranging Service”, Adv. Space Res., 30(2), pp. 135-143, 2002.

[2] Hugentobler, U., P. Fridez, S. Schaer: “Bernese GPS Software Version 5.0”, Druckerei der Universität Bern, Switzerland, 2005.

Satellite Laser Ranging in the National (Australian) Collaborative Research Infrastructure Proposal for Geospatial R&D

Kurt Lambeck[1]

1. The Australian National University, Canberra, Australia

The presentation is at:

http://www.ilrscanberraworkshop2006.com.au/workshop/day2/Monday1400.pdf

Time-variable gravity from SLR and DORIS tracking

Frank G. Lemoine[1], Steven M. Klosko[2], Christopher M. Cox [3], Thomas J. Johnson[4]

1. Planetary Geodynamics Laboratory, NASA Goddard Space Flight Center, Greenbelt, Maryland, USA
2. SGT, Inc., Greenbelt, Maryland, USA
3. Raytheon Integrated Defense Systems, Arlington, Virginia, USA
4. National Geospatial-Intelligence Agency, Reston, Virginia, U.S.A.

Abstract

One of the significant strengths of the tracking of satellites with satellite laser ranging (SLR) is the long time base of data available. This has been exploited to provide us with monthly snapshots of the variations of the low-degree field from approximately 1980 to the present. The analysis of these data by Cox and Chao [2002] revealed an anomaly in the zonal rate for J_2. Cox and Chao [2002] clearly indicated that the contributions to this zonal rate from the cryosphere and surface hydrology, such as glacier melt and ground water storage, are just as important as post-glacial rebound. In this paper, we extend the time series of low degree variations through 2006, describing the satellite data incorporated into the solutions, the method of analysis, and the satellite performance. We compare the SLR/DORIS recovered low-degree variations with those derived from GRACE from 2003 to 2005, through degree four, and investigate the climatological and geophysical connections revealed by the new time series.

Introduction

Although GRACE provides us with a valuable source of high-resolution data for assessment of surface mass transport, the analysis of SLR and DORIS tracking data to low Earth orbiting satellites still provides valuable information. Intercomparison of the GRACE and independent SLR & DORIS results can provide a validation of the GRACE results where the data overlap after launch of GRACE, and an improvement in the quality of the time series through improvements in the dynamic modeling, for example through usage of the GRACE-derived geopotential. In this manner, the joint analysis of GRACE and the SLR and DORIS tracking data can help to leverage these data into the pre-GRACE era. In this manner we can obtain a snapshot of surface mass transport on the Earth over the past 25 years.

Data and Processing

The gravity solutions are based on data to nine satellites: Lageos 1 & 2, Starlette, Stella, Ajisai, Westpac, GFZ-1, TOPEX/Poseidon, and BE-C. The temporal coverage of the tracking data is depicted in Figure 1. For most of the 1980's, only three satellites are available. From the 1990's onward, between six and nine satellites are used, including the SLR & DORIS tracking data to TOPEX/Poseidon.

The modeling applied the ITRF2000 reference frame [*Altamimi et al.*, 2002] with corrections for certain stations, derived principally by the TOPEX/POD team (N. Zelensky, NASA GSFC, personal communications). The GGM01C GRACE-derived gravity model was used [*Tapley et al.*, 2004]. The IERS2003 solid Earth tides were applied including anelasticity [*McCarthy and Petit*, 2004]. The GOT00.2 T/P-derived ocean tide model was applied [*Ray*, 1999]. The atmospheric gravity was forward modeled using atmospheric pressure data from NCEP to 20x20, with an inverse

barometer correction assumed over the oceans. The observed annual gravity terms to 4x4 were forward modeled a priori, based on a previous SLR time series solution. After 1992, the daily arcs are 10 days in length, and constructed to be commensurate with the start and stop times of the near-ten day ground track cycle of TOPEX/Poseidon. Prior to 1992, the arc length was 30 days for Lageos-1, and 15-days for Starlette and Ajisai. For all the arcs, global station biases are adjusted for the SLR data. The gravity solutions consisted of a 30x30 static field, a 6x6 field for the secular rates of the geopotential, annual and semi-annual terms to 4x4, and a 4x4 monthly time series.

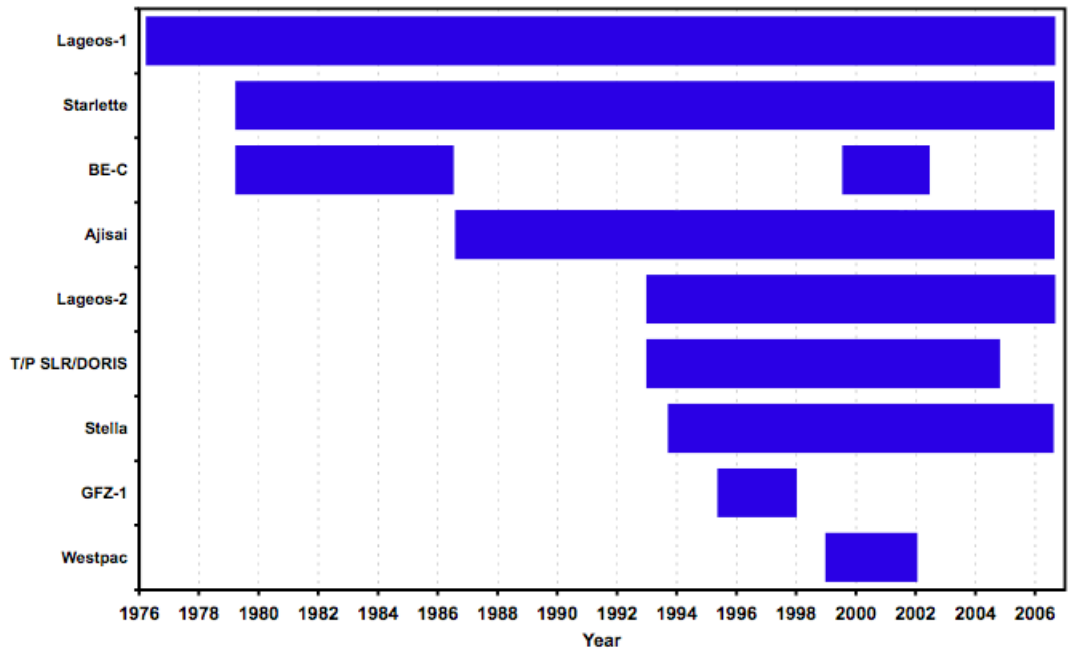

Figure 1. *Temporal coverage of SLR and DORIS tracking data used in the monthly gravity solutions, the solutions for the annual and semi-annual harmonics and the solutions for the secular rates.*

Analysis of the J_2 signal

The full time series is depicted in Figure 2, with respect to the GGM01C. The 1998 J_2 (- C_{20}) anomaly discussed in *Cox and Chao* [2002], appears as an inter-annual variation. The slope in J_2 obtained from 1980 to 1997 of 1.34 x 10^{-11}/year is similar to the post 1997 slope of 1.36 x 10^{-11}/year. It now appears, especially after the application of an annual filter, that a similar interannual variation was observed in 1987-1988. The J_2 time series is visibly much noisier before 1983. The addition of Starlette to the solution, especially after 1983, acts to stabilize the solutions for J_2 and the other low degree harmonics. An additional consideration is that the strength of the network and the quality of the data for 1983 and later is far superior to the pre-1983 SLR data. For reference, we note that a ± 1 x 10^{-10} in J_2 corresponds to a ± 2 mm change for the geoid in a zonal sense from pole to equator.

In Figure 3 we compare the C_{20} time series for GRACE, and from the SLR & DORIS solutions from 2002 to 2006. We show the comparisons for the CSR Release 01 fields (constrained and unconstrained), the NASA GSFC GRACE solutions based solely on GRACE K Band Range-Rate data (KBRR) from *Luthcke et al.* [2006[, and the corresponding SLR & DORIS solution. The unconstrained CSR release 01 (RL01)

C_{20} data have the worst agreement, especially around the period in late 2004 when GRACE entered a deep resonance driven by a close ground track repeat. The solutions lightly constrained by a Kaula constraint are smoother in their performance. The C_{20} from the NASA GSFC spherical harmonic time series is smoother, but still does not have good agreement with the SLR & DORIS solution. We conclude that the GRACE spacecraft are not a good sensor of this very long wavelength harmonic.

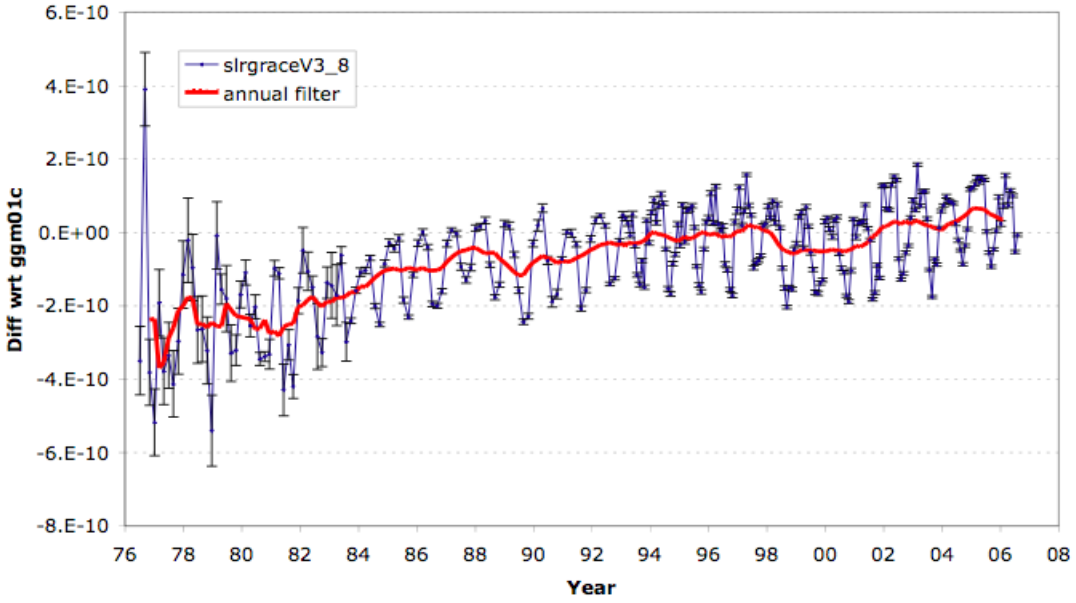

Figure 2. *Monthly J2 solutions from SLR and DORIS tracking from 1976 through 2006. The solutions are shown w.r.t. the GGM01C solution, and with the application of an annual filter (red line).*

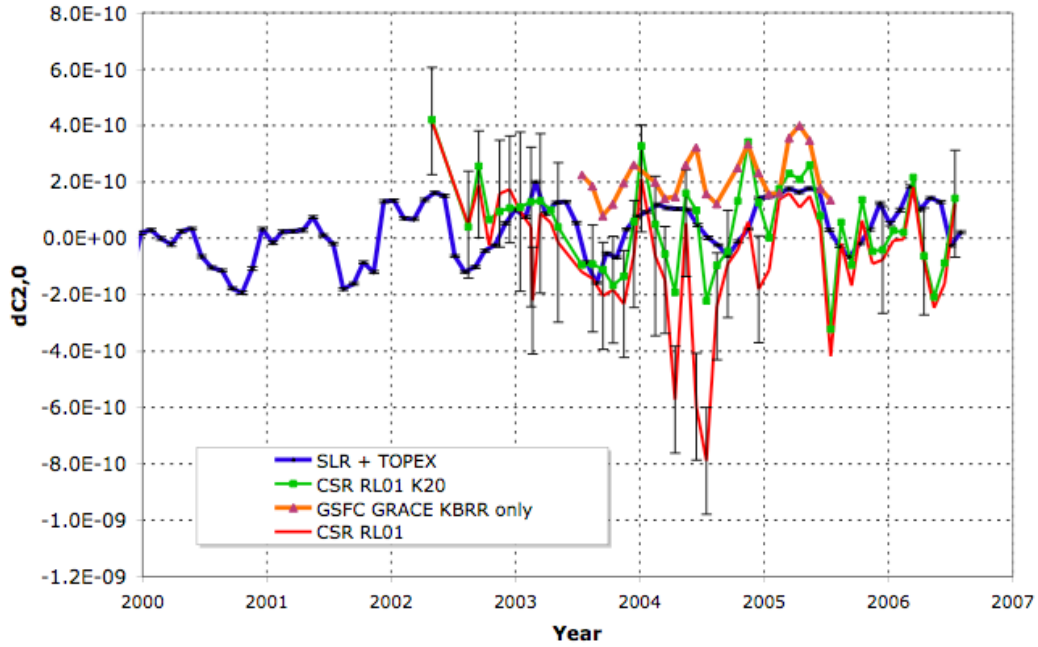

Figure 3. *Comparison of solutions for C_{20} from the SLR and DORIS solutions, and from GRACE.*

Comparison of Other Low Degree Harmonics

The SLR and DORIS monthly time series is compared to the GRACE solutions in Figure 4 for the other low degree harmonics (C_{21}, S_{21}, C_{22}, S_{22}, C_{30} and C_{40}). For C_{21} and S_{22}, the agreement is exceptionally good; For S_{21} and C_{22} there is some agreement on the amplitude of the variation, but the phases really do not match. For C_{30} we obtain the interesting result that the time series for the two GRACE solutions (CSR RL01, and NASA GSFC, KBRR-only) agree perfectly. The SLR and DORIS time series matches more closely the GRACE C_{30} + C_{50} solutions, suggesting that for the C_{30} harmonic, what the SLR and DORIS time series discerns is really a lumped harmonic. In contrast for the C_{40} harmonic, the GRACE solutions completely fail to discern the variations that are visible in the SLR and DORIS time series. We conclude that for C_{40}, just as for C_{20}, the GRACE spacecraft are simply not good sensors of this harmonic.

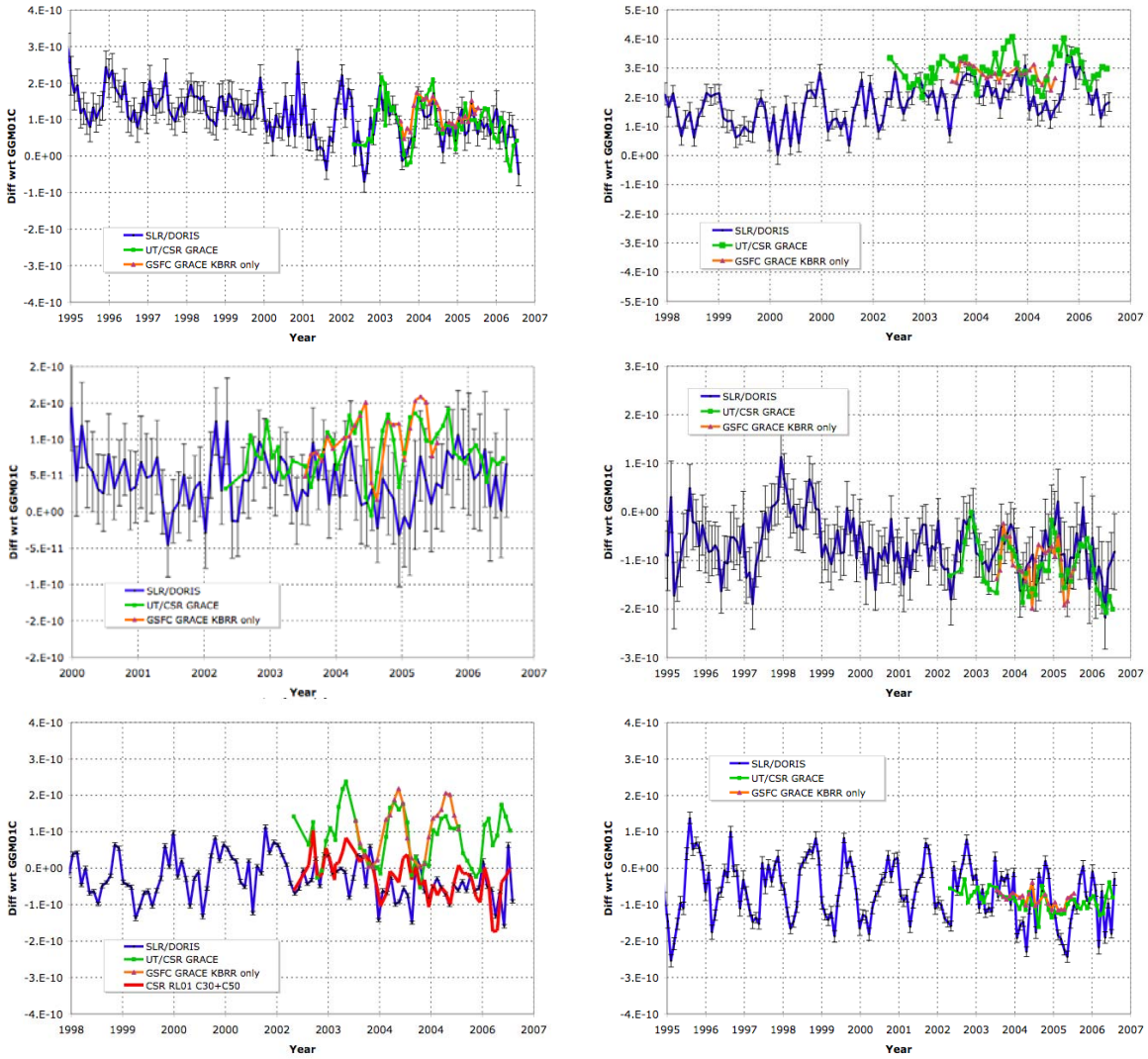

Figure 4. *Comparison time series for the low-degree harmonics between GRACE and the SLR and DORIS solutions (C_{21}, S_{21}; C_{22}, S_{22}; C_{30}, C_{40}). We show the formal errors for the SLR/DORIS solutions. The agreement is exceptionally good for the C21 and S22 harmonics. For the two GRACE solutions tested, the variations in the C40 harmonic cannot be properly resolved.*

Recovery of Annual and Semiannual Harmonics

We are able to use the entire time series of SLR and DORIS data to recover the annual variations in the geopotential through degree six, and the semiannual variations through degree four. In Figure 5, the signal of the annual harmonics recovered from the CSR RL01 GRACE series, is compared to the signal recovered from the SLR & DORIS time series, and the formal uncertainties of the SLR and DORIS recovery. Thus, from this comparison of the degree variances, the SLR and DORIS data can recover signals between degrees five and six.

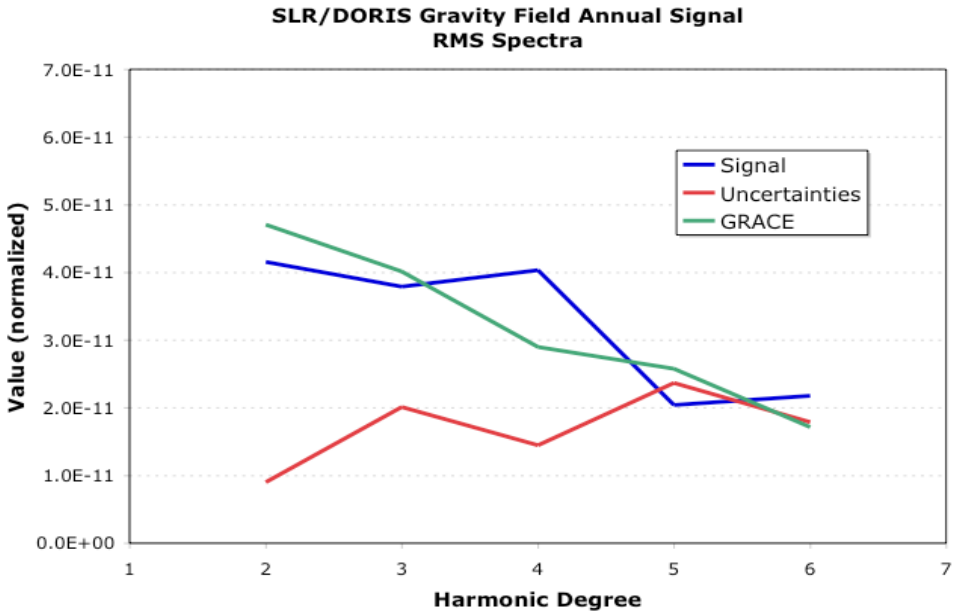

Figure 5. *Degree variances of the annual harmonics recovered from the SLR and DORIS data, and from the GRACE monthly solutions, compared to the formal uncertainties in the SLR/DORIS solutions. The SLR & DORIS time series can resolve the annual variations in the geopotential through degree five over a period of 25 years.*

The SLR/DORIS time series is sufficiently long that we can reliably recover annual and semiannual harmonics over different time scales. For example, if we compare the time-variable gravity variations for two SLR/DORIS solutions (1979-1997, and 1998-2005), we can observe for the most part overall similarities between the solutions. Both show the same patterns of geoid highs and geoid lows in the Amazon region, and Southeast Asia associated with the expected hydrology variations. If we compare the 1998-2005 SLR/DORIS solution to the annual and semiannual harmonics recovered from GRACE (in this case the CSR RL01), both observe the geoid highs in the Amazon in April and May, and the geoid lows in south east Asia and the Bay of Bengal. In addition, both data sets observe the same phase of the Southeast Asia monsoon with a prominent high in August and September over the Bay of Bengal, Bangladesh and the Indian subcontinent. The geoid low observed over the Amazon in November with the GRACE results is more prominent than with the SLR/DORIS observed variations.

Recovery of Secular Geoid Rates

The long time series of SLR and DORIS data allows to solve for secular rates in the geopotential, not just with the zonal harmonics, but for all coefficients through degree

six. The recovered geoid rates are illustrated in Figure 6 for the period from 1979 through 1997. In this figure, the general pattern of post-glacial rebound is observed over Antarctica, Greenland and the Arctic consistent with post-glacial rebound models. Globally the scale of the variations is ± 1 mm/year, with an error of 0.14 mm/year. Secular geoid changes occur in other regions, for example over the Indian subcontinent (+0.5 mm/yr). While we may ascribe the secular changes in the polar regions for the most part to changes in the solid Earth (cf. post-glacial rebound), in other regions, other considerations (long-term hydrology or ocean mass variations) may also play a role. If secular solutions are obtained on shorter time scales (five years) the solutions differ considerably, indicating that on those time scales, annual and inter-annual variations in the geopotential are more prominent than the secular variations.

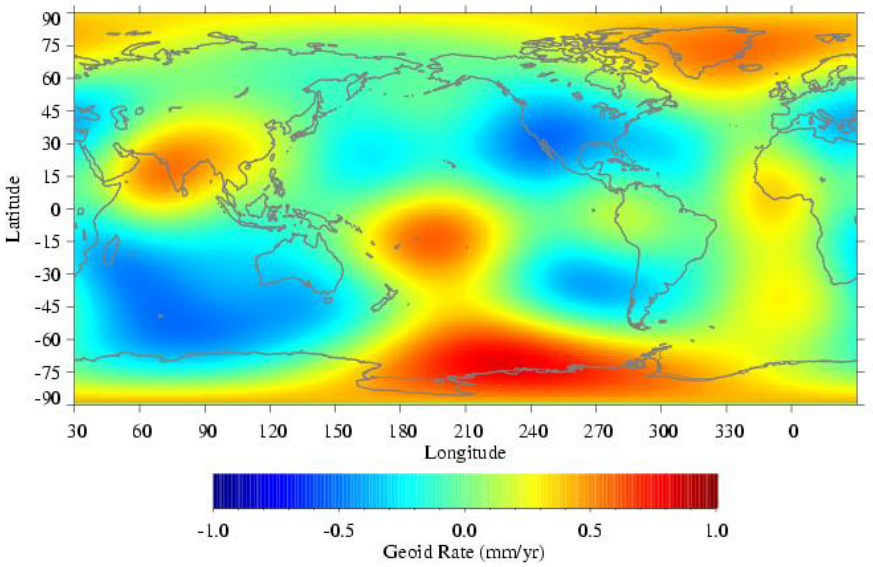

Figure 6*. Geoid rates observed from 1979 through 1997 from SLR and DORIS data. The global error is 0.14 mm/yr.*

Summary

The long time series of SLR and DORIS data allow us to resolve periodic time variations on the time scale of months, and secular variations over the period of many years. These data allow us a window into geophysical mass flux variability over a period prior to the launch of GRACE. We discern that that 1998 C_{20} anomaly was in fact an interannual variation, and that similar variations are observable over the course of the 25-year time series. The GRACE solutions for the low degree even zonals do not agree with those obtained from SLR and DORIS data, although in an overall sense the annual variations observed are similar. The SLR and DORIS data have sufficient strength to resolve secular changes in the geopotential through degree 6 corresponding to a spatial scale of 3300 km.

Acknowledgements

The authors acknowledge the ILRS [*Pearlman et al.*, 2002] and the IDS [*Tavernier et al., 2006*] for making the SLR and DORIS data available for this study as well as for overseeing the networks and the stations responsible for providing the data. Jennifer

Wiser Beal1 (Raytheon Corp, Upper Marlboro, MD) performed most of the GEODYN processing for the SLR and DORIS solutions.

References

[1] Altamimi Z., P. Sillard, and C. Boucher, ITRF2000: A new release of the International Terrestrial Reference Frame for earth science applications, *J. Geophys. Res., 107(B10),* 2214, doi:10.1029/2001JB000561.

[2] Cox, C.M., and B.F. Chao, Detection of a large-scale mass redistribution in the terrestrial system since 1998, *Science, 297,* 831, Aug. 2., 2002.

[3] Luthcke, S.B., D.D. Rowlands, F. G. Lemoine, S.M. Klosko, D. Chinn, and J.J. McCarthy, Monthly spherical harmonic gravity field solutions determined from GRACE inter-satellite range-rate data alone, *Geophys. Res.Lett.,33,* L02402,

[4] doi:10.1029/2005GL024846.

[5] McCarthy, D.D., and G. Petit (Eds.), IERS Conventions, IERS Tech. Note, vol. 32, Verl. Des Bundesamts für Kartogr. Und Geod., Frankfurt am Main, Germany, 2003.

[6] Pearlman, M.R., J. Degnan, and J.M. Bosworth (2002), The International Laser Ranging Service (ILRS), *Adv. Space Research, 30,* 135-143, 2002.

[7] Ray, R.D., A global ocean tide model from TOPEX/Poseidon altimetry: GOT99.2, *NASA Technical Memo. 209478,* NASA Goddard Space Flight Center, 58 pp., 1999.

[8] Tapley, B.D., S. Bettadpur, M. Watkins, and C. Reigber, The gravity recovery and climate experiment: Mission overview and early results, *Geophys. Res. Lett., 31, L09607,* doi:10.1029/2004GL019920, 2004.

[9] Tavernier, G. et al., The International DORIS Service: Genesis and early achievements, *J. Geodesy, 80,* 403-417, doi:10.1007/S00190-006-0082-4, 2006.

Global Glacial Isostatic Adjustment: Target Fields for Space Geodesy

W.R. Peltier[1]

1. Department of Physics, University of Toronto, Toronto, Ontario, Canada M5S-1A7.

Contact: peltier@atmosp.physics.utoronto.ca

Abstract

A very detailed theory of the global process of glacial isostatic adjustment (GIA) is now available that is being employed to address a number of significant problems in both solid Earth geophysics and climate dynamics. A recent focus of the work in this area has been upon the impact of changes in the Earth's rotational state upon postglacial sea level history and the modern field of geoid height time dependence that is being measured by the GRACE dual satellite system that is now in space. Satellite laser ranging continues to play a critical role in the understanding of these processes. This paper summarizes recent progress in modelling the impact of the GIA process upon Earth's rotational state.

Introduction

The origins of highly significant anomalies in the Earth's rotational state, respectively the so-called non-tidal acceleration of the rate of axial rotation and the secular drift (true polar wander) of the pole of rotation relative to the surface geography, have been associated for some time with the influence of the glacial isostatic adjustment (GIA) process. The non-tidal acceleration is equivalent to a value for the time dependence of the degree 2 zonal coefficient in the spherical harmonic expansion of Earth's gravitational field, commonly represented as $\dot{J}_2$ of (-2.67 ± 0.15) x 10^{-11} $year^{-1}$ (e.g. Cheng et al. 1989). The value for the rate of polar wander reported by Vincente and Yumi (1969, 1970) using the data of the International Latitude Service (ILS) was (0.95 ± 0.15) degree/million years, a value that is close to the most recent estimation by Argus and Gross (2004) of 1.06 degree/million years. The latter authors have suggested that the observed direction and speed of polar wander should be corrected for the influence of plate tectonic motions and that this could be a significant effect, depending upon the assumptions on the basis of which the correction is made (see Table 1 of Argus and Gross, 2004).

The development of theoretical explanations for the above discussed anomalies in Earth rotation has been dominated by work over the past two decades that has suggested a close connection of them both to GIA. The earliest discussion of the impact upon polar wander that should be expected due to time dependent surface loading of a visco-elastic model of the Earth was that of Munk and MacDonald (1960) who employed a simple homogeneous model to suggest that wander of the pole could only occur in response to simultaneous variability in the surface mass load. This point was obscured in the later papers by Nakiboglu and Lambeck (1980, 1981) and Sabadini and Peltier (1981) whose analysis was based upon the application of a homogeneous viscoelastic model similar to that employed by Munk and MacDonald (1960). These authors, however, suggested that polar wander would continue on a homogeneous visco-elastic model of the Earth even after all temporal variations of the surface mass load had ceased. This significant error of interpretation was corrected in Peltier (1982) and Wu and Peltier (1984) who showed that, in the case of cyclic loading and unloading, as is appropriate for the computation of the GIA

effect following the series of glacial loading and unloading events that have characterized the Late Quaternary period of Earth history (e.g. Broecker and van Donk, 1970), there would be no polar wander effected once the cycle ended. The homogeneous visco-elastic model of the planet would therefore exhibit no memory of the past history of loading and unloading as correctly pointed out by Munk and McDonald. This was traced to the fact that, specifically for the homogeneous visco-elastic model, there exists an exact annihilation of the polar wander forced by the internal redistribution of mass due to the free relaxation of Earth's shape and that forced by the deformation due to the changing rotation itself (see e.g. Figure 2 of Wu and Peltier 1984).

Based upon the prior analysis of Peltier (1974, 1976), however, it was known that realistic viscoelastic models of the planetary interior were significantly more complex then could be accommodated by the homogeneous visco-elastic model of Munk and MacDonald (1960). Whereas the relaxation under surface forcing of a homogeneous visco-elastic model of the Earth is described by a single relaxation time that is unique for each spherical harmonic degree in the deformation spectrum, realistically layered spherical visco-elastic models have a much more complex relaxation spectrum, a unique spectrum consisting of an (often essentially) finite number of modes for each spherical harmonic degree. In Peltier (1982) and Wu and Peltier (1984) it was demonstrated that this realistic level of complexity endowed the Earth model with a memory of its history of surface loading and unloading such that the pole of rotation would continue to wander even after the surface load had ceased to vary. Deep sea core oxygen isotopic data based upon $\delta^{18}0$ measurements on benthic foraminifera were employed as basis for the construction of a model of cyclic ice-sheet loading and unloading of the continents following the interpretation of such data as proxy for the variation of continental ice volume through time (Shackleton 1967, Shackleton and Opdyke 1973). Analysis based upon the application of rather crude models of the growth and decay of the Laurentide, Fennoscandian and Antarctic ice sheets then demonstrated that both the speed and direction of true polar wander as well as the non-tidal acceleration of rotation could be fit by the model and that the radial visco-elastic structure required to fit both of these observations was essentially the same. This was construed to strongly suggest that both anomalies might to be entirely explained as a consequence of the ongoing global process of glacial isostatic adjustment.

A recent objection to this interpretation was raised in the paper by Mitrovica, Wahr et al. (2005; hereafter MW) who have suggested that the theoretical formulation employed in Peltier (1982) and Wu and Peltier (1984) was mathematically "unstable" insofar as the computation of the polar wander component of the response to the GIA process is concerned. This objection appears to be based upon an error of mathematical comprehension as explicit analyses to be presented in what follows will demonstrate.

Computation of the rotational response of the Earth to the GIA process

The time dependent impact on the Earth's rotational state of the glacial isostatic adjustment process is determined as a solution of the classical Euler equation describing the conservation of angular momentum of a system subjected to no external torques, as:

$$\frac{d}{dt}(J_{ij}\,\omega_i) + \in_{ijk}\,\omega_j\,J_{k\ell}\,\omega_\ell = 0 \tag{1}$$

in which the J_{ij} are the elements of the moment of inertia tensor, the ω_i are as previously and $\in_{ijk}$ is the Levi-Civita (alternating) tensor. Restricting attention to small departures from the modern state of steady rotation with angular velocity Ω_o, we may construct a solution to (1), accurate to first order in perturbation theory, by expanding:

$$\omega_i = \Omega_o\,(\delta_{i3} + m_i)\,;\, m_i = \omega_i / \Omega_o \tag{2a}$$

$$J_{11} = A + I_{11} \tag{2b}$$

$$J_{22} = B + I_{22} \tag{2c}$$

$$J_{33} = C + I_{33} \tag{2d}$$

$$J_{ij} = I_{ij},\, i \neq j \tag{2e}$$

Substitution of these expansions into equation (1), keeping only terms of first order, leads to the standard set of governing equations for polar wander and the length of day, respectively (see Munk and McDonald, 1960), as:

$$\left.\begin{aligned} \frac{dm_1}{dt} + \frac{(C-B)}{A}\Omega_o\,m_2 &= \Psi_1 \\ \frac{dm_2}{dt} + \frac{(C-A)}{B}\Omega_o\,m_1 &= \Psi_2 \end{aligned}\right\} \text{ polar wander} \tag{3a,b}$$

$$\left.\frac{dm_3}{dt} = \Psi_3\right\} \text{ length of day} \tag{3c}$$

in which the "excitation functions" are defined as:

$$\Psi_1 = \left(\frac{\Omega_o}{A}\right) I_{23} - \frac{(dI_{13}/dt)}{A} \tag{4a}$$

$$\Psi_2 = -\left(\frac{\Omega_o}{B}\right) I_{13} - \frac{(dI_{23}/dt)}{B} \tag{4b}$$

$$\Psi_3 = -\left(\frac{I_{33}}{C}\right) \tag{4c}$$

Now it is critical to recognize that there exist perturbations Iij to the inertia tensor due to two distinct causes, namely due to the direct influence of change in the mass distribution of the planet that accompanies the change in planetary shape due to surface loading and unloading and that due to the additional deformation induced by the changing rotation triggered by the surface mass loading and unloading process. The contribution due to the former process may be represented as (e.g. Peltier, 1982):

$$I_{ij}^{GIA} = \left(1 + k_2^L(t)\right) * I_{ij}^R(t) \tag{5}$$

in which $k_2^L(t)$ is the surface mass load Love number of degree 2 and the I_{ij}^R are the perturbations of inertia that would obtain due to the variation in surface mass load if the Earth were rigid. The symbol * in equation (5) represents the convolution operation. The contribution to the perturbations of inertia due to the changing rotation

follows from an application of a linearized version of MacCullagh's formula (e.g. see Munk and MacDonald, 1960) as:

$$I_{13}^{ROT} = \left(\frac{k_2^T * a^5 \, \omega_1 \omega_3}{3G} \right) = \left(\frac{k_2^T}{k_f} \right) * m_1 \, (C - A) \tag{6a}$$

$$I_{23}^{ROT} = \left(\frac{k_2^T * a^5 \, \omega_2 \omega_3}{3G} \right) = \left(\frac{k_2^T}{k_f} \right) * m_2 \, (C - A) \tag{6b}$$

with

$$k_f = \left(\frac{3G}{a^5 \, \Omega_o^2} \right) (C - A) \tag{6c}$$

the value of which is determined entirely by the observed flattening of the Earth's figure. Assuming the validity of the data in Yoder (1995) as listed on the web site: (www.agu.org/references/geophys/4_Yoder.pdf), one obtains the value $k_f \cong 0.9414$, a value that deviates somewhat from the value of 0.9382 employed in MW.

The General Solution for the Rotational Response in the Laplace Transform Domain

Since the solution of equation (3c) for the change in the axial rate of rotation is uncomplicated, it will suffice to focus first in what follows on the solution of (3a) and (3b) for the polar wander component of the response to surface loading. Substitution of (6a) and (6b) into (3a,b), the Laplace-transformed forms of the equations that follow are simply:

$$s \, m_1 + \sigma \left(1 - \frac{k_2^T(s)}{k_f} \right) m_2 = \Psi_1(s) \tag{7a}$$

$$s \, m_2 + \sigma \left(1 - \frac{k_2^T(s)}{k_f} \right) m_1 = \Psi_2(s) \tag{7b}$$

where

$$\sigma = \Omega_o \frac{(C - A)}{A} \tag{7c}$$

is the Chandler Wobble frequency of the rigid Earth, "s" is the Laplace transform variable, and again A=B has been assumed. The Laplace-transformed forms of the excitation functions in (4a) and (4b) are simply:

$$\Psi_1(s) = \left(\frac{\Omega_O}{A} \right) I_{23}(s) - \left(\frac{s}{A} \right) I_{13}(s) \tag{8a}$$

$$\Psi_2(s) = \left(\frac{\Omega_O}{A} \right) I_{13}(s) - \left(\frac{s}{A} \right) I_{23}(s) \tag{8b}$$

with

$$I_{ij}(s) = \left(1 + k_2^L(s) \right) I_{ij}^{Rigid}(s) \tag{8c}$$

Now equations (7a) and (7b) are elementary algebraic equations for $m_1(s)$ and $m_2(s)$ and these may be solved exactly to write:

$$m_1(s) = \left[\frac{1 + k_2^L(s)}{s^2 + \sigma^2 \left(1 + \frac{k_2^T(s)}{k_f} \right)^2} \right] \left[\left(\frac{\Omega_o \sigma}{A} \right) \left(1 - \frac{k_2^T(s)}{k_f} \right) - \frac{s^2}{A} \right] I_{13}^{Rigid}(s) \quad (9a)$$

$$m_2(s) = \left[\frac{1 + k_2^L(s)}{s^2 + \sigma^2 \left(1 + \frac{k_2^T(s)}{k_f} \right)^2} \right] \left[\left(\frac{\Omega_o \sigma}{A} \right) \left(1 - \frac{k_2^T(s)}{k_f} \right) - \frac{s^2}{A} \right] I_{23}^{Rigid}(s) \quad (9b)$$

If we now neglect terms of order s^2/σ^2 in (9a,b), which delivers a highly accurate approximation free of the influence of the Chandler wobble, we obtain:

$$m_1(s) = \left(\frac{\Omega_o}{A\sigma} \right) \left[\frac{1 + k_2^L(s)}{1 - \frac{k_2^T(s)}{k_f}} \right] I_{13}^{Rigid}(s) = H(s)\, I_{13}^{Rigid}(s) \quad (10a)$$

$$m_2(s) = H(s)\, I_{23}^{Rigid}(s) \quad (10b)$$

A convenient short-hand form for the solution vector $(m_1, m_2) = \underline{m}$ is to write:

$$\underline{m}(s) = \frac{\underline{\Psi}^L(s)}{\left[1 - \frac{k_2^T(s)}{k_f} \right]} = H(s) \left(I_{13}^{Rigid}(s), I_{23}^{Rigid}(s) \right) \quad (11a)$$

where $$\underline{\Psi}^L(s) = \left[\left(\frac{\Omega_o}{A\sigma} \right) (1 + k_2^L(s) \left(I_{13}^{Rigid}(s), I_{23}^{Rigid}(s) \right) \right] \quad (11b)$$

An Exact Inversion of the Laplace Transform Domain Solution

From equations (11) it will be clear that the polar wander solution m(s) will depend critically upon the ratio $k_2^T(s)/k_f$. This fact was more fully exposed in the analysis of Peltier (1982) and Wu and Peltier (1984) who re-wrote the Laplace transform domain forms of $k_2^T(s)$ and $k_2^L(s)$ as (e.g. see equation 61 of Wu and Peltier 1984):

$$k_2^T(s) = k_2^T(s=0) - s \sum_{j=1}^{N} \frac{(q'_j / s_j)}{(s + s_j)} \quad (12a)$$

$$k_2^L(s) = (-1 + \ell_s) - s \sum_{j=1}^{N} \frac{(q_j / s_j)}{(s + s_j)} \quad (12b)$$

in which the superscript ℓ=2 on q_j^2, r_j^2, s_j^2 has been suppressed for convenience. Substituting (12a) into (11a) this may be re-written as:

$$\underline{m}(s) = \frac{\underline{\Psi}^L(s)}{\left[1 - \frac{k_2^T(s=0)}{k_f}\right] + \frac{s}{k_f}\sum_{j=1}^{N}\frac{(q'_j / s_j)}{(s+s_j)}} \qquad (13)$$

In their discussion of the formal inversion of (13) into the time domain, Peltier (1982) and Wu and Peltier (1984) made the approximation that the term in square brackets in the denominator of 13 could be safely neglected. In MW it is claimed that this renders the numerical structure employed to compute the time domain response unstable. This appears to be connected to a misunderstanding of the Tauberian Theorem (eg Widmer, 1983) which asserts that the infinite time limit of **m**(t) will be equal to the s->0 limit of the product s**m**(s). Clearly the approximation in which the square bracketed term in the denominator of (13) is neglected, in which case one is assuming that $k_2^T(s=0) = k_f$, the multiplication by "s" on the lhs of (13) cancels the "s" in the denominator of (13), thus rendering the infinite time limit of the approximate form of (13) entirely stable. In this brief paper my purpose is to

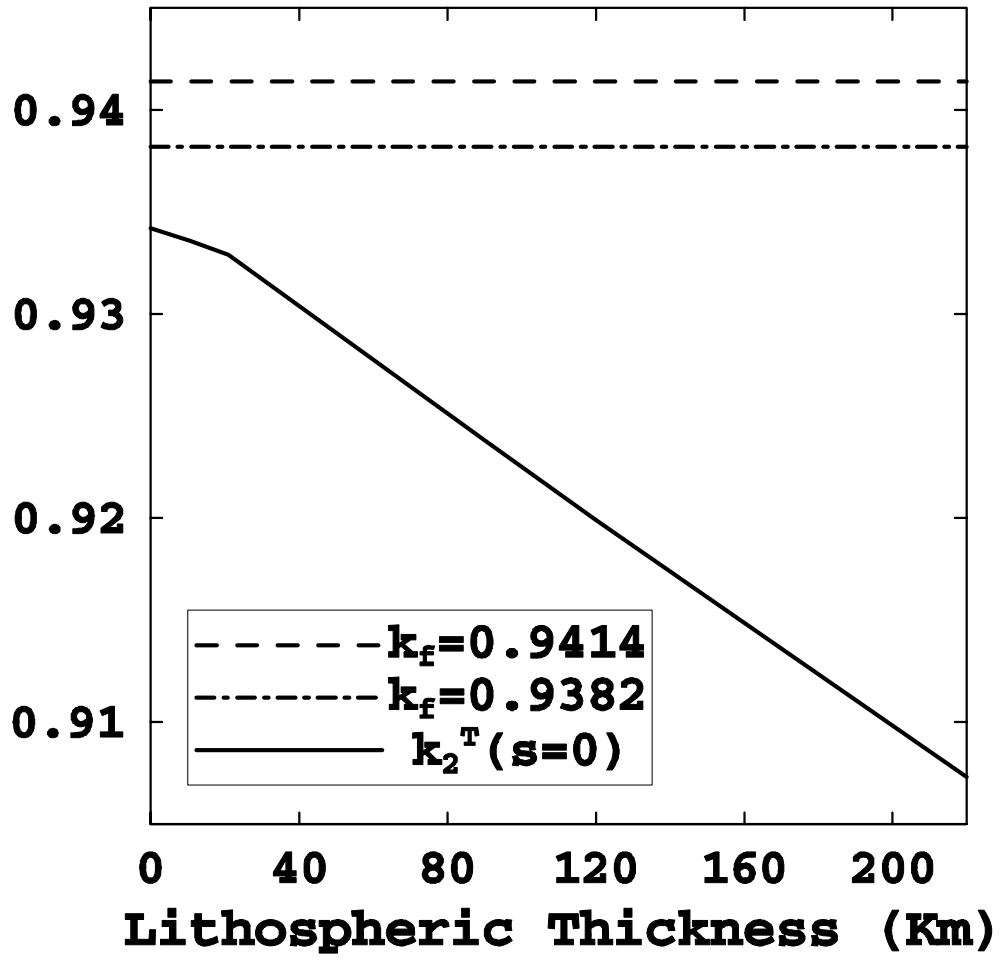

Figure 1. *Compares the value of the degree 2 "tidal Love number" in the limit of zero frequency (s=0) with the two estimates of the "fluid Love number" discussed in the text*

demonstrate this fact by computing exact solutions for the inverse of (13) without making the approximation involved in the neglect of the term in square brackets in the denominator of (13). It is nevertheless useful to start this process by showing explicitly that this term is small. This is demonstrated in Figure 1 where I show $k_2^T(s=0)$ as a function of lithospheric thickness "L". It will be clear by inspection of this Figure, on which the two previously cited values for k_f are also shown, that in the limit of zero lithospheric thickness the approximation made in the analyses of Peltier (1982) and Wu and Peltier (1984) becomes increasingly more valid. That the Earth might be expected to respond to the GIA process such that the flattening of its figure was accurately predictable by the infinite time limit of the first order linear visco-elastic field theory of Peltier (1974) is entirely expected. The fact that it is not "exactly" predictable by this field theory (see Figure 1) is also entirely expected because processes other than the basic rotation of the object, such as mantle convection, may also contribute to this flattening. To demonstrate the impact of the approximation previously made in constructing the solutions for the polar wander speed and direction caused by the GIA process we must invert the Laplace transform domain solution (13) exactly. This was not done in MW and this appears to have clouded their judgement as to what the impact might be.

When the assumption $k_2^T(s=0) = k_f$ is abandoned , the Laplace transform domain impulse response may then be written n the form:

$$H(s) = \left(\frac{\Omega_o}{A\sigma}\right) \frac{1 + k_2^L(s)}{\frac{s}{k_f}\sum_{j=1}^{N}\frac{(q_j/s_j)}{(s+s_j)} + \varepsilon} \tag{14a}$$

where

$$\varepsilon = 1 - \frac{k_2^T(s=0)}{k_f}. \tag{14b}$$

As will become clear, even though ε is a small quantity (especially in the case that the finite thickness of the lithosphere may be neglected in the limit $t \rightarrow \infty$), retaining it in expression (14a) for the impulse response could have a significant impact upon the solution as the rotational stability of the system would be modified. Now the construction of the solution for the time-domain form of the impulse response H(t) proceeds in this case as in the case based upon the Equivalent Earth Model assumption, although the result differs somewhat from a physical perspective. In this case it is useful to make the distinction between the Chandler wobble frequency of a rigid Earth σ and the Chandler wobble frequency of the visco-elastic Earth σo, by employing the definition:

$$\sigma_0 = \frac{\left(k_2^T(s=0) - k_2^{TE}\right)}{k_2^T(s=0)}\sigma. \tag{15}$$

We must then re-write the expression for H(s) as:

$$H(s) = \left(\frac{\Omega}{A\,\sigma_o}\right) \frac{\left(1 + k_2^L(s)\right)}{\left((1-\varepsilon)s\sum_{i=1}^{N}\frac{g_j}{s+s_j}\right) + \varepsilon'} \tag{16a}$$

with

$$\varepsilon' = \varepsilon \frac{\sigma}{\sigma_o}, \tag{16b}$$

and,

$$g_j = \frac{q'_j / s_j}{\sum_j (q'_j / s_j)}. \tag{16c}$$

The inversion of H(s) into the time domain now proceeds by expanding the sum in the denominator of (16a) in the form:

$$\sum_{j=}^{N} \frac{g_j}{(s+s_j)} = \frac{Q_{N-1}(s)}{\prod_{j=1}^{N}(s+s_j)} = \frac{\prod_{j=1}^{N-1}(s+\lambda_j)}{\prod_{j=}^{N}(s+s_j)} \tag{17}$$

since $\sum_j g_j \equiv 1$. Then we have, suppressing for the moment the factor (Ω_o / $A\sigma_o$),

$$H(s) = \frac{\prod_{j=1}^{N}(s+s_j)\left[1+k_2^L(s)\right]}{(1-\varepsilon)s\prod_{i=1}^{N-1}(s+\lambda_i) + \varepsilon'\prod_{j=1}^{N}(s+s_j)}. \tag{18}$$

Now substituting for the function $1 + k_2^L(s)$ from (12b) we obtain:

$$H(s) = \frac{\prod_{j=1}^{N}(s+s_j)\,\ell_s}{(1-\varepsilon)s\prod_{i=1}^{N-1}(s+\lambda_i) + \varepsilon'\prod_{i=1}^{N}(s+s_i)} + \sum_{j=1}^{N} \frac{(-q_j/s_j)s\prod_{i\neq j}^{N}(s+s_i)}{(1-\varepsilon)s\prod_{i=1}^{N-1}(s+\lambda_i) + \varepsilon'\prod_{i=1}^{N}(s+s_i)} \tag{19a}$$

$$= \frac{\prod_{j=1}^{N}(s+s_j)\,\ell_s}{(1-\varepsilon+\varepsilon')\prod_{i=1}^{N}(s+\kappa_i)} + \sum_{j=1}^{N} \frac{(-q_j/s_j)s\prod_{i\neq j}^{N}(s+s_j)}{(1-\varepsilon+\varepsilon')\prod_{i=1}^{N}(s+\kappa_i)}. \tag{19b}$$

Where now the κ_i are the N roots of the polynomial in the denominator of the 2 terms in (19a). This expression for the impulse response may be further reduced by re-writing the ratios of products as follows:

$$\frac{\prod_{j=1}^{N}(s+s_j)}{\prod_{j=1}^{N}(s+\kappa_i)} = 1 - \frac{q'(s)}{\prod_{i=1}^{N}(s+\kappa_i)} \tag{20a}$$

where now

$$q'(s) = \prod_{j=1}^{N}(s+\kappa_i) - \prod_{j=1}^{N}(s+s_j) \tag{20b}$$

and
$$\frac{s\prod_{i\neq j}^{N}(s+s_i)}{\prod_{j=1}^{N}(s+\kappa_i)} = 1 - \frac{R'_j(s)}{\prod_{i=1}^{N}(s+\kappa_i)} \tag{21a}$$

with
$$R'_j(s) = \prod_{i=1}^{N}(s+\kappa_i) - s\prod_{i\neq j}^{N}(s+s_i) \tag{21b}$$

We then have, for the Laplace transform of the impulse response, the expression:

$$H(s) = \frac{\ell_s}{(1-\varepsilon+\varepsilon')}\left\{1 - \frac{q'(s)}{\prod_{i=1}^{N}(s+\kappa_i)}\right\} + \frac{1}{(1-\varepsilon+\varepsilon')}\sum_{j=1}^{N}\left(-\frac{r_j}{s_j}\right)\left\{1 - \frac{R'_j(s)}{\prod_{i=1}^{N}(s+\kappa_i)}\right\} \tag{22a}$$

or

$$H(s) = \frac{\ell_s - \sum_{j=1}^{N} r_j/s_j}{(1-\varepsilon+\varepsilon')} - \frac{\ell_s\, q'(s)}{(1-\varepsilon+\varepsilon')\prod_{i=1}^{N}(s+\kappa_i)} + \frac{1}{(1-\varepsilon+\varepsilon')}\sum_{j=1}^{N}\frac{(q_j/s_j)\,R'_j(s)}{\prod_{i=1}^{N}(s+\kappa_i)} \tag{22b}$$

Denoting $\ell_s - \sum_{j=1}^{N} r_j/s_j = 1 + k_2^{LE} = D_1$, say, then we may further reduce the expression for the impulse response to:

$$H(s) = \frac{D_1}{(1-\varepsilon+\varepsilon')} - \frac{1}{(1-\varepsilon+\varepsilon')}\left\{\frac{\ell_s\, q'(s) - \sum_{j=1}^{N}(q_j/s_j)R'_j(s)}{\prod_{i=1}^{N}(s+\kappa_i)}\right\} \tag{23}$$

The inverse Laplace transform of this expression is such that the solution in the present case, in which $k_2^T(s=0) \neq k_f$, is just:

$$m_1(t) = \frac{1}{(1-\varepsilon+\varepsilon')}\left(\frac{\Omega_o}{A\sigma_o}\right)\left\{\left[\ell_s - \sum_{j=1}^{N}\frac{r_j}{s_j}\right] I_{13}^{Rigid}(t) + \sum_{i=1}^{N} E'_i\, e^{-\kappa_i t} * I_{13}^{Rigid}(t)\right\} \tag{24a}$$

$$m_2(t) = \frac{1}{(1-\varepsilon+\varepsilon')}\left(\frac{\Omega_o}{A\sigma_o}\right)\left\{\left[\ell_s - \sum_{j=1}^{N}\frac{r_j}{s_j}\right] I_{23}^{Rigid}(t) + \sum_{i=1}^{N} E'_i\, e^{-\kappa_i t} * I_{23}^{Rigid}(t)\right\} \tag{24b}$$

where

$$E'_i = \left\{-\ell_s\, q'(-\kappa_i) + \sum_{j=1}^{N}\frac{r_j}{s_j}R'_j(-\kappa_i)\right\} / \prod_{i=j}^{N}(\kappa_j - \kappa_i). \tag{24c}$$

The polar wander velocity vector components are obtained simply by time differentiation of equations (24a) and (24b). It is useful to compare the result in (24) to the solutions that obtain under the approximation previously employed. In the limit $\varepsilon \to o$ we have κN = 0 and κi = λi the N-1 relaxation times that govern the system in this limit. In this case, the parameter E'N in the above becomes:

$$E'_N = -\frac{\ell_1 \, q\,(o)}{\prod_{j=1}^{N-1} (\kappa_j - \kappa_N)} = -\frac{\ell_s \, q(o)}{\prod_{j=1}^{N-1} \lambda_i} \qquad (25)$$

And the previous approximate result is fully recovered.

In order to compare the temporal histories of the rotational anomalies in the two cases, it will be important to proceed by keeping as many features of the Earth model fixed as possible. To this end and for the remainder of this paper, I will focus entirely upon the nature of the solutions that obtain when the recently published ICE-5G model of the glaciation and deglaciation process of Peltier (2004) is employed to determine the rotational excitation functions required for the evaluation of the solution (24). In the next section results will be discussed for a sequence of simple two layered viscosity structures as a function of the parameter ε in order to explicitly demonstrate the highly stable nature of the solution in the limit that this parameter vanishes.

Results

Of particular importance for the purpose of this paper is the sensitivity of the predictions of polar wander speed to the assumption that $k_2^T(s=o)$ may be assumed to be equal to k_f. When this assumption is not made, then the solution is given by equation (24). In the latter, there appears the quantity (1- $\varepsilon+\varepsilon'$), the values in which for the Earth model (VM2) in question are respectively 0.034, 0.05, and 1.017 (for ε, ε' and $1-\varepsilon+\varepsilon'$) when the thickness of the lithosphere is taken to be 90 km. In Figure 2 (bottom) are plotted the predictions of polar wander speed based upon equations (24) as a function of the viscosity of the lower mantle with the upper mantle viscosity held fixed to the value in the VM2 model of Peltier (1996). Results are also shown for several different values of a parameter $\Delta = \varepsilon$ / 0.034 including the value ε = 0.034 (Δ = 1) which is appropriate for the VM2 model with a lithospheric thickness of 90 km, in which case $k_2^T(s=0)$= 0.9263, but also for significantly smaller values of ε including the value ε = 0 (Δ = 0) so as to investigate the "smoothness" of the transition from the value ε = 0 which obtains when k_2^T (s = 0) is assumed to be equal to k_f. The two intermediate values of Δ for which results are shown on Figure 2 correspond to the two values of k_f shown on Figure 1 when the lithospheric thickness L is assumed to be equal to zero. Also shown on Figure 2 (top) is the dependence of the predicted value of the non-tidal acceleration as a function of lower mantle viscosity.

Inspection of Figure 2 clearly demonstrates the fact that the solutions for polar wander speed that obtain in the limit $\Delta = 0$ are almost identical to those that obtain for either of the two non-zero values that correspond to zero lithospheric thickness. This demonstrates that the formulation of Peltier (1982) and Wu and Peltier (1984) based upon the approximation $k_2^T(s=0) = k_f$ was not mathematically unstable as claimed in WM. In fact, careful inspection of Figure 2 will show that the preferred solution for BOTH the non-tidal acceleration and polar wander speed is the model

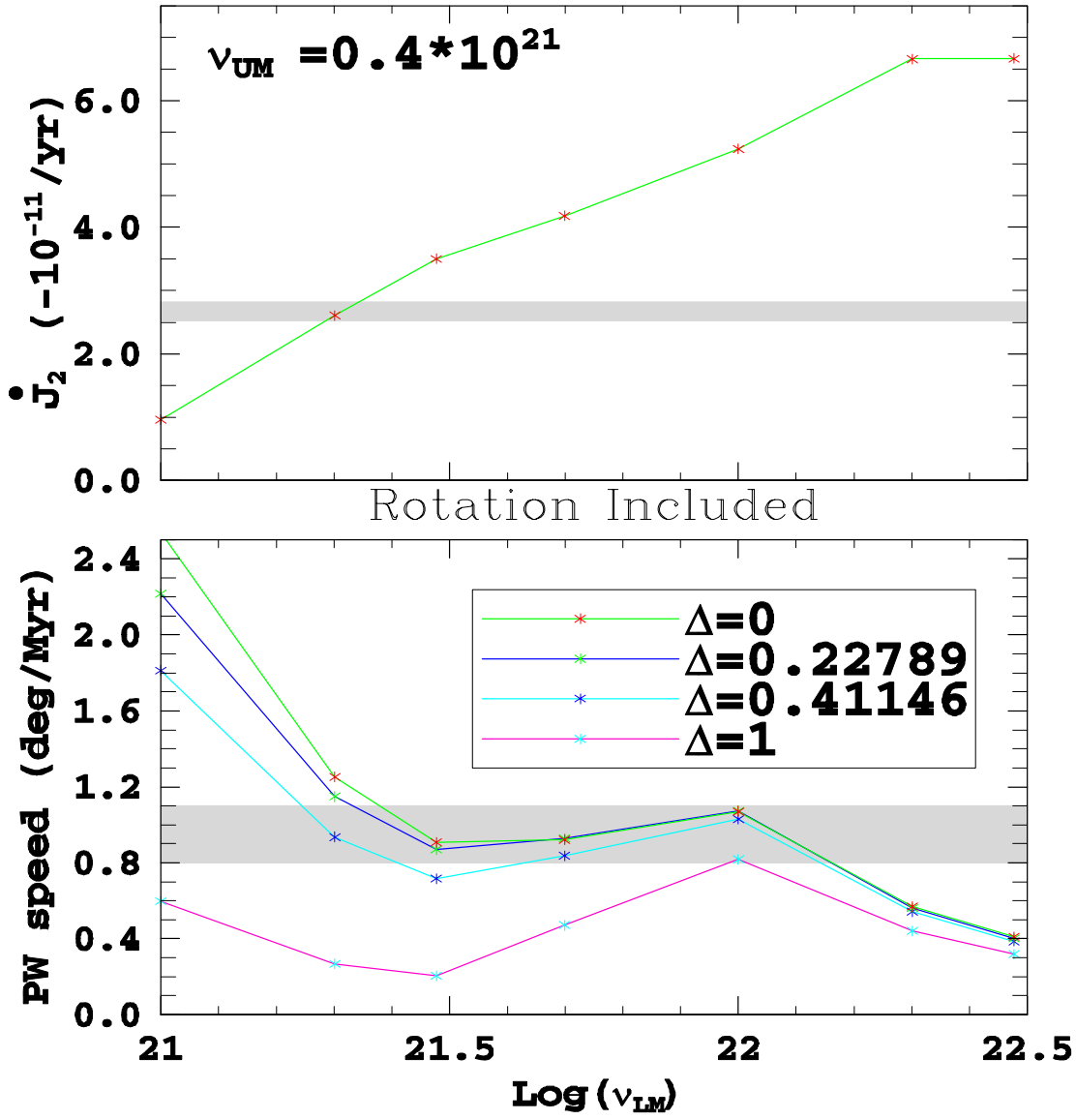

Figure 2. *This Figure compares model predictions of the non-tidal acceleration of rotation (top) and of the speed of polar wander (bottom) as a function of the viscosity of the lower mantle when the upper mantle viscosity is held fixed to the value in the VM2 viscosity model of Peltier (1996). The polar wander speed predictions are shown for several values of the parameter* Δ *which measures the importance of the difference between the fluid Love number* k_f *and* $k_2^T(s=0)$. *The two values of* Δ *that are less than unity, 0.22789 and 0.41146, correspond respectively to the* k_f *values of 0.9382 and 0.9414 and are those that obtain in the limit of vanishing lithospheric thickness. The value* $\Delta = 1$ *is the value appropriate for a finite lithospheric thickness of 90 km.*

with $\Delta = 0.41146$ AND L=0.0. This solution amounts to a very modest adjustment of the earlier result obtained with $\Delta = 0.0$ and L=0.0. The results for finite non-zero lithospheric thickness cannot fit the observed polar wander speed except, marginally, for a model with an upper mantle-lower mantle viscosity contrast that is incompatible with the observed non-tidal acceleration. Such high contrast viscosity models are also firmly rejected by relative sea level data from the previously ice covered area of North America.

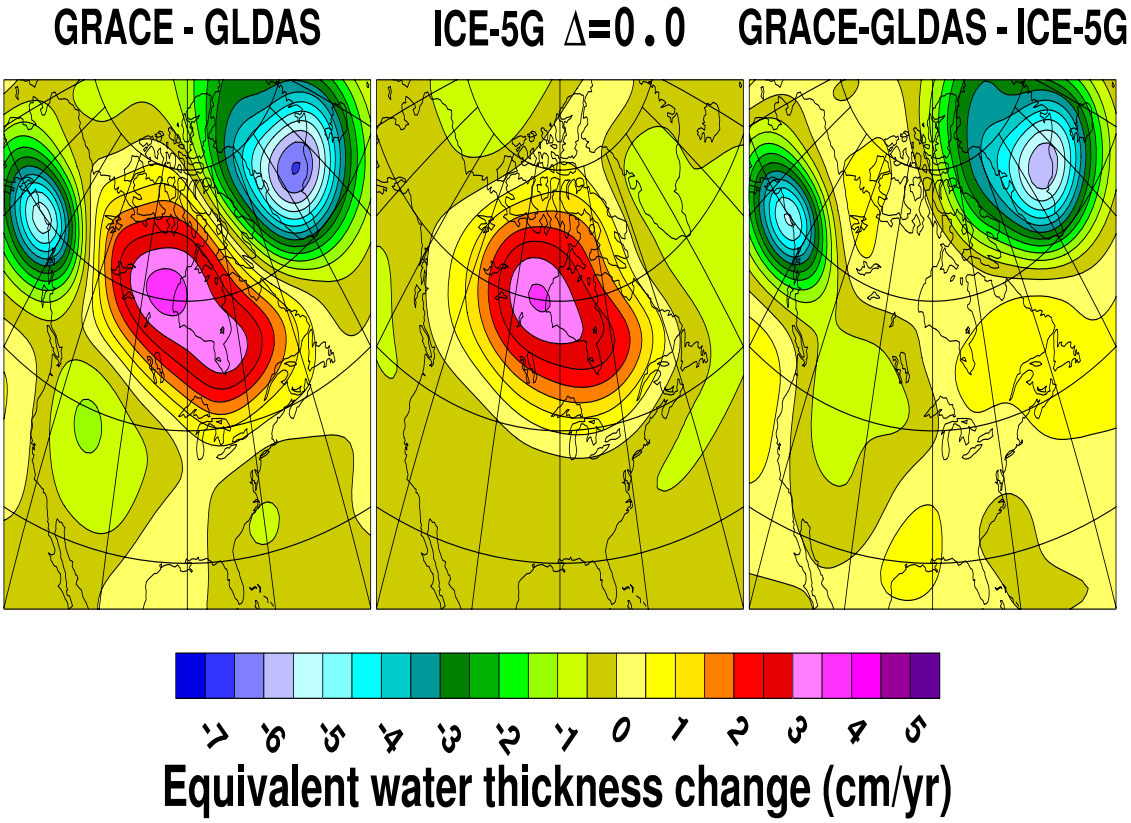

Figure 3. *Demonstrates the ability of the GIA model of Peltier(2004) to accurately explain the observed time dependence of the gravity field over the North American continent. This field is represented by the time rate of change of the thickness of an equivalent layer of water at the earth's surface. This analysis is based upon the level 2 release of the GRACE Stokes coefficients. In this comparison, the degree 2 terms have been excluded, a consequence of the fact that GRACE does not provide accurate measures of these coefficients.*

The quality of this low contrast model is also strongly re-enforced by the recently obtained time dependent gravity field data from the GRACE satellite system. Figure 3 compares the GRACE observed and hydrology corrected GRACE time dependent gravity field observations with the ICE-5G(VM2) GIA model prediction of the same field. In the third frame of Figure 3 the difference between these two data sets is also shown, thus demonstrating the extremely high quality of the ICE-5G(VM2) model. The neglect of the degree 2 coefficients, which are very large for the ICE-5G(VM2) model, as demonstrated in Peltier (2004), is required by virtue of the inability of GRACE to accurately observe these coefficients..

Conclusion

The analyses described in the previous sections of this paper have considerably extended the previously published theory that is employed to compute the response of

the earth's rotational state to the global process of glacial isostatic adjustment. These analyses suffice to refute the claim in MW that the formalism described in Peltier (1982) and Wu and Peltier (1984) was fundamentally unstable mathematically. This error of interpretation appears to have been due to a lack of understanding of the Tauberian Theorem that may be employed to predict the infinite time limit of a solution from the Laplace transform of this solution. The extended version of the theory described herein has allowed a direct investigation of the question of the extent to which the finite thickness of a globally continuous and unbroken lithosphere may contribute to the rotational response to surface mass load forcing. These analyses demonstrate that, in this long timescale limit, the most accurate representation of the rotational response of the Earth is that based upon the assumption of vanishing lithospheric thickness. This is understandable on the basis of the fact that the lithosphere of the planet is "broken" into a series of weakly coupled plates. For planets whose lithospheres are not unbroken in this way, the same assumption would clearly not be appropriate.

References

[1] Argus, D.F. & Gross, R.S. An estimate of motion between the spin axis and the hotspots over the past century. *Geophys. Res. Lett.* **31**, L06614, doi:10.1029/2004GL019657,2004

[2] Broecker, W.S. & Van Donk, J. Insolation changes, ice volumes, and the $\delta^{18}0$ record in deep sea cores. *Geophys. Space Phys.* **8**, 169-198, 1970.

[3] Cheng, Mik, Eanes, R.J., Shum, C.K., Schutz, B.E. & Tapley, B.D. Temporal variations in low degree zonal harmonics from Starlette orbit analysis. *Geophys. Res. Lett.* **16**, 393-396, 1989.

[4] Clark, J.A., Farrell, W.E. & Peltier, W.R. Global changes in postglacial sea levels: A numerical calculation. *Quat. Res.* **9**, 265-287, 1978.

[5] Dahlen, F.A. The passive influence of the oceans upon the rotation of the Earth. *Geophys. J.R. Astron. Soc.* **46**, 663-406, 1976.

[6] Domack, E., Duran, D., Leventer, A., Ishman, S., Doane, S., McCullum, S., Amblas, D. Ring, J. Gilbert, R. & Prentice, M. Stability of the Larsen B ice shelf on the Antarctic Peninsula during the Holocene epoch. *Nature* **436**, 681-685, 2005.

[7] Dziewonski, A.M. & Anderson, D.L. Preliminary reference Earth model. *Phys. Earth Planet. Int.* **25**, 297-356, 1981.

[8] Farrell, W.E. Deformation of the Earth by surface loads. *Rev. Geophys.* **10**, 761-797, 1972.

[9] Farrell, W.E. & Clark, J.A. On postglacial sea level. *Geophys. J.R. Astron. Soc.* **46**, 647-667, 1976.

[10] Imbrie, J., Hays, J.D., Martinsen, D.G., McIntyre, A., Mix, A.C., Morley, J.J., Pisias, N.G., Prell, W.L. & Shackleton, N.J. The orbit theory of Pleistocene climate: Support from a revised chronology of the marine $\delta^{18}0$ record in Milankovitch and Climate, edited by A. Berger et al., pp. 269-306. D. Reidel, Norwell, Mass., 1984.

[11] Lambeck, K. & Chappell, J. Sea level change through the last glacial cycle. *Science* **292**(5517), 679-686, 2001.

[12] Mitrovica, J.X., Wahr, J., Matsuyama, I. & Paulson, A. The rotational stability of an ice-age Earth. *Geophys. J. Int.* **161**, 491-506, 2005.

[13] Nakiboglu, S.M. & Lambeck, K. Deglaciation effects on the rotation of the Earth. *Geophys. J.R. Astron. Sco.* **62**, 49-58, 1980.

[14] Nakiboglu, S.M. & Lambeck, K. Deglaciation related features of the Earth's gravity field. *Tectonophysics* **72**, 289-303, 1981.

[15] Peltier, W.R. The impulse response of a Maxwell Earth. *Rev. Geophys. Space Physics.* **12**, 649-669, 1974.

[16] Peltier, W.R. Glacial isostatic adjustment, II: The inverse problem. *Geophys. J. Roy. Astron. Soc.* **46**, 669-706, 1976.

[17] Peltier, W.R. Dynamics of the ice-age Earth. *Advances in Geophysics*, **24**, 1-146, 1982.

[18] Peltier, W.R. The LAGEOS constraint on deep mantle viscosity: Results from a new normal mode method for the inversion of visco-elastic relaxation spectra. *J. Geophys. Res.* **90**, 9411-9421, 1985.

[19] Peltier, W.R. Ice-age paleotopography. *Science* **265**, 195-201, 1994.

[20] Peltier, W.R. Mantle viscosity and ice-age ice-sheet topography. *Science* **273**, 1359-1364, 1976.

[21] Peltier, W.R. Postglacial variations in the level of the sea: implications for climate dynamics and solid-Earth geophysics. *Rev. Geophys.* **36**, 603-689, 1998.

[22] Peltier, W.R. Comments on the paper of Yokoyama et al. (2000) entitled "Timing of the last glacial maximum from observed sea level minima" *Quat. Sci. Rev.* **21**, 409-414, 2002a.

[23] Peltier, W.R. One eustatic sea level history, Last Glacial Maximum to Holocene. *Quat. Sci. Rev.* **21**, 377-396, 2002b.

[24] Peltier, W.R. Global glacial isostatic adjustment: paleo-geodetic and space-geodetic tests of the ICE-4G (VM2) model. *J. Quat. Sci.* **17**, 491-510, 2002c.

[25] Peltier, W.R. On the hemispheric origins of meltwater pulse 1a. *Quat. Sci. Rev.* **24**, 1655-1671, 2005.

[26] Peltier, W.R., Farrell, W.E., & Clark, J.A. Glacial isostatsy and relative sea-level: a global finite element model. *Tectonophysics*, **50**, 81-110, 1978.

[27] Peltier, W.R. & Jiang, X. Glacial isostatic adjustment and Earth rotation: Refined constraints on the viscosity of the deepest mantle. *J. Geophys. Res.* **101**, 3269-3290, 1996 (Correction, *J. Geophys. Res.* **102**, 10,101-10,103, 1997).

[28] Peltier, W.R., Shennan, I., Drummond, R. & Horton, B. On the postglacial isostatic adjustment of the British Isles and the shallow visco-elastic structure of the Earth. *Geophys. J. Int.*, **148**, 443-475, 2002.

[29] Peltier, W.R. & Fairbanks, R.G. Global glacial ice-volume and Last Glacial Maximum duration from an extended Barbados Sea Level record. *Quat. Sci. Rev.*, 2006.

[30] Sabadini, R. & Peltier, W.R. Pleistocene deglaciation and the Earth's rotation: implications for mantle viscosity. *Geophys. J. Roy. Astron. Soc.* **66**, 553-578, 1981.

[31] Stephenson, E.R. & Morrison, L.V. Long term fluctuations in the Earth's rotation: 700 B.C. to A.D. 1990. *Philos. Trans. R. Soc. London, Serc. A*, **351**, 165-202, 1995.

[32] Shackleton, N.J. Oxygen isotope analysis and Pleistocene temperatures re-addressed. *Nature* **215**, 15-17, 1967.

[33] Shackleton, N.J. & Opdyke, N.D. Oxygen isotope and paleomagnetic stratigraphy of equatorial Pacific core V28-238: Oxygen isotope temperatures and ice volumes on a 10^5-year time scale. *Quaternary Res.* **3**, 39-55, 1973.

[34] Vincente, R.O. & Yumi, S. Co-ordinates of the pole (1899-1968) returned to the conventional international origin. *Publ. Int. Latit. Obs. Mizusawa* **7**, 41-50, 1969.

[35] Vincente, R.O. & Yumi, S. Revised values (1941-1961) of the co-ordinates of the pole referred to the CIO. *Publ. Int. Latit. Obs. Mizusawa* **7**, 109-112, 1970.

[36] Waelbroecke, C., Labyrie, L., Michel, E., Duplessy, J.-C. McManus, J.F., Lambeck, K., Balbon, E. & Labracherie, M. Sea-level and deep water temperature changes derived from benthic foraminifera isotopic records. *Quat. Sci. Rev.* **21**, (1-3), 295-305, 2002.

[37] Wu, P. & Peltier, W.R. Pleistocene deglaciation and the Earth's rotation: A new analysis. *Geophys. J.R. astr. Soc.* **76**, 202-242, 1984.

[38] Yoder, C.F., Williams, J.G., Dickey, J.O., Schutz, B.E., Eanes, R.J. & Tapley, B.D. Secular variation of the Earth's gravitational harmonic J_2 coefficient from LAGEOS and non-tidal acceleration of Earth rotation. *Nature* **303**, 757-762, 1983.

[39] Yoder, C.F., 1995. www.agu.org/references/geophys/4_Yoder.pdf

[40] Yokoyama, Y., Lambeck, K., DeDekkar, P., Johnston, P. & Fifield, L.K Timing of the Last Glacial Maximum from observed sea level minima. *Nature* **406**, 713-716, 2000. (Correction, 2001, *Nature* **412**, 99).

Recent Results from SLR Experiments in Fundamental Physics: Frame Dragging observed with Satellite Laser Ranging.

E. C. Pavlis[1], I. Ciufolini[2], R. König[3]

1. Joint Center for Earth Systems Technology (JCET), UMBC, Baltimore, MD, USA.
2. Università degli Studi di Lecce, Lecce, Italy
3. GeoForschungsZentrum (GFZ), Potsdam, Germany.

Contact: epavlis@JCET.umbc.edu / Fax: +1 410 455 5868

Abstract

Satellite laser ranging provided for decades the most precise measurement of positions and velocities of earthbound tracking stations, as well as the most precise orbits of earth-orbiting artificial satellites. While the latter applies to any satellite carrying the appropriate reflectors, the use of these orbits for precise geodetic products requires the use of specially designed target satellites in high altitude orbits, such as the two LAGEOS satellites. To achieve such high quality, the motion of these satellites must be described with equally accurate models, such as those made available recently, thanks to missions like CHAMP and GRACE. This led to the synergistic application of such precise products to devise tests of fundamental physics theories. Nearly twenty years after conceiving and proposing an initial concept for a General Relativity (GR) prediction test, our recent experiment resulted in a positive and convincing measurement of the Lense-Thirring effect, also known as the gravitomagnetic effect of the rotating Earth. Using state-of-the-art Earth gravitational field models based on data from the CHAMP and GRACE missions, we obtained an accurate measurement of the Lense–Thirring effect predicted by GR, analyzing eleven years of LAGEOS and LAGEOS 2 Satellite Laser Ranging (SLR) data. The new result, in agreement with the earlier one based on Earth models JGM-3 and EGM96, is far more accurate and more robust. The present analysis uses only the nodal rates of the two satellites, making NO use of the perigee rate, thus eliminating the dependence on this unreliable element. Using the EIGEN-GRACE02S model, we obtained our optimal result: $\mu = 0.99$ (vs. 1.0 in GR), with a total error between ± 0.05 and ± 0.1, i.e., between 5% and 10 % of the GR prediction. Results based on processing with NASA and GFZ s/w will be presented, along with preliminary tests with very recent improved GRACE models. Further improvement of the gravitational models in the near future will lead to even more accurate tests. We discuss the LAGEOS results and some of the crucial areas to be considered in designing the future LARES mission dedicated to this test.

Introduction

One of the most fascinating theoretical predictions of general relativity is “frame–dragging” (Misner et al. 1973, Ciufolini and Wheeler 1995), also known as the Lense-Thirring effect, after the two Austrian physicists who predicted the effect based on Einstein’s General Relitivity (GR) theory (Lense and Thirring, 1918). The equivalence principle, at the basis of Einstein’s gravitational theory, states that “locally”, in a sufficiently small spacetime neighbourhood, in a freely falling frame, the observed laws of physics are the laws of special relativity. However, the axes of these inertial frames where “locally” the gravitational field is “unobservable”, rotate with respect to “distant stars” due to the rotation of a mass or in general due to a

current of mass–energy. In general relativity the axes of a local inertial frame can be realized by small gyroscopes, as shown in Figure 1.

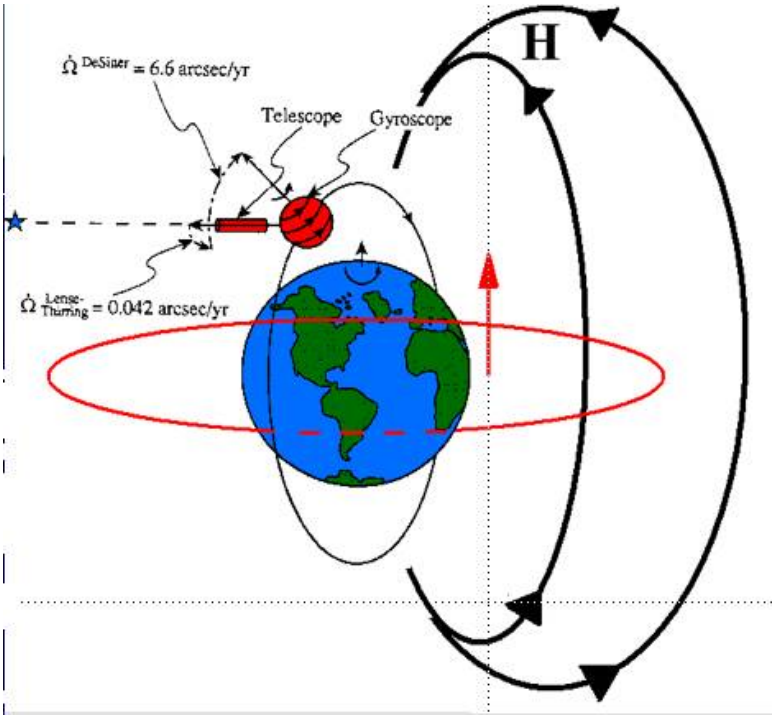

Figure 1. *The gravitomagnetic field and the mass-energy currents that produce the frame-dragging effect on the node of the orbiting gyroscope.*

Methodology

The gravitomagnetic force is by far smaller than the gravitational monopole, so we can use the tools of celestial mechanics and consider this force as a perturbation on an orbiting satellite. From the integrated (to first order) perturbation equations we obtain the most significant effects on the orbital elements, the secular rates of the node and perigee:

$$\begin{cases} \dot{\Omega}^{L-T} = \dfrac{2GJ}{c^2 a^3 (1-e^2)^{3/2}} \\ \dot{\omega}^{L-T} = \dfrac{-6GJ}{c^2 a^3 (1-e^2)^{3/2}} \cos I \end{cases}$$

In the past we used both quantities in our methodology (Ciufolini *et al.*, 1998) due to the lack of accurate enough gravitational models. Since the release of improved models from the CHAMP and GRACE missions though, we only use the node rate in our experiments. Our methodology uses as “source” of the field Earth with its angular momentum, as a test particle the geodetic satellites LAGEOS and LAGEOS 2 at present (and in the future LARES, see more on this later), and our basic observations are the two-way precise ranging with laser pulses from the ground network of the International Laser Ranging Service (ILRS), (Pearlman *et al.*, 2002).

Perturbations due to J_2 are much larger than the Lense-Thirring (LT) effect, so we need to be able to eliminate such uncertainties in order to extract the sought-for LT signal from our data. Thanks to Ciufolini's 1986 idea however, (using a "butterfly" configuration of counter-orbiting satellites in supplementary inclination orbits, Figure 2), the effect of J_2 uncertainties is cancelled.

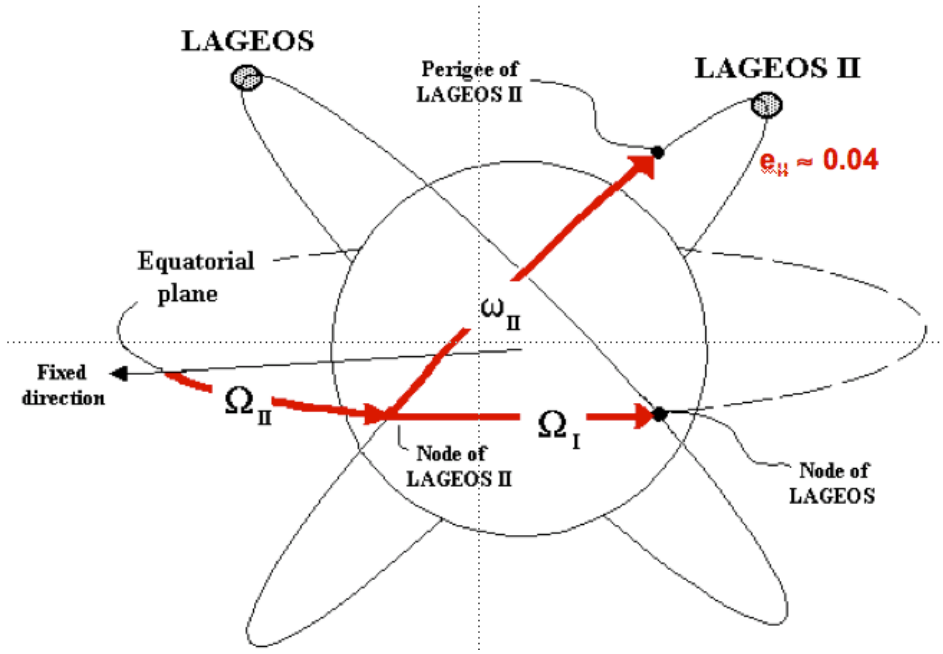

Figure 2*. The nearly-"butterfly" configuration of the retrograde LAGEOS (i = 109.8°) and the prograde LAGEOS 2 (i = 52.6°) orbits.*

When the two orbits are supplementary, one-half the sum of their nodal rate variations would provide a direct observation of the LT effect. However, Ciufolini (1989) generalized his original idea of the butterfly configuration to configurations of *N* nodes of various orbits, to cancel out the effects of the first *N-1* even zonals on the nodal rates of these orbits. Using this modified constraint for the case of two orbits in near- (but not exact) butterfly configuration, such as the LAGEOS and LAGEOS 2 orbits, we obtain:

$$\delta\dot{\Omega}_I + k\,\delta\dot{\Omega}_{II} = 48.2\mu + other\,errors \quad [mas/y]$$

where k ($\approx$ 1/2) is a function of the elements of the two orbits, and μ is our LT parameter to be determined. If μ = 1, GR is correct, if μ = 0 the Newtonian physics are correct. Under "*other errors*" we lump a number of higher order errors and the uncertainty in the background models mapped on the estimated quantity μ. Extensive error analysis of the experiment provides bounds on these errors and allows for a realistic error budget for the result (Ciufolini, Pavlis and Peron, 2006). We separate the error sources in two groups, the gravitational and the non-gravitational. A summary of the results published in detail in (*ibid.*) are given in Figures 3 and 4.

This study supports the errors quoted for our most recent published results for μ, (Ciufolini and Pavlis, 2004), between 5 and 10% of the expected value of 1 for GR. This improved (in accuracy) result compared to our 1998 result, is a direct consequence of the highly improved gravitational model accuracy, thanks to the use

of gravity mapping data from the CHAMP and GRACE missions (Reigber *et al.*, 2002, 2003, 2005 and Tapley *et al.*, 2002 and 2003). These products are the enabling factors for the success of these experiments. Pavlis (2002) and Ries *et al.* (2003) had already forewarned of this leap in accuracy for these models and proposed the continuation of the LAGEOS experiments in anticipation of their release.

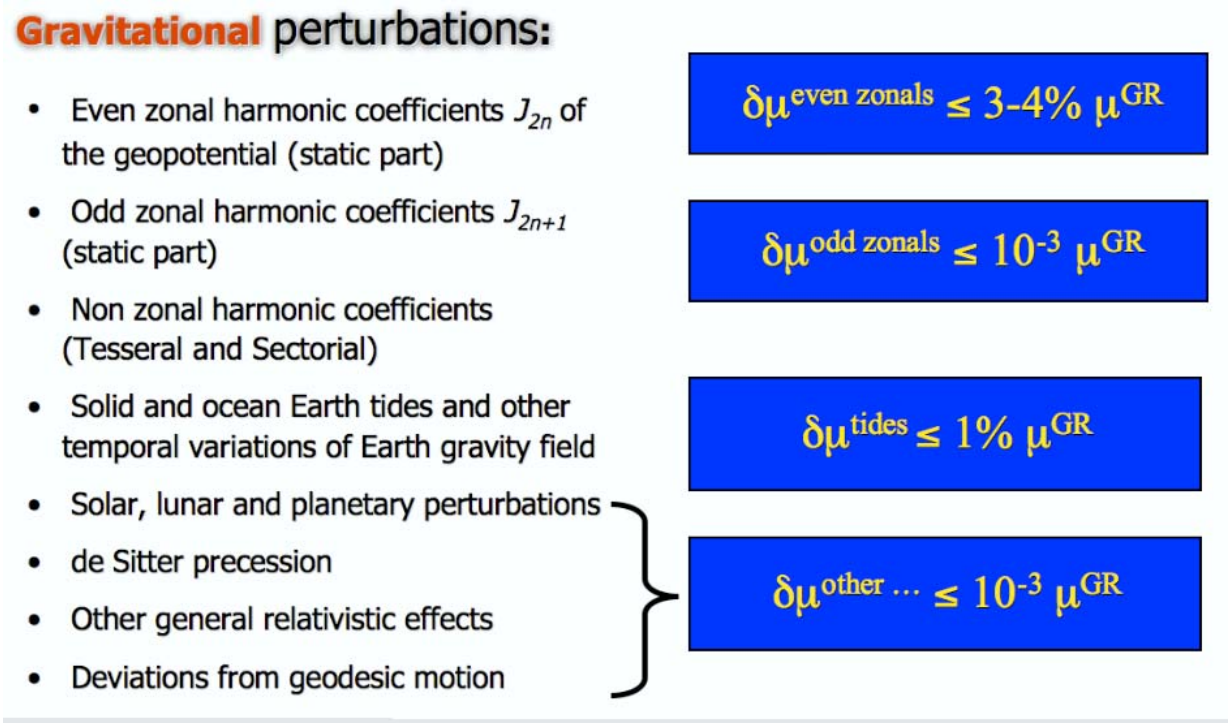

***Figure 3**. The calibrated errors on μ, due to realistic uncertainties of the gravitational parameters.*

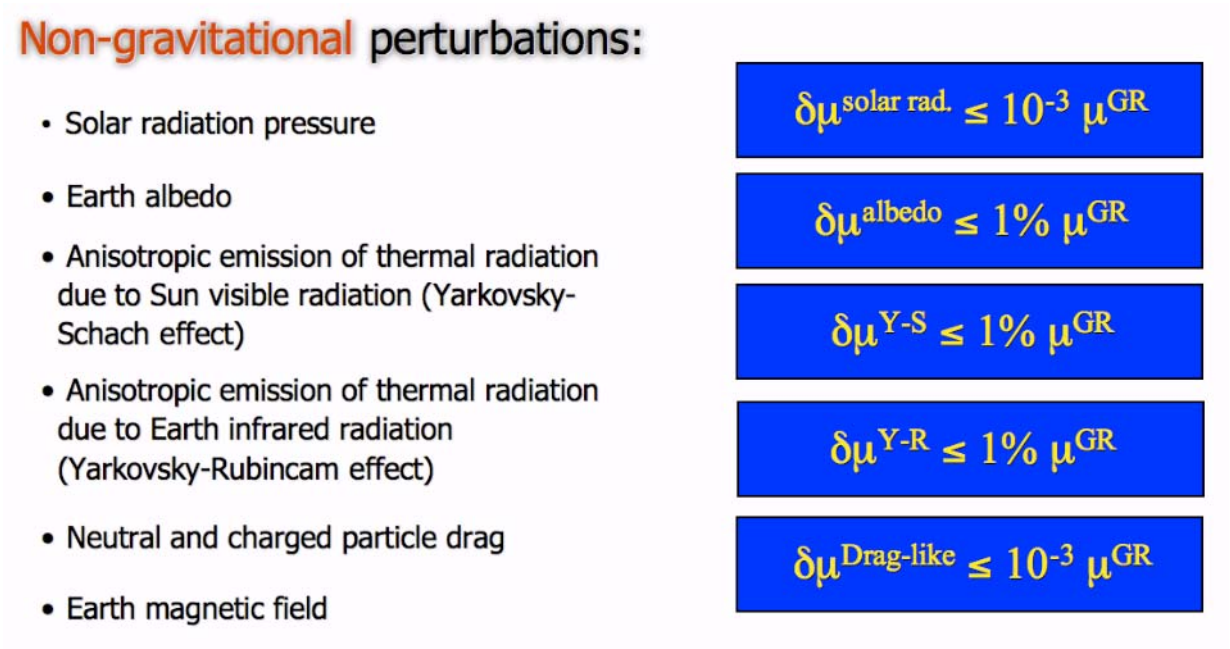

***Figure 4**. The calibrated errors on μ, due to realistic uncertainties of the non-gravitational parameters.*

The 2004 experiment results

The most accurate results on the measurement of the LT effect were published in (Ciufolini and Pavlis, 2004). The methodology and error analysis were subsequently detailed in (Ciufolini, Pavlis and Peron, 2006). These two references describe in detail the technique and the data that were used for the 2004 experiment. The basic points to be noted here are that the analysis covered the period from 1993 (just after the launch of LAGEOS 2) up to 2004, including all SLR data from the two LAGEOS satellites. The data were reduced using 15-day orbital arcs with a one-day overlap. The models used were the most accurate and consistent with the IERS Conventions 2003. All known perturbations were modeled **except** for the LT effect (set to zero). Once all arcs were converged, for each LAGEOS we formed a time series of consecutive arcs' nodal longitude differences, i.e. the nodal longitude at $t_d^{ARC=n+1}$ and the same quantity obtained for the same time from the previous arc at $t_d^{ARC=n}$. These were then integrated and combined using our constraint equation to generate a single time series. The secular trend of these series is the sought-for estimate of the μ LT parameter. Figure 5 shows the final result for the 2004 experiment.

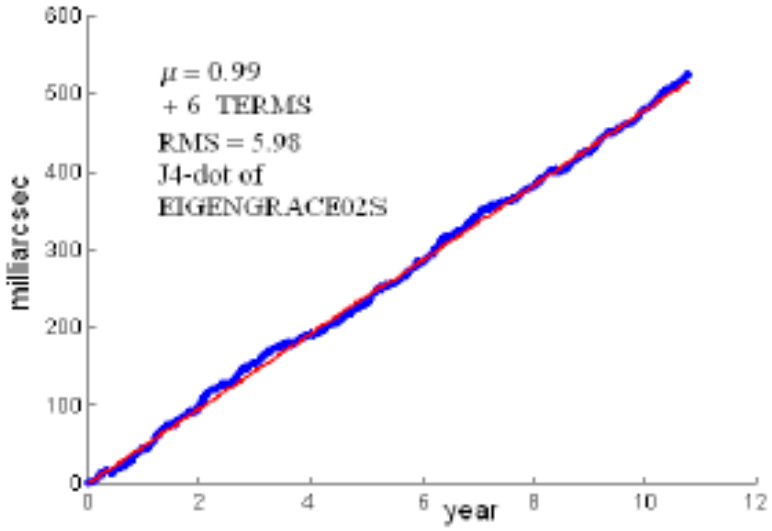

Figure 5*. The linear trend of the LAGEOS and LAGEOS 2 integrated nodal longitude differences time series for the EIGEN-GRACE02S gravitational model. Six periodic signals associated with well-known periods were filtered at the same time.*

We have already discussed the accuracy estimates associated with the 2004 result and the extensive work done to validate these error estimates as much as possible. It is worth noting that the gravitational model improvements from additional years of GRACE data result in an ever-improving estimate of these errors. The converging progression of these accuracy estimates provides a means to validate our quoted accuracy estimates for previous experiments. It is this point that makes the forthcoming new and much improved GRACE model GGM03S so anxiously awaited by all.

Beyond the 2004 experiment

The LAGEOS experiments are a zero-budget verification experiment for the much more accurate (~0.1%) and expensive (>$700M) result expected from NASA's Gravity Probe B mission (Buchman et al., 2000). In particular, with the recent

discovery of unanticipated errors in the gyro design of GP-B (Tomlin, 2007), it is doubtful that the GP-B results will ever break the 10% accuracy level (Kahn, 2007), so the LAGEOS experiments may eventually take a totally unforeseen center role in the area of fundamental physics tests.

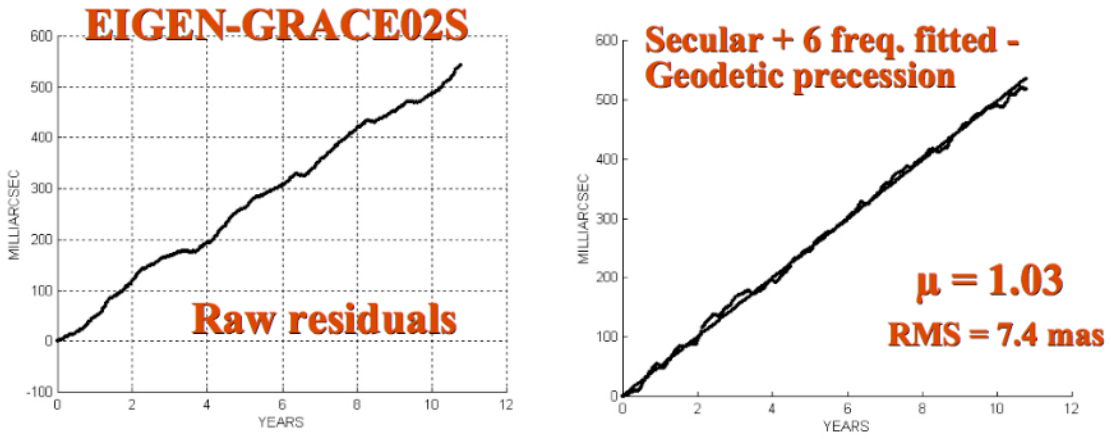

Figure 6. *Results from the GFZ software package EPOS, replicating the 2004 experiment (preliminary, pending small s/w improvements in the force model).*

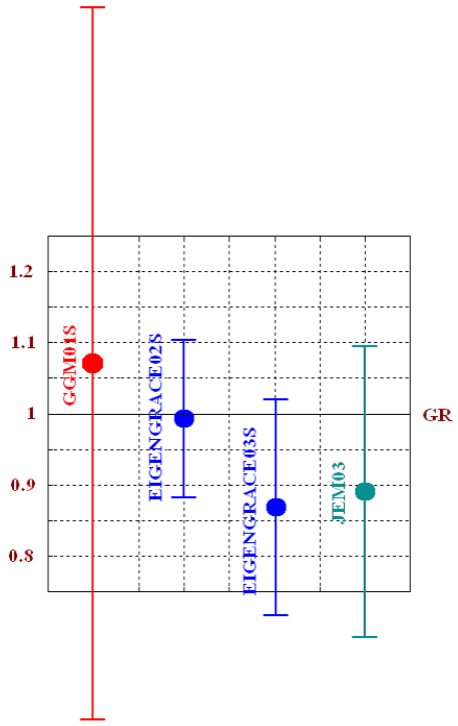

Figure 7. *Results from the joint analysis for four different gravitational models from GRACE (plotted is the value of the recovered μ, with unity signifying GR is correct).*

To improve the validation of our results our original group was extended to encompass analysts from other institutions and allow an independent check of the results with multiple software packages and alternate reduction philosophy. So far, the GFZ group has become an integral and active participant with their software package EPOS. First results from their initial attempts to replicate our 2004 experiment are shown in Fig. 6. The small discrepancy with respect to our 2004 result is due to the

fact that their software needs some small improvements to match the modeling that was used in Geodyn. In addition to the test results for 2004, new models developed by various GRACE science team groups were also used to derive new estimates of μ. Using different gravitational models we also get a good sense of the variability of the μ-estimates due to the change in the model, the development group's strategy and their ability to properly calibrate the errors of their model. The results are shown in a summary plot in Figure 7.

LAGEOS results and LLR claims

It is sometimes claimed that gravitomagnetism, measured already by SLR with the LAGEOS satellites, (might also be detected after refining the GP-B data analysis, see Tomlin, 2007), has already been observed by Lunar Laser Ranging (LLR), (Murphy in these proceedings and Murphy *et al.,* 2007); however the gravitomagnetic effects measured by LLR and the LAGEOS satellites are intrinsically different.

The gravitomagnetic effect measured by LLR depends on the motion of a gyroscope (the Earth-Moon system in the case of the LLR analysis) with respect to a central mass (the mass of the Sun in the LLR analysis) and, by changing the frame of reference used in the analysis, is equivalent to the geodetic precession, already well measured by LLR. The second gravitomagnetic effect measured by the LAGEOS satellites is an intrinsic gravitomagnetic effect (Ciufolini, 1994 and Ciufolini and Wheeler, 1995, Ciufolini 2007) that cannot be eliminated by means of any coordinate transformation.

In general relativity, in the frame in which a mass is at rest the so-called "magnetic" components g_{0i} of the metric are zero (in standard PPN coordinates). However, if an observer is moving with velocity **v** relative to the mass, the "magnetic" components g_{0i} are no longer nonzero in his local frame. These "magnetic" components g_{0i} can be simply eliminated by a Lorentz transformation back to the original frame. This is precisely what has been observed by LLR since the first measurements of the geodetic precession of the lunar orbit. In contrast, a mass object (such as Earth) with angular momentum J generates a gravitomagnetic field intrinsic to the structure of spacetime that therefore cannot be eliminated by a simple coordinate transformation or choice of reference frame. This is the field producing the LT effect on Earth orbiting satellites such as LAGEOS, measured by SLR.

In general relativity, given explicitly a general metric $\boldsymbol{g}$, with or without magnetic components g_{0i}, in order to test for intrinsic gravitomagnetism (i.e. which cannot be eliminated with a coordinate transformation), one should use the Riemann curvature tensor **R** and the spacetime invariants built using it (Ciufolini, 1994 and Ciufolini and Wheeler, 1995). Ciufolini and Wheeler (1995) give the explicit expression of the Riemann curvature invariant ***R•R**, where ***R** is the dual of **R**. Irrespective of the frame of choice, this invariant is non-zero in the case of the Kerr metric generated by the angular momentum and the mass of a rotating body. When however we evaluate it for the Schwarzschild metric generated by the mass of a non-rotating body, it is equal to zero for any frame and coordinate system of choice. In (*ibid.*) it is shown that the gravitomagnetic effect measured by LAGEOS and LAGEOS 2, due to Earth's angular momentum, is intrinsic to the spacetime's curvature and cannot be eliminated by a simple change of frame of reference since the spacetime curvature invariant ***R•R** is different from zero. However, the effect measured by LLR is just a gravitomagnetic effect that depends on the velocity of the Earth-Moon system and whose interpretation depends on the frame used in the analysis.

Murphy *et al.* (2007) show that on the lunar orbit there is a gravitomagnetic acceleration that changes the Earth-Moon distance by about 5 meters with monthly and semi-monthly periods. In a frame of reference co-moving with the Sun, the lunar gravitomagnetic acceleration in the Moon's equation of motion, is $\sim \mathbf{v}_M \times (\mathbf{v}_E \times \mathbf{g}_{ME})$; where $\mathbf{v}_M$ and $\mathbf{v}_E$ are the velocities of Moon and Earth in the frame of reference co-moving with the Sun and $\mathbf{g}_{ME}$ is the standard Newtonian acceleration vector on the Moon due to the Earth mass; this is the term discussed in (Murphy *et al.*, 2007). However, in a geocentric frame of reference co-moving with Earth, the lunar gravitomagnetic acceleration can be written: $\sim \mathbf{v}_M \times (\mathbf{v}_S \times \mathbf{g}_{MS})$: where $\mathbf{v}_M$ and $\mathbf{v}_S$ are the velocities of Moon and Sun in the frame of reference co-moving with Earth and $\mathbf{g}_{MS}$ is the standard Newtonian acceleration vector on the Moon due to the Sun mass. This acceleration can be simply rewritten as a part equivalent to the geodetic precession (Ciufolini 2007) and another one too small to be measured at the present time.

This argument can be made rigorous by using the curvature invariant ***R•R**. This invariant is formally similar to the invariant ***F•F** equal to **E•B** in electromagnetism. In the case of a point-mass metric generated by Earth and Sun, this invariant is: $\sim$ **G•H**, where **G** is the standard Newtonian electric-like field of the Sun and Earth and **H** the magnetic-like field of the Sun and Earth; this magnetic-like field is $\sim \mathbf{v} \times \mathbf{G}$ and then clearly, on the ecliptic plane, the invariant ***R•R** is null. Indeed, this invariant has been calculated (Ciufolini 2007) to be zero on the ecliptic plane, even after considering that the lunar orbit is slightly inclined on the ecliptic plane, this component would only give a contribution to the change of the radial distance too small to be measured at the present time.

***Figure 8**. A 1:2 model of the proposed LARES (Bosco et al., 2006) geodetic satellite for SLR applications in relativistic tests and geodetic TRF development.*

Summary and future plans

The analysis of nearly twelve years of SLR data from LAGEOS and LAGEOS 2 has demonstrated the measurement of the LT effect at the 5-10% level for the first time. This result was possible because of the extremely precise gravitational models developed from the gravity-mapping missions CHAMP and GRACE. The results have been validated with independently developed s/w and our future plans include further additional validation with even more groups.

Interim results are also exchanged and compared with John Ries of Univ. of Texas, who is now using the UTEX software UTOPIA, in a similar reduction approach and obtains similar results. We hope to have UTOPIA results regularly in the near future, as the UTEX group makes time for participation in these experiments. It is our intention to have a new experiment using the new and soon to be released 3rd-generation UTEX model GGM03S, using all s/w packages (GEODYN, EPOS and UTOPIA) and groups, extending our LAGEOS data span by several years (3+) to the present, and incorporating many small but significant model improvements, especially in the temporally varying gravitational signals area due to climate change and global mass redistribution.

In a parallel process we are actively pursuing the optimal design and likely contribution of a new dedicated mission, LARES (Bosco *et al.*, 2006), which is currently in pre-phase B and expected to be in orbit in the next two years. Although not identical to LAGEOS, the improved design of LARES will result in a better LT measurement and expand the list of high-accuracy geodetic targets for TRF and low-degree temporal gravity observations. As explained in (*ibid.*), LARES is being designed with the utmost care for the definition of its "signature", i.e. the precise offset between the effective reflection plane and its CoM, to minimize errors that affect the origin and scale of the TRF. A half-scale model of LARES is shown in

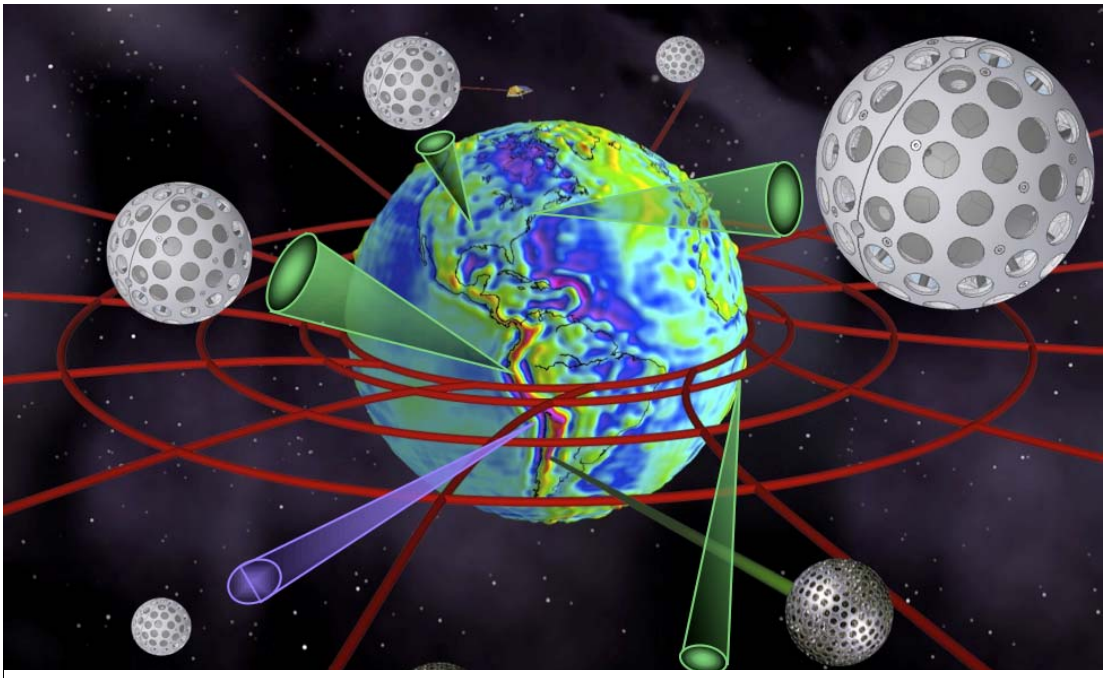

Figure 9*. A visualization of the LT effect on frame coordinate lines and a constellation of geodetic satellite targets which with a small effort could be a reality by the end of this decade.*

Figure 8 along with a mechanical drawing of the current design.

The future launch of LARES and other similar geodetic targets will go a long ways towards the development of a "SLR" constellation (Figure 9). The near-continuous availability of targets at all SLR stations and the improved geometry from the mix of inclinations and nodal longitudes, etc., will lead to a more robust set of SLR products for TRF and POD. Improvement of the gravitational static and temporal models and the availability of other data sets from Earth observing missions will soon allow us to use most of the currently available and future geodetic satellites with laser arrays for highly precise geophysical products.

References

[1] Bosco, A. *et al.*, 2006. "Probing Gravity in NEO with High-Accuracy Laser-Ranged Test Masses," proceedings of "*Quantum to Cosmos"* NASA Int. Workshop, Warrenton, VA, USA, May 2006, *Int. J. Mod. Phys. D*, 8.

[2] Buchman, S. *et al*, 2000. "The Gravity Probe B Relativity Mission," *Adv. in Space Res.* 25(6), p. 1177.

[3] Ciufolini, I., 1989. *Int. J. Mod. Phys.* A 4, 3083.

[4] Ciufolini, I., 1994. *Class. Quantum Grav.* 11, 958.

[5] Ciufolini, I. and J.A. Wheeler, 1995. *Gravitation and Inertia*, Princeton University Press, Princeton, New Jersey.

[6] Ciufolini, I. et al., 1998. Science 279, 2100.

[7] Ciufolini, I. and E. C. Pavlis "A confirmation of the general relativistic prediction of the Lense-Thirring effect", *Nature*, 431, 958-960, 2004.

[8] Ciufolini, I., E. C. Pavlis and R. Peron, 2006. Determination of frame-dragging using Earth gravity models from CHAMP and GRACE, *New Astronomy*, 11, 527-550, 10.1016/j.newast.2006.02.001, Elsevier Science B.V., Amsterdam.

[9] Ciufolini, I., 2007, to be published (arXiv:0704.3338v2).

[10] Everitt, C.W.F., *et al.*, 1980. Report on a program to develop a gyro test of General Relativity in a satellite and associated technology, Stanford University.

[11] Kahn, B., 2007. *StanfordNews*, Press release of April 14, 2007, http://www.stanford.edu/dept/news/pr/.

[12] Lense, J., Thirring, H., 1918. *Phys. Z.* 19, 156. See also English translation by Mashhoon, B., Hehl, F.W., Theiss, D.S., 1984. Gen. Relativ. Gravit. 16, 711.

[13] Murphy, T.W., K. Nordtvedt and S.G. Turyshev, 2007. *Phys. Rev. Lett.* 98, 071102.

[14] Pavlis, E. C., 2002. Geodetic Contributions to Gravitational Experiments in Space, in *Recent Developments in General Relativity, Genoa 2000*, R. Cianci, R. Collina, M. Francaviglia, P. Fré eds., 217-233, Springer-Verlag.

[15] Pearlman, M.R., Degnan, J.J., and Bosworth, J.M., 2002. "The International Laser Ranging Service", *Adv. in Space Res.*, Vol. 30, No. 2, pp. 135-143, 10.1016/S0273-1177(02)00277-6.

[16] Reigber, Ch., *et al*., 2002. GRACE Orbit and Gravity Field Recovery at GFZ Potsdam - First Experiences and Perspectives, Eos. *Trans. AGU*, 83(47), Fall Meet. Suppl., Abstract G12B-03.

[17] Reigber, Ch., *et al.*, 2003. The CHAMP-only Earth Gravity Field Model EIGEN-2, *Adv. in Space Res.* 31(8), 1883-1888 (doi: 10.1016/S0273–1177(03)00162-5).

[18] Reigber, C., Schmidt, R., Flechtner, F., König, R., Meyer, U., Neumayer, K. H., Schwintzer, P., and Zhu, S. Y., 2005. An Earth gravity field model complete to degree and order 150 from GRACE: EIGEN-GRACE02S, *J. Geodyn.* 39, 1.

[19] Ries, J.C., Eanes, R.J., Tapley, B.D., 2003. In: *Non-Linear Gravitodynamics*, The Lense–Thirring Effect. World Scientific, Singapore.

[20] Tapley, B. D., 2002. The GRACE Mission: Status and Performance Assessment, Eos. *Trans. AGU*, 83(47), Fall Meet. Suppl., Abstract G12B-01.

[21] Tapley, B.D., Chambers, D.P., Bettadpur, S., Ries, J.C., 2003. *Geophys. Res. Lett.* 30 (22), 2163.

[22] Tomlin, S., 2007. Interim view from NASA relativity probe, *Nature*, 446, 19 April 2007.

A "Web Service" to Compare Geodetic Time Series

Florent Deleflie[1]

1. Geodesie and Mecanique Celeste Team, Grasse, France

Abstract

We have developed a geodetic database built on the concept of "Virtual Observatory" (http://www.ivoa.net). These time series come from our solutions of Earth Orientation Parameters, stations coordinates and velocities, polar motion, and start at the beginning of the 1990's. Solutions deduced from various techniques are available (SLR data, combined or not...)

This tool enables one to directly compare, in an easy, homogeneous and coherent way, results coming, for example, from various groups. One of the scientific goals consists in making different results be comparable one from another, and to check, for example, if there is or not systematic differences, or if the used reference frames are fully compatible or not.

I will show how this database works (directly through the Web, if it is possible), and I will mention some interesting scientific applications for the future.

Least-square mean effect: Application to the Analysis of SLR Time Series

D. Coulot[1], P. Berio[2], A. Pollet[1]

1. IGN/LAREG - Marne-la-Vallée – France
2. CNRS/OCA/GEMINI - Grasse - France

Contact: David.Coulot@ensg.ign.fr Fax: +33-1-64-15-32-53

Abstract

In this paper, we evidence an artifact due to the least square estimation method and, in particular, to the current modeling used to derive station position time series from space-geodetic measurements. Indeed, to compute such series, we in fact estimate constant (typically over one week) updates of station positions with respect to a priori models (ITRF2000, solid Earth tides, polar tide and oceanic loading effects). Thus, these estimations must underline the physical models which were not taken into account in the a priori modeling (atmospheric and hydrologic loading effects and even unknown signals, in our case).

As shown through the example of the Satellite Laser Ranging measurement processing, it is not the case: the weekly position time series exhibit weekly means of these physical signals but with a supplementary signal at the level of a few millimeters. This is the so-called "least square mean effect".

To avoid this effect, alternative modeling such as periodic series can be used. A method to compute such periodic series for the station positions together with the geocenter motion is also presented in this paper.

Introduction

This paper comprises four parts. First of all, we present the least square mean effect from two points of view, theoretical and numerical. Secondly, we propose alternative models to reduce this effect. Then, we study a new method to process Satellite Laser Ranging (SLR) data. This method should help to use alternative modeling for a global network. Finally, we provide some conclusions and prospects.

1. Least square mean effect

The quality presently reached by space-geodetic measurements allows us to study geodetic parameters (Earth Orientation Parameters (EOPs), station positions, Earth's gravity field, etc.) under the form of time series. The modeling currently used to derive such time series is the following. The physical effects which are well understood are modeled (take as examples solid Earth tides or oceanic loading effects for station positions). These models are used to compute a priori values for the parameters worthy of interest and we compute the parameters with respect to these a priori values. These estimations are supposed to be constant over a given time (typically one day for EOPs and one week for station positions). And these estimations should help us to study the underlying physical effects (atmospheric loading effects, for instance). But, to do so, we need exact and judicious representations. We show that it is not really the case for the current modeling in this section.

1.1. Theoretical considerations

We consider a vector of physical parameters $\vec{X}$ which vary with time. According to the modeling used, we split this vector in two parts: the modeled effects $\vec{X}_0$ and the effects we

want to study through time series $\delta\vec{X}$, $\vec{X}(t) = \vec{X}_0(t) + \delta\vec{X}(t)$ .We know that the vector $\delta\vec{X}$ varies with time but, in order to get a robust estimation, we suppose it constant over a given interval $[t_1, t_m]$. And, doing so, we hope that the constant estimations $\delta\hat{\vec{X}}$ will correspond to the averages of the underlying physical signals over this interval. The measurements used are modeled with a function f ($m(t) \cong f(t, \vec{X})$) which is linearized

$$m(t) \cong f(t, \vec{X}_0(t)) + \frac{\partial f}{\partial \vec{X}}(t, \vec{X}_0(t)).\delta\vec{X} \qquad \text{with} \frac{\partial f}{\partial \vec{X}}(t, \vec{X}_0(t)),$$

the partial derivative matrix of f at the point $(t, \vec{X}_0(t))$) to get the least square model. Furthermore, we can also linearize the measurements but with respect to the true signal to be studied ($m(t) \cong f(t, \vec{X}_0(t)) + \frac{\partial f}{\partial \vec{X}}(t, \vec{X}_0(t)).\delta\vec{X}(t)$).

As a consequence, on one hand, we have a relation between the measurements and the constant updates to be estimated and, on the other hand, a relation between these measurements and the true physical signal to be studied. From these two relations, we get the following observation equation:

$$f(t, \vec{X}_0(t)) + \frac{\partial f}{\partial \vec{X}}(t, \vec{X}_0(t)).\delta\vec{X} \cong f(t, \vec{X}_0(t)) + \frac{\partial f}{\partial \vec{X}}(t, \vec{X}_0(t)).\delta\vec{X}(t)$$

This observation equation allows us to build the following system:

$$A.\delta\vec{X} \cong \widetilde{A}.\delta\vec{\vec{X}}$$

$$\text{with } A = \begin{bmatrix} \frac{\partial f}{\partial \vec{X}}(t_1, \vec{X}_0(t_1)) \\ \frac{\partial f}{\partial \vec{X}}(t_2, \vec{X}_0(t_2)) \\ \vdots \\ \frac{\partial f}{\partial \vec{X}}(t_m, \vec{X}_0(t_m)) \end{bmatrix},$$

$$\widetilde{A} = \begin{bmatrix} \frac{\partial f}{\partial \vec{X}}(t_1, \vec{X}_0(t_1)) & 0 & \cdots & 0 \\ 0 & \frac{\partial f}{\partial \vec{X}}(t_2, \vec{X}_0(t_2)) & \cdots & 0 \\ \vdots & \vdots & \ddots & \vdots \\ 0 & 0 & \cdots & \frac{\partial f}{\partial \vec{X}}(t_m, \vec{X}_0(t_m)) \end{bmatrix},$$

$$\text{and } \delta\vec{\vec{X}} = \begin{pmatrix} \delta\vec{X}(t_1) \\ \delta\vec{X}(t_2) \\ \vdots \\ \delta\vec{X}(t_m) \end{pmatrix}.$$

This system is then used to compute the least square solution with a weight matrix *P*:

$$\hat{\vec{\delta X}} \cong \vec{\delta X}_{average} + \left(A^T P A\right)^{-1} A^T P \tilde{A}.(\tilde{\vec{\delta X}} - \tilde{\vec{\delta X}}_{average})$$

$$\text{with } \tilde{\vec{\delta X}}_{average} = \begin{pmatrix} \vec{\delta X}_{average} \\ \vec{\delta X}_{average} \\ \vdots \\ \vec{\delta X}_{average} \end{pmatrix} \text{ and } \vec{\delta X}_{average} = \frac{1}{t_m - t_1} \int_{t_1}^{t_m} \vec{\delta X}(u) du \,.$$

In this solution, we can see that the estimations effectively contain the averages of the involved signals over the time interval but with a complementary term. We have called this term the "least square mean effect".

1.2. Numerical examples

In this section, we provide some numerical examples based on simulations. Here is the method used to carry out these simulations (cf. Fig.1). The first step is the two LAGEOS satellite orbit computation with GINS software. These orbits are used, in a second step, with ITRF2000 [Altamimi et al., 2002a] and a model for atmospheric loading effects to compute simulated range measurements and partial derivatives of these latter with respect to station positions. Then, we estimate station positions without any atmospheric loading effect in the a priori model. Thus, the estimated positions must reflect these non modeled effects. These estimations are finally compared with the temporal averages of the atmospheric loading effect models. We use real orbits and real SLR measurement epochs in order to get the most realistic simulations. European Center for Medium-range Weather Forecasts (ECMWF, http://www.ecmwf.int/) pressure fields were used to derive the atmospheric loading effect models.

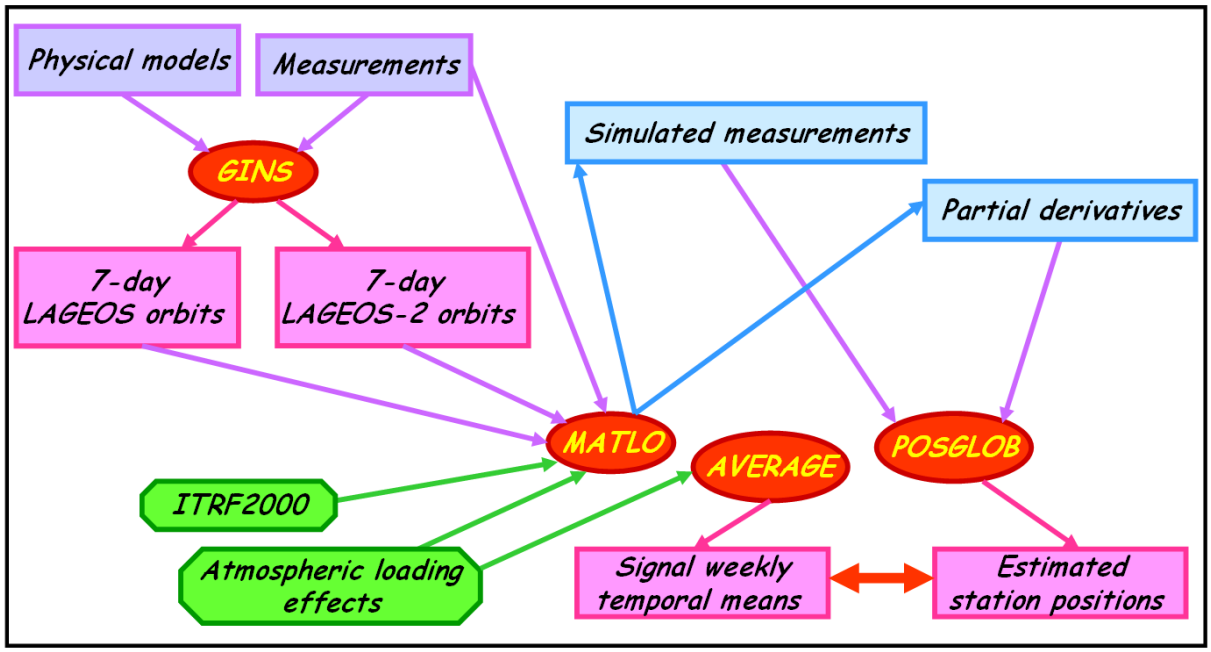

Figure1. *Simulation method.*

Fig. 2 shows the results produced for the station Yarragadee (7090) regarding the three components East, North and Up, in mm. In the graphs above, black curves correspond to the weekly temporal averages of the atmospheric loading effects and red curves to the estimated

weekly time series. The graph below shows the absolute differences between black and red curves, so the least square mean effects.

Table 1 provides maximum values of differences of a few millimeters (2 mm for the Up component). And, on average, the least square mean effect is approximately 10 % of the amplitude of the loading effects.

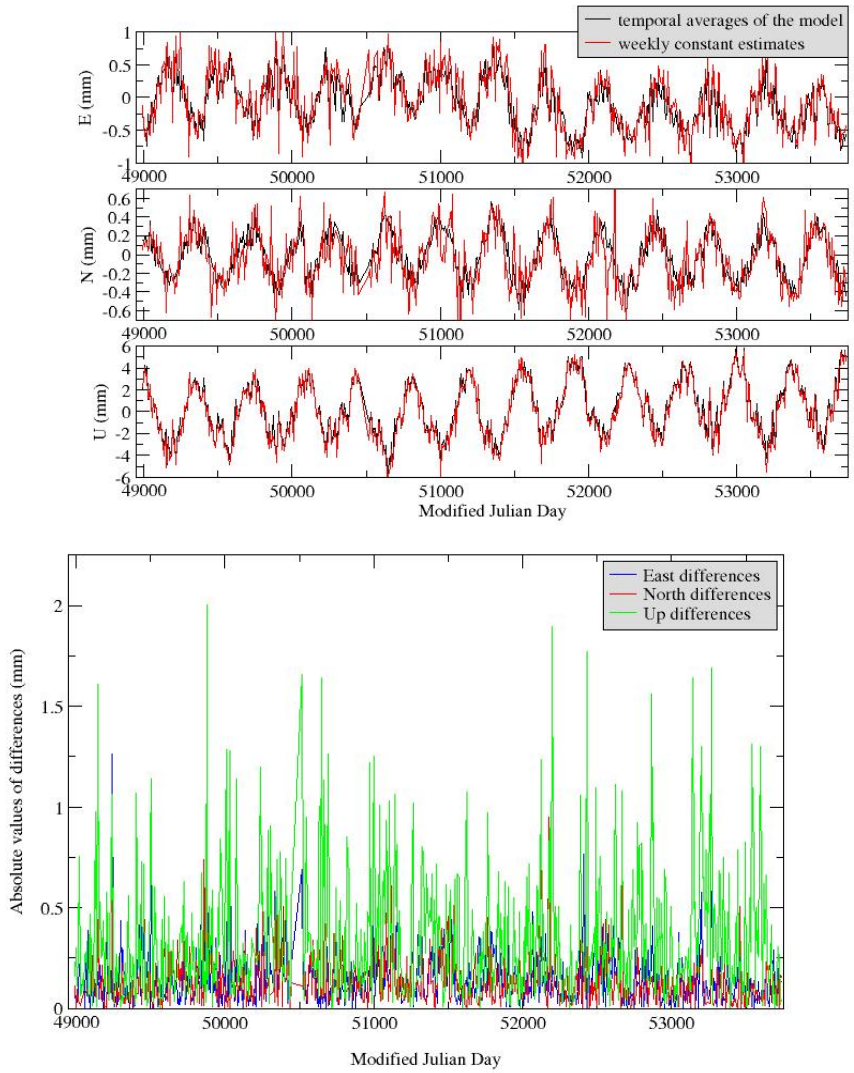

Figure 2. *Simulation results for the station Yarragadee (7090).*
Graphs above: black (resp. red) curves correspond to the weekly temporal averages of the atmospheric loading effects (resp. to the estimated weekly time series) in mm.
Graph below: absolute values of least square mean effects per component in mm.

Table 1. *Statistics of the results shown on Fig. 2.*

Values (mm)	Minimum	Maximum	Average	RMS
East	2.37 10-4	1.26	0.15	0.13
North	1.86 10-5	0.95	0.13	0.12
Up	2.29 10-5	2.00	0.34	0.32

Fig. 3 shows the equivalent results for the Monument Peak station (7110).

Table 2. *Statistics of the results shown on Fig. 3.*

Values (mm)	Minimum	Maximum	Average	RMS
East	1.57 10-4	2.28	0.19	0.21
North	3.87 10-4	1.96	0.19	0.22
Up	3.14 10-5	4.49	0.42	0.51

As shown in Table 2, the effects are even stronger than those obtained for Yarragadee (see Fig.2 and Tab. 1). Indeed, the maximum effect is 4.5 mm for the Up component.

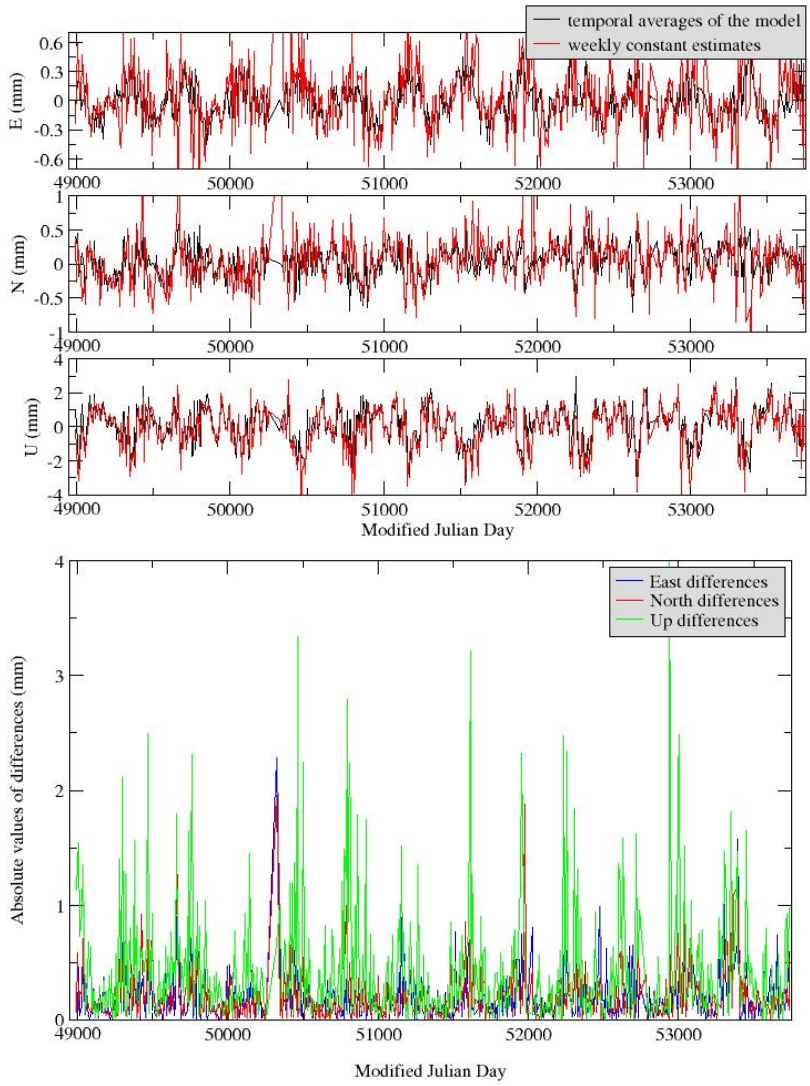

Figure 3. *Simulation results for the station Monument Peak (7110).*
Graphs above: black (resp. red) curves correspond to the weekly temporal averages of the atmospheric loading effects (resp. to the estimated weekly time series) in mm.
Graph below: absolute values of least square mean effects per component in mm.

Thus, this effect is clearly not negligible and we have to take it into account in a geodynamical framework. Indeed, due to this effect, weekly station position time series can not be directly compared to geodynamical models, [Coulot and Berio, 2004] and [Coulot,

2005]. Furthermore, the results provided in [Penna and Stewart, 2003], [Stewart et al., 2005], and [Penna et al., 2007] show that this effect could create spurious periodic signals in the estimated time series. To reduce this effect, we have studied some alternative models.

2. Alternative models

We have studied two alternative modeling. The first one uses periodic terms and the second one is based on wavelets.

2.1. Periodic series

The first model is a periodic one. Each of the three positioning components φ is modeled as periodic series: $\varphi(t) \cong \sum_{i=1}^{n} a_i \cos(\frac{2\pi}{T_i}t) + b_i \sin(\frac{2\pi}{T_i}t)$ where the periods $(T_i)_{i=1,n}$ are the characteristic periods of the involved signals. Instead of estimating weekly φ time series, all available measurements are stacked to compute the coefficients $(a_i)_{i=1,n}$ and $(b_i)_{i=1,n}$.

Fig. 4 shows the results (in mm) provided by simulations for the station Yarragadee (7090). The computational scheme is the same than the one shown on Fig. 1 but the simulated measurements are now used to compute the periodic series. On Fig. 4, blue curves correspond to the model of atmospheric loading effects used to compute the simulated measurements and red curves to the estimated periodic series. We can see a good coherence for the Up component and artifacts near the limits of the considered interval for all components. The less satisfying agreement for the horizontal components is certainly due to the low amplitude of the involved signals and to the poorest sensitivity of SLR measurements with respect to horizontal motions.

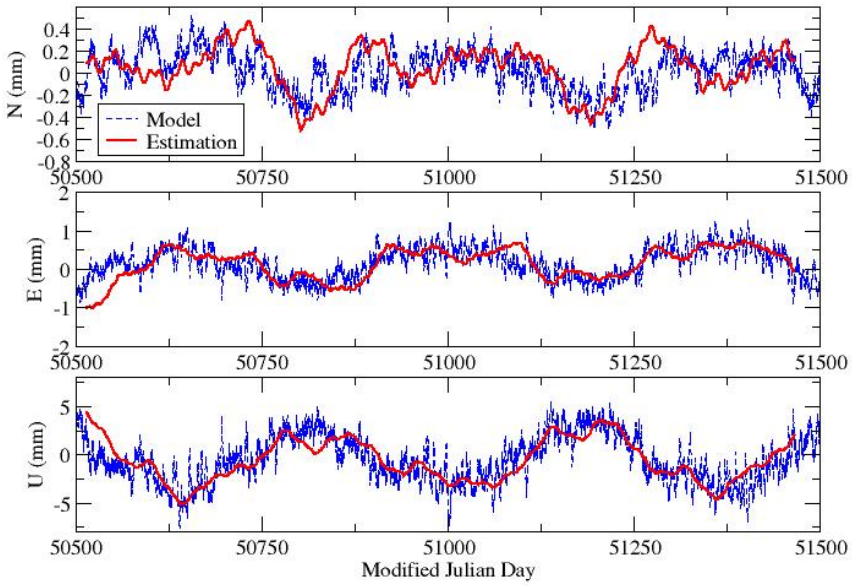

Figure 4. *Periodic series estimated with simulated measurements for Yarragadee station (7090), in mm. Blue (resp. red) curves correspond to the atmospheric loading effect models used to simulate the range measurements (resp. to the estimated periodic series).*

The main advantage of this approach is that no sampling is a priori imposed for estimations but

- the minimal period to be estimated may be imposed by the measurement sampling;

- regarding unknown signals, it will probably be difficult to find the involved periods;
- this model can difficultly take into account discontinuities such as earthquakes.

2.2. Wavelets

To go further, we have also studied a model based on wavelets. We have used, as a first test, the simplest wavelet, Haar's wavelet, for which the core function ψ is defined as follows:

$$\psi(t) = \begin{cases} 1 \text{ if } 0 \le t < \frac{1}{2} \\ -1 \text{ if } \frac{1}{2} \le t < 1 \\ 0 \text{ if not} \end{cases} .$$

Each of the three positioning components φ is modeled by the decomposition of the involved physical signal on the wavelet basis: $\varphi(t) = \sum_{j=-j_1}^{j_2} \sum_{n=0}^{n_{\max}} a_{j,n} \psi_{j,n}(t)$ with

$$n_{\max} = \begin{cases} 2^j - 1 \text{ if } j < 0 \\ 0 \text{ if not} \end{cases} \text{ and } \psi_{j,n}(t) = \frac{1}{\sqrt{2^j}} \psi\left(\frac{t - 2^j n}{2^j} \right).$$

All available measurements are stacked to compute the coefficients $a_{j,n}$. The discontinuities can now be taken into account with the help of this time-frequency representation.

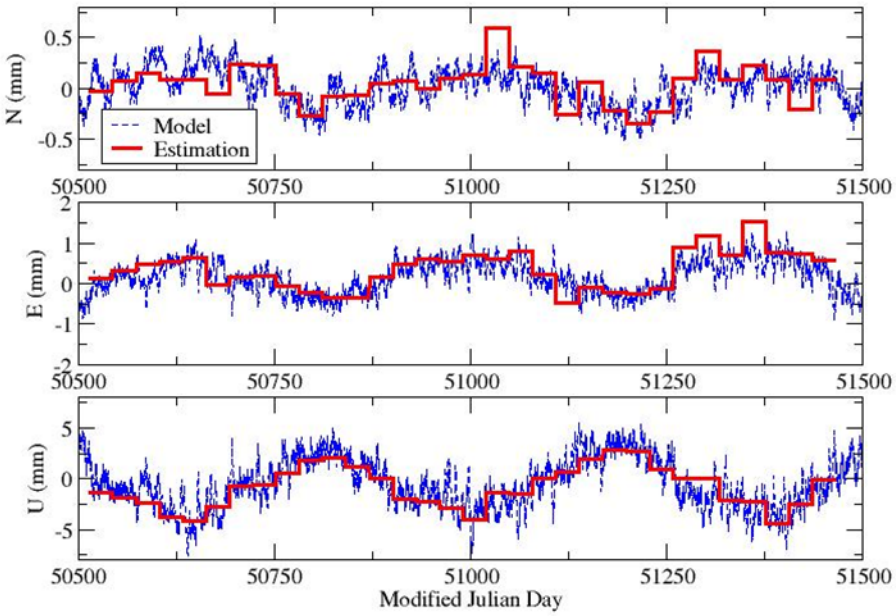

Figure 5. *Wavelet decompositions estimated with simulated measurements for Yarragadee station (7090), in mm. Blue (resp. red) curves correspond to the atmospheric loading effect models used to simulate the range measurements (resp. to the estimated wavelet decompositions).*

Fig. 5 shows the results provided by simulations for Yarragadee station (7090). We can notice the good agreement for the Up component and also the great importance of the smallest scale used for wavelets.

These preliminary results are encouraging but, whatever the model used, we need to guarantee the homogeneity of the involved Terrestrial Reference Frames (TRFs) to carry out such

computations for a station network. Furthermore, we can take the opportunity of such global computation to derive geodynamical signals contained in global parameters such as translations. To reach this goal, we have developed a new approach to process SLR data [Pollet, 2006].

3. New model for SLR data processing

3.1. General considerations

In the "classical approach", the starting point is the observation system Y=A.δX composed by the pseudo measurements Y, the design matrix A and the parameters to be computed δX. By applying weak or minimum constraints, we are able to derive weekly solutions [Altamimi et al., 2002b] (usually, daily EOPs together with weekly station positions for the considered network). On the basis of these weekly solutions, with the help of Helmert's transformation - here are the well-known formulae for station positions and for EOPs [Altamimi et al., 2002a]:

Station positions

$$\delta X = T + DX_0 + RX_0$$

with $T=(T_X, T_Y, T_Z)^T$

and $R=\begin{bmatrix} 0 & -R_Z & R_Y \\ R_Z & 0 & -R_X \\ -R_Y & R_X & 0 \end{bmatrix}$

Earth Orientation Parameters

$$\begin{cases} \delta x_P = R_Y \\ \delta y_P = R_X \\ \delta UT_1 = -\frac{1}{f} R_Z \end{cases}$$

with f=1.002737909350795

we can compute station positions in the a priori reference frame (ITRF2000, for instance) together with coherent EOPs and also 7-parameter transformation between involved TRFs.

The new model we have developed allows us to compute all these parameters in the same process, directly at the observational level. To derive this new approach, we have directly translated Helmert's transformations at the level of the previous observation system: Y=A.δX with δX=δXC+T+DX0+RX0 and δEOP=δEOPC+εR{X,Y,Z}. Doing so, we have replaced the parameters δX and δEOP by new ones: δXC, T, D, R{X,Y,Z} and δEOPC.

Theoretical considerations and numerical tests with SLR data have shown that the rotations R{X,Y,Z} were not needed at all in this model. We did not keep them.

The normal matrices provided by this new approach present a rank deficiency of 7, coming from:

- the fact that SLR data do not carry any orientation information (deficiency of 3);
- the estimation of three translations and a scale factor (deficiency of 4).

This rank deficiency in fact corresponds to the definition of the totally unknown TRF underlying the estimated δXC for which the seven degrees of freedom need to de defined. To do so, minimum constraints [Sillard and Boucher, 2001] are applied with respect to the ITRF2000 and with the help of a minimum network.

3.2. First results

In this section, we provide the preliminary results produced with this new model for SLR data processing over 13 years.

Fig. 6 shows the minimum network used to apply the minimum constraints to define the homogenous weekly TRFs.

Figure 6. *Minimum network used to apply the minimum constraints to define the homogeneous weekly TRFs.*

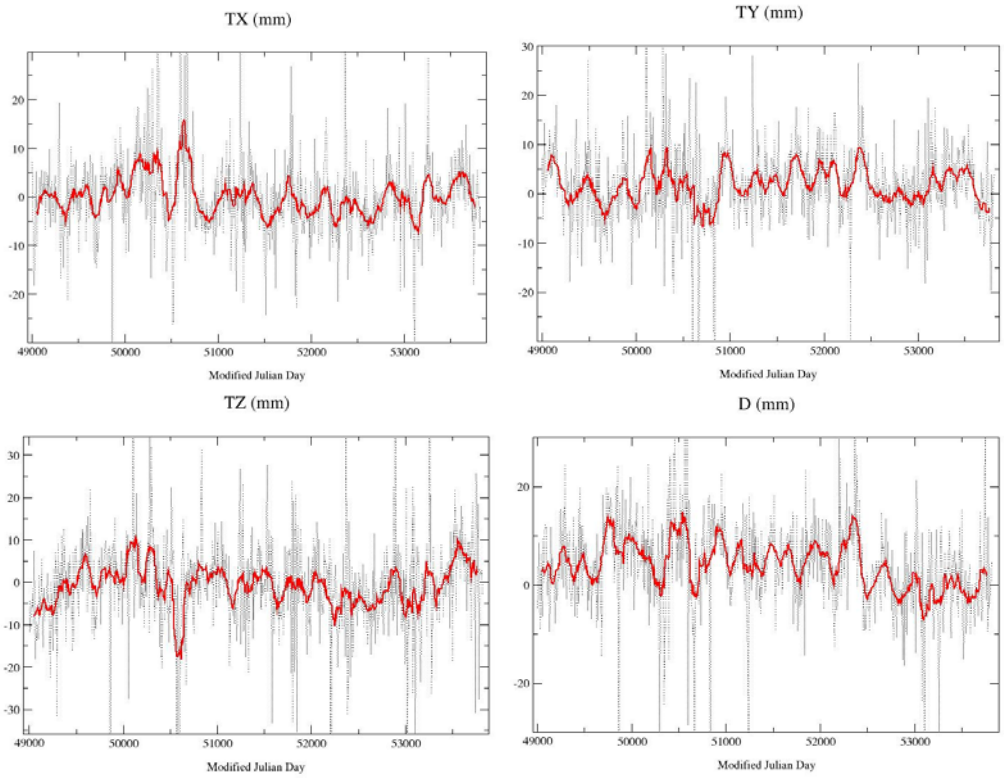

Figure 7. *Weekly time series of the three translations and the scale factor, in mm. Red curves correspond to running averages.*

Fig. 7 shows the four estimated transformation parameters between the weekly TRFs underlying the SLR measurements and directly linked to the two LAGEOS orbit references and the weekly TRFs constrained to be realized in ITRF2000. The three translations exhibit periodic signals (mainly annual) certainly linked to the geocenter motion.

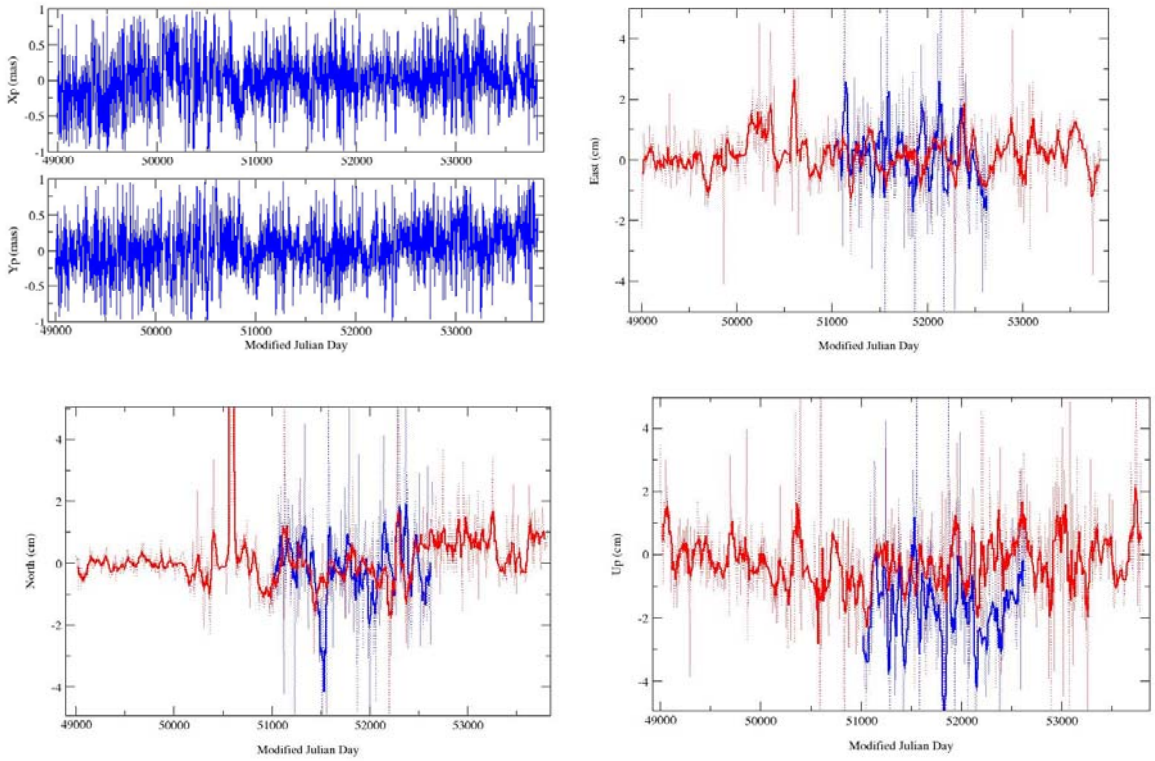

Figure 8. *Results produced with the new method for EOPs and station positions. Graph up left: EOP residuals (mas) with respect to EOPC04 time series [Gambis, 2004] consistent with the estimated station positions. Three other graphs: Mount Stromlo - 7849, in blue- and Yarragadee - 7090, in red- station three positioning component estimated time series (cm).*

Fig. 8 shows the results provided by the new method for EOPs and two Australian SLR stations, Mount Stromlo (blue curves) and Yarragadee (red curves). Regarding EOPs, the weighted biases (resp. the WRMS) are respectively 5µas for Xp and 23µas for Yp (resp. 280µas for Xp and Yp). Regarding the station position time series, we can notice the similarities between these series. The constant difference between the two Up time series is certainly due to range biases which were not taken into account for these computations.

3.3. Toward global estimations over long period

How this new model can help us to reduce the least square mean effect? We can replace the new parameters of the model by previous alternative models such as periodic series in the following example (new parameters to be estimated are underlined in green):

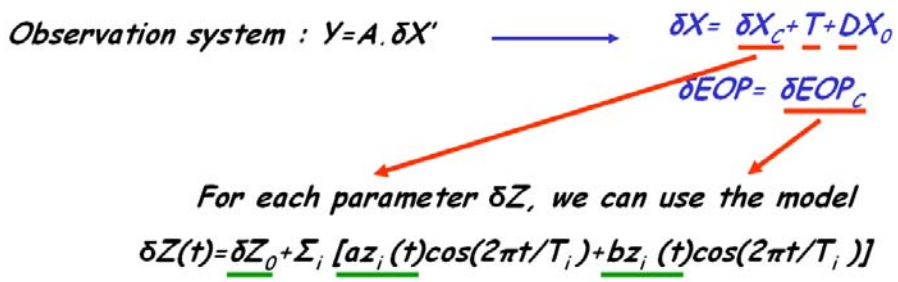

But, each harmonic estimated on station positions generates new rank deficiencies. Consequently, we have to generalize the minimum constraints for harmonic vectors. Furthermore, the number of involved parameters is very large (close to 50 000 in the next example).Thus, we have to use tools allowing the handling of large normal systems.

As a very preliminary computation, we have used this approach to compute amplitudes of annual signals contained in the four global parameters involved. The computation was carried out over 3 years of data. Amplitudes obtained are relatively satisfying (*TX*: 2.1 mm, *TY*: 3.6 mm, *TZ*: 1.1 mm and *D*: 0.9 mm). Moreover, the periodic series really absorb the annual signals as the annual harmonic totally disappears in the residual weekly parameters (the previous parameters called δZ_0) computed with respect to this annual term.

4. Conclusions and Prospects

All these results are satisfying but we of course need to go further by:

- using this periodic approach not only for global parameters but also for station positions;
- computing periodic series directly linked to oceanic loading effects together with series corresponding to atmospheric and hydrologic loading effects;
- deriving diurnal and semi-diurnal signals affecting EOPs with this approach;
- studying the spurious effects provided by this least square mean effect in the International Laser Ranging Service (ILRS) operational products.

We could also couple periodic series with more complex wavelet bases to get a more robust model and, eventually, with stochastic modeling in a filtering framework.

References

[1] Altamimi, Z., P. Sillard, and C. Boucher: "ITRF2000: a new release of the International Terrestrial Reference Frame for Earth science applications", J. Geophys. Res., 107(B10), 2214, doi: 10.1029/2001JB000561, 2002a.

[2] Altamimi, Z., C. Boucher, and P. Sillard: "New trends for the realization of the International Terrestrial Reference System", Adv. Space Res., 30(2), p. 175-184, 2002b.

[3] Coulot, D. and P. Berio: "Effet de moyenne par moindres carrés, application à l'analyse des séries temporelles laser", Bulletin d'Information Scientifique & Technique de l'IGN, 75, p. 129-142, IGN (Eds), IGN-SR-03-083-G-ART-DC, 2004.

[4] Coulot, D.: "Télémétrie laser sur satellites et combinaison de techniques géodésiques. Contributions aux Systèmes de Référence Terrestres et Applications", Ph. D. thesis, Observatoire de Paris, 2005.

[5] Gambis, D: "Monitoring Earth orientation using space-geodetic techniques: state-of-the-art and prospective", J. Geod., 78, p. 295-305, 2004.

[6] Penna, N.T. and M.P. Stewart: "Aliased tidal signatures in continuous GPS height time series", Geophys. Res. Lett., 30(23), p. 2184-2187, doi: 10.1029/2003GL018828, 2003.

[7] Penna, N.T., M.A. King, and M.P. Stewart: "GPS height time series: Short-period origins of spurious long-period signals", J. Geophys. Res., 112, B02402, doi: 10.1029/2005JB004047, 2007.

[8] Pollet, A.: "Combinaison de mesures de télémétrie laser sur satellites. Contributions aux systèmes de référence terrestres et à la rotation de la Terre.", Master research course report, Observatoire de Paris, 2006.

[9] Sillard, P. and C. Boucher: "Review of algebraic constraints in terrestrial reference frame datum definition", J. Geod., 75, p. 63-73, 2001.

[10] Stewart, M.P., N.T. Penna, and D.D. Lichti: "Investigating the propagation mechanism of unmodelled systematic errors on coordinate time series estimated using least squares", J. Geod., 79(8), p. 479-489, doi: 10.1007/s00190-005-0478-6, 2005.

Some Aspects Concerning the SLR Part of ITRF2005

H. Mueller[1], D. Angermann[1]

1. Deutsches Geodaetisches Forschungsinstitut (DGFI) Alfons-Goppel-Str. 11 80539 Muenchen.

Contact: mueller@dgfi.badw.de Fax: +49 89 23031 1240

Abstract

Two combined solutions for the ITRF2005 were generated independently by two ITRS Combination Centres, IGN, Paris and DGFI, Munich. A comparison of the two ITRF2005P solutions shows in general a good agreement, but the scale and scale rate of the SLR network differs significantly. To investigate this difference a number of tests were performed. It was found that the actual SLR results are consistent with the ITRF2005 solution of DGFI, whereas there is a bias of about 2 ppb compared to the IGN solution. The translation parameters between both ITRF2005 solutions are in good agreement. We also compared the VLBI and SLR scale through co-locations with GPS. This comparison showed the importance of a proper choice and weighting of local ties at co-location sites for the connection of the technique-dependent reference frames. Especially the sites at the southern hemisphere influence the resulting scale of the combined product.

Introduction

Within the re-organized IERS structure, there are three Combination Centres for the International Terrestrial Reference System (ITRS) at Deutsches Geodätisches Forschungsinstitut (DGFI), Munich, Institute Géographique National (IGN), Paris, and National Resources Canada (NRCan), Ottawa. The ITRS Product Center at IGN is coordinating the processing. DGFI and IGN provided each one solution for ITRF2005. Both used their own software and applied their preferred strategy. This guarantees independent results and allows a decisive validation and quality control of the results.

The combination strategy of IGN is based on the solution level by simultaneously estimating similarity transformation parameters w.r.t. the combined frame along with the adjustment of station positions and velocities. The ITRF2005 computations done at DGFI use unconstrained normal equations from the solutions of the different techniques.

This paper briefly summarizes the combination methodology of the ITRS Combination Center at DGFI. Main subject is a comparison of the ITRF2005 solutions of IGN and DGFI. The focus thereby is on the SLR part of ITRF2005.

Combination methodology of DGFI

The general concept of the ITRS Combination Center at DGFI is based on the combination of normal equations and the common adjustment of station positions, velocities and EOP. The computations are performed with the DGFI Orbit and Geodetic Parameter Estimation Software (DOGS). Details on the combination procedure and the mathematical background are given in various publications (e.g., Angermann et al., 2004; Angermann et al., 2006; Drewes et al., 2006; Krügel and Angermann, 2006; Meisel et al., 2005). Figure 1 shows the data flow and the combination methodology for the ITRF2005 computation.

The combination methodology of DGFI comprises the following major steps:

- Analysis of ITRF2005 input data and generation of normal equations
- Analysis of time series and accumulation per-technique (intra-technique combination)
- Comparison and combination of different techniques (inter-technique combination)
- Generation of the ITRF2005 solution by applying minimum datum conditions

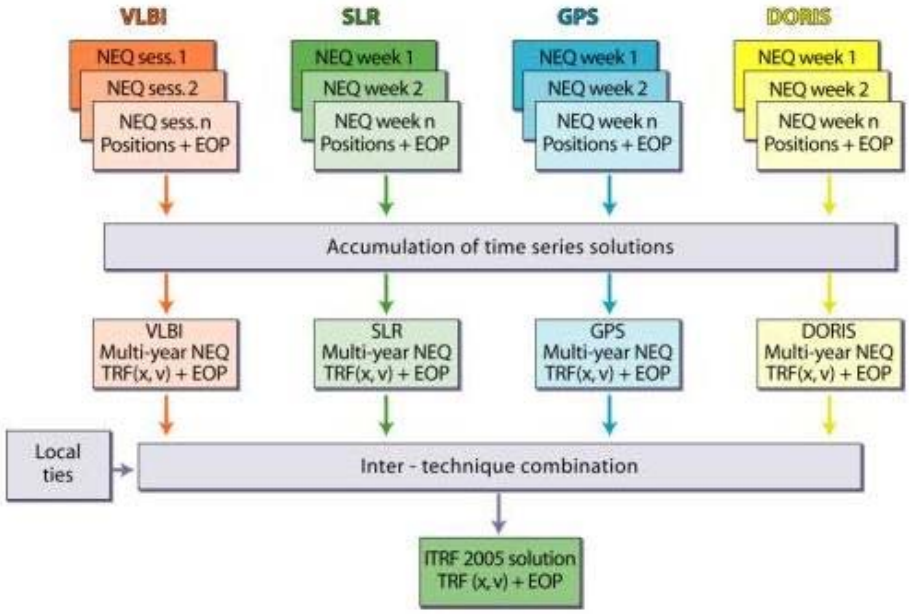

***Figure 1**. Data flow and computation procedure for the ITRF2005 solution of DGFI*

The final ITRF2005 solution comprises station positions, velocities and daily EOP estimates as primary results. In addition epoch position residuals and geocenter coordinates are obtained from the time series combination. The reference epoch for station positions is 2000.0. The rather inhomogeneous data quality and quantity of the space geodetic observation stations is reflected in the accuracy and reliability of the ITRF2005 station position and velocity estimations. This holds in particular for a number of SLR and VLBI stations, but also for some GPS and DORIS stations with few observations. Another aspect is that the new type of ITRF2005 solution contains many stations with several solution ID's. As a consequence the station positions and velocities are valid only for a certain period of time, which has to be known and considered by the users. Furthermore co-location sites may have different station velocities for co-located instruments, if their estimated velocities differ significantly.

Comparison of the ITRF2005 solutions of DGFI and IGN

For comparisons we performed similarity transformations between both solutions. These transformations were done separately for each technique by using good reference stations. The RMS differences for station positions and velocities show a very good agreement (after similarity transformations). This holds in particular for "good" stations with several years of continuous observations without discontinuities (Table 1). For weakly estimated stations (e.g., observation time < 2.5 years, different solutions caused by discontinuities) larger discrepancies do exist, which are in most cases within their standard deviations.

Most of the transformation parameters agree within their estimated standard deviations, except for the scale and its time variation of the SLR network. A significant difference of about 1 ppb (offset) and 0.13 ppb/yr (rate) between the ITRF2005P solutions of DGFI and IGN has been found, which accumulates to nearly 2 ppb in 2006 (see Table 2). The scale difference is not visible in the pure SLR intra-technique solutions of IGN and DGFI. This indicates that the difference between both ITRF2005P solutions is caused within the inter-technique combination.

From these comparisons it is obvious that the major problem of the ITRF2005 is the significant difference in the SLR scale. The analysis of weekly SLR solutions in 2006 has shown that the scale is in good agreement with the ITRF2005P solution of DGFI, whereas

there is a significant scale bias of about 2 ppb w.r.t. the IGN solution (see Figure 2), which is equivalent to a difference of 1.3 cm in SLR station heights. It was argued by IGN that this "scale problem" is a consequence of a scale bias between VLBI and SLR. Because of the apparent discrepancies the scale of the IGN solution was defined by VLBI only, whereas the scale of the DGFI solution is defined by the SLR and VLBI data.

***Table 1**. RMS differences for station positions and velocities between IGN and DGFI solutions for ITRF2005 for "good" Reference stations (25 VLBI, 22 SLR, 57 GPS, 40 DORIS stations).*

ITRF2005P DGFI - IGN	Positions [mm]	Velocities [mm/yr]
GPS	0.31	0.14
VLBI	0.79	0.34
SLR	1.82	0.66
DORIS	3.32	1.11

***Table 2**. Scale differences between the pure intra-technique and the ITRF2005P solutions of DGFI and IGN.*

	SLR		VLBI	
	offset [ppb]	drift [ppb/yr]	offset [ppb]	drift [ppb/yr]
Pure intra-technique solutions (IGN – DGFI)	-0.17 ± 0.06	0.01 ± 0.02	0.16 ± 0.05	0.01 ± 0.02
ITRF2005 P solutions (IGN – DGFI)	**0.86 ± 0.12**	**0.13 ± 0.03**	-0.12 ± 0.06	0.03 ± 0.03

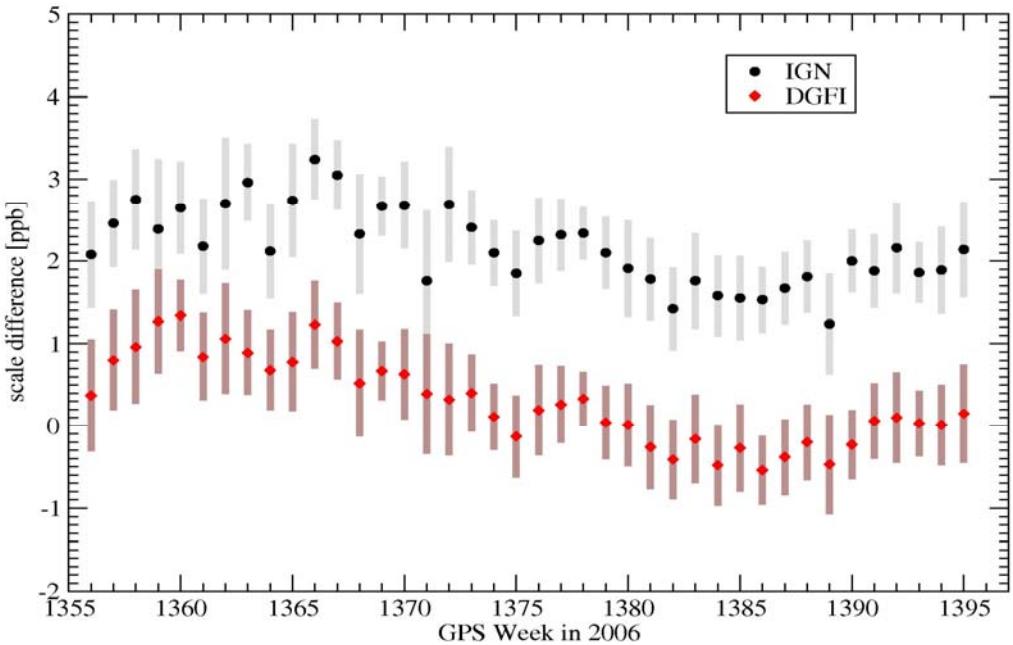

***Figure 2**. Scale of ITRF2005P solutions of IGN and DGFI w.r.t. to the combined SLR solution (ILRSA)*

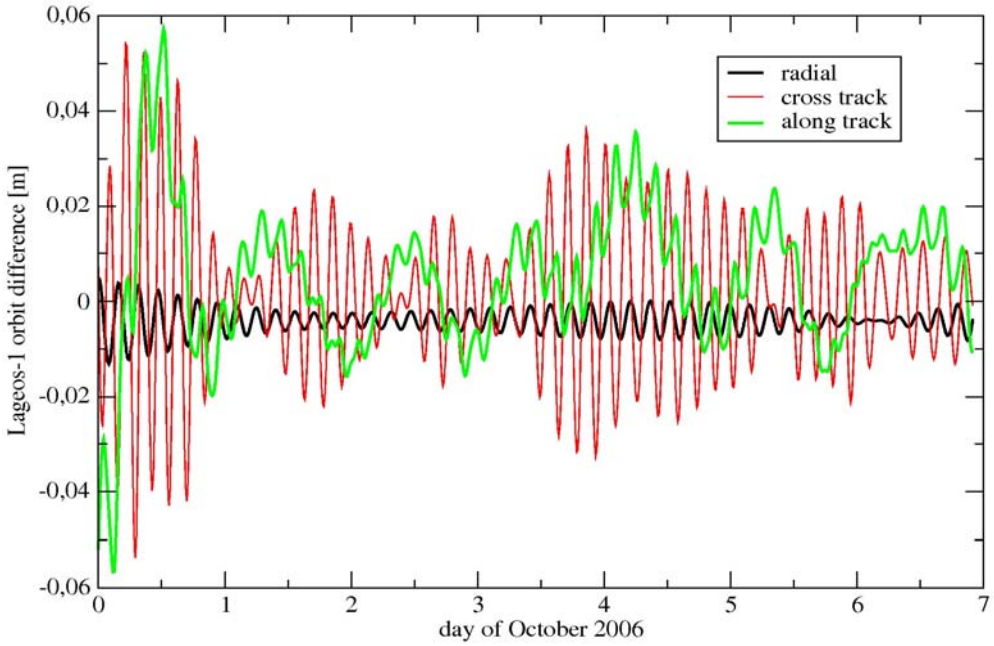

***Figure 3**. Difference between IGN and DGFI solution for a weekly Lageos-1 orbit.*

This scale difference is also reflected in the resulting satellite orbits. For a comparison we solved a weekly Lageos-1 orbit with fixed station coordinates, one with the DGFI solution, the other with the IGN solution, solving for all internal arc parameters and polar motion (X-, Y- pole and dUT1). The resulting orbits were compared in radial, cross- and along track to investigate the influence of the scale difference. In figure 3 the radial offset of about 5 mm is clearly visible. The cross and along track components only show a revolution dependent signal which results from the radial orbit bias, but there is no systematic error. This comparison indicates that the scale of the IGN solution will produce biased satellite orbits.

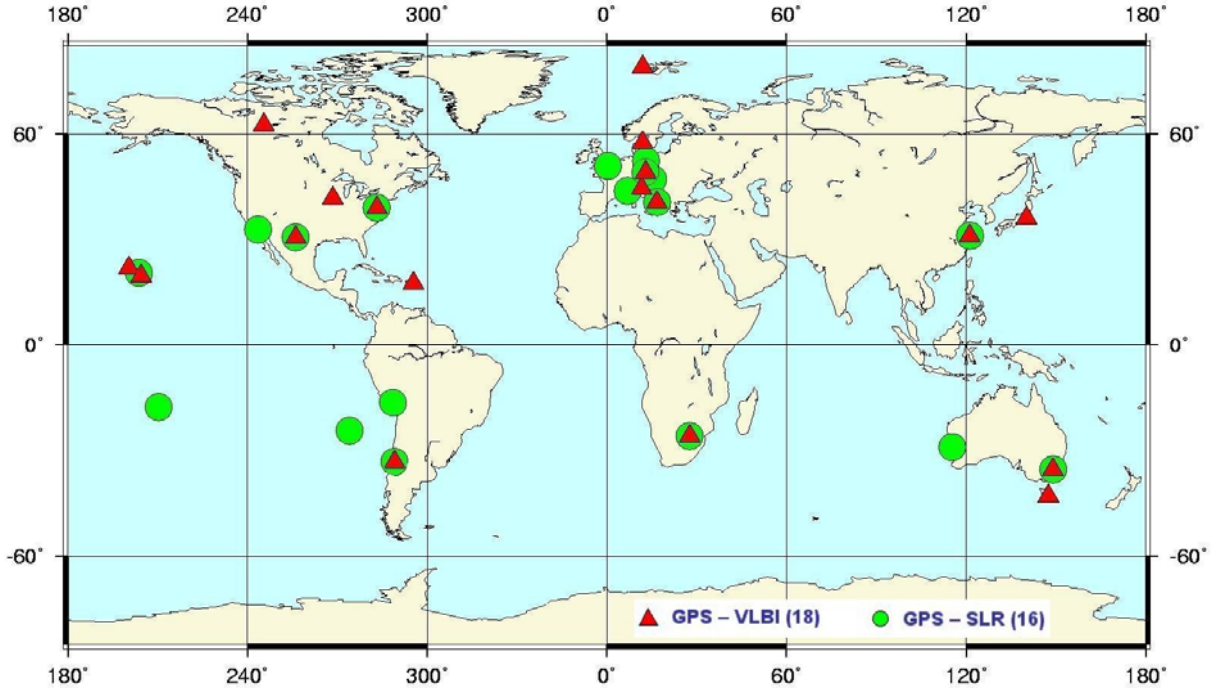

***Figure 4**. Available co-location sites between GPS, SLR and VLBI*

***Figure 5**. Observation period of southern hemisphere collocation sites*

Investigation of the scale differences

We used the intra-technique solutions of the DGFI combination for ITRF2005 to investigate the scale of VLBI and SLR. Since the number and spatial distribution of good co-location sites between VLBI and SLR is not sufficient to get reliable results for a direct comparison of the scale, we used an "indirect" approach via the GPS network and consider the GPS intra-technique solution as reference for this specific study. We used "good" co-location sites and local ties to refer the VLBI and SLR solutions to an "arbitrary" GPS frame (see Fig. 4).

The geographical distribution and quality of SLR tracking stations is in particular problematic in the Southern hemisphere. Therefore we focus on these stations and on the co-locations with GPS. Fig. 5 shows the GPS and SLR observation periods and the estimated ITRF 2005 precision for 8 SLR-GPS co-location sites on the southern hemisphere. DGFI used for the connection of the reference frames all stations except Easter Island and Conception because of poor SLR data. In the IGN solution the Australian sites Yarragadee, Mt. Stromlo, Orroral and Tahiti are down-weighted. Thus the reference frame connection in the IGN solution was realized mainly via the remaining 4 co-location sites on the Southern hemisphere, from which Easter Island and Conception are poorly observed by SLR. This indicates that the integration of GPS and SLR networks in the Southern hemisphere is rather poor in the IGN solution.

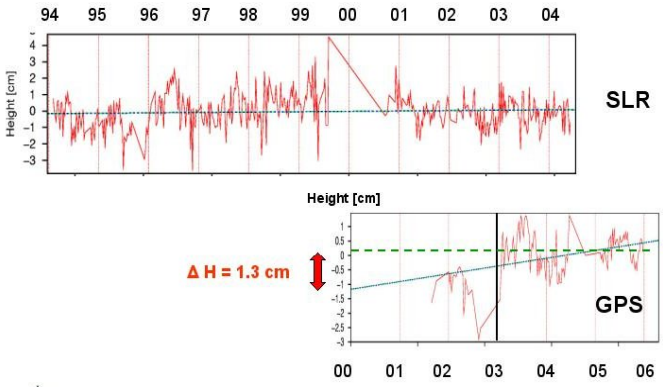

***Figure 6**. Jump in the Haleakala time series*

***Table 3**: Scale difference between SLR and VLBI obtained from DGFI ITRF2005P solution.*

	Δ Scale offset [ppb]	Δ Scale drift [ppb/yr]
SLR - VLBI	0.40 ± 0.42	0.04 ± 0.10
SLR – VLBI *	**0.26 ± 0.41**	**0.03 ± 0.09**

*** : Discontinuity for GPS station Maui introduced**

We also investigated the position time series of co-location sites. As an example Fig. 6 shows the GPS and SLR position time series for the co-location site Maui on Hawaii. A clear jump is visible in the GPS time series at the end of 2002, which affects the height estimation by about 1.3 cm. We have introduced a discontinuity for the GPS station Maui and we solved for two solutions. To test the influence of the jump we performed a 14 parameter similarity transformation between the GPS and SLR solutions and compared the resulting residuals. As shown in Fig. 7 the relatively large height residual for Maui disappeared completely.

The scale parameters obtained from the singularity transformations of the SLR and VLBI solutions w.r.t. GPS are arbitrary numbers, but the difference of the scale parameters is independent from the "arbitrary" GPS scale. The estimated scale difference between VLBI and SLR are shown in Table 3. If the discontinuity for GPS station Maui is introduced the scale differences are 0.26 ± 0.41 ppb for the offset and 0.03 ± 0.09 ppb/yr for the drift. Thus the results of the DGFI ITRF2005P solution do not indicate any evidence for a scale bias between VLBI and SLR.

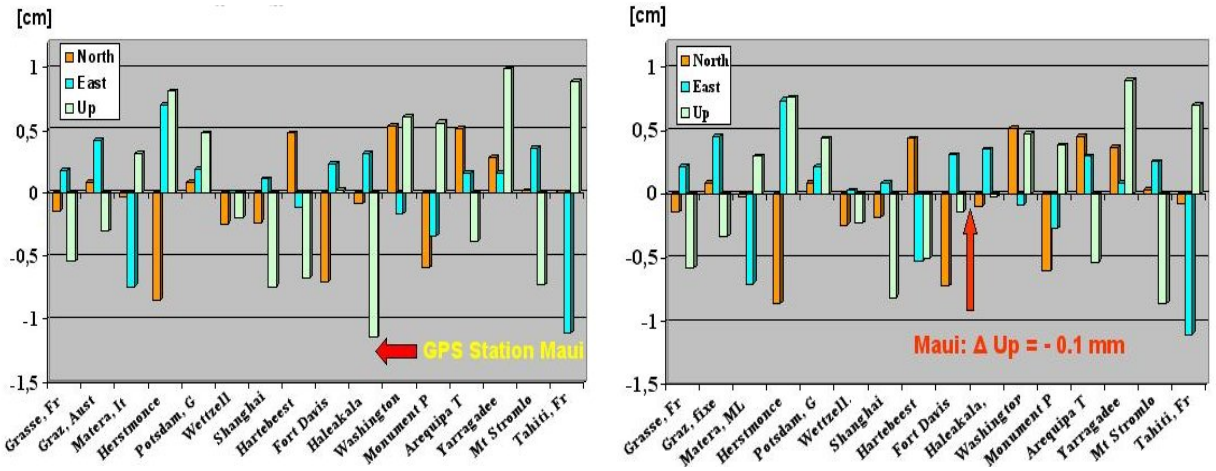

***Figure 7**. Station position residuals for 16 SLR-GPS colocation sites. The left figure shows a height residual for Maui of 1.2 cm, which is reduced to almost zero, if the jump for GPS station is introduced (see right figure).*

Conclusion

The DGFI and IGN for the ITRF2005 are in good agreement for the station positions and velocities (after similarity transformations), but a significant difference has been observed for the scale of the SLR network. As the discrepancies are not visible in the pure SLR intra-technique solutions of IGN and DGFI, they are most likely caused by a different combination procedure and in particular by the implementation of local tie information. Furthermore the IGN solution reveals an apparent difference in SLR and VLBI scales, which led to the exclusion of SLR data for the scale definition of the ITRF2005. The ITRF2005 solution of DGFI does not show this apparent scale difference between SLR and VLBI and it relies on the data of both techniques to define the scale. The analysis of the actual SLR tracking data show a good agreement with the scale of the ITRF2005 solution of DGFI, whereas there is a misfit of about 2 ppb w.r.t. the IGN solution.

Acknowledgement

The authors thank the ILRS (Pearlman et al,2002) for providing the SLR data and the combined weekly SLR intra-technique solutions. For the investigations on the SLR scale we used also the time series of GPS and VLBI intra-technique solutions kindly provided by the IGS and the IVS, respectively.

References

[1] Angermann D, Drewes H, Krügel M, Meisel B, Gerstl M, Kelm R, Müller H, Seemüller W, Tesmer V (2004) ITRS Combination Center at DGFI: A terrestrial reference frame realization 2003, Deutsche Geodätische Kommission, Reihe B, Heft Nr. 313.

[2] Angermann D, Drewes H, Krügel M, Meisel B (2006) Advances in terrestrial reference computations, IAG Symposia Cairns, Springer.

[3] Drewes H, Angermann D, Gerstl M, Krügel M, Meisel B, Seemüller W (2006) Analysis and Refined Computations of the International Terrestrial Reference Frame, Observation of the Earth System from Space, Flury, Rummel, Reigber, Rothacher, Boedecker, Schreiber (Eds), 343-356, Springer.

[4] Krügel M and Angermann D (2006) Frontiers in the combination of space geodetic techniques Proceedings of IAG Symposia Cairns, Springer.

[5] Meisel B, Angermann D, Krügel M, Drewes H, Gerstl M, Kelm R, Müller H, Seemüller W, Tesmer V (2005) Refined approaches for terrestrial reference frame computations, Adv Space Res 36, 350-357, Elsevier.

[6] Pearlman, M.R., Degnan, J.J., and Bosworth, J.M., "The International Laser Ranging Service", Advances in Space Research, Vol. 30, No. 2, pp. 135-143, July 2002.

Determination of the Temporal Variations of the Earth's Centre of Mass from Multi-Year Satellite Laser Ranging Data

Ramesh Govind[1]

1. Geoscience Australia, Canberra, Australia

Abstract

Temporal variation of geodetic parameters (station positions, Earth's gravity field) that are used to monitor global change are referred to a time-varying terrestrial reference system (geocentre, orientation). The time evolution of the geocentre referred to the origin of the terrestrial reference system can be determined from estimates of degree one spherical harmonic representation of the Earth's gravity field. Weekly estimates of the degree one coefficients were undertaken for the period spanning 1993.0 to 2006.8 using SLR data from the global network for four satellites (Lageos-1, Lageos-2, Stella, Starlette). The data set, computation process and results of the geocentre estimates are presented. A comparison of the geocentre estimates from the satellite pairs at two different altitudes is shown. A system to "visualise" the motion of the geocentre as an indicator of mass transport is proposed.

Contribution of Satellite and Lunar Laser Ranging to Earth Orientation Monitoring

D.Gambis[1], R. Biancale[2]

1. Paris Observatory, France
2. CNES Toulouse, France

Abstract

Lunar and Satellite Laser Ranging have been contributing for several decades to Earth orientation variations monitoring. UT0 derived from LLR was used for the period 1976 to 1982 and made the transition between Astrometry and VLBI techniques. Polar motion derived from Lageos observations has a significant contribution in the IERS combinations, mainly thanks to its long term stability. So far Earth orientation parameters and ITRF are derived separately leading to inconsistencies. Rigorous approaches to simultaneously determine a terrestrial reference frame (TRF) and Earth Orientation Parameters (EOP) are now being developed either using SINEX files derived from the different techniques or at the observation level. We present here the results from a coordinated project within the Groupe de Recherches de Geodesie Spatiale (GRGS). Observations of the different techniques VLBI, SLR, LLR, DORIS and GPS) are separately processed by different Analysis centres using the software package GINS DYNAMO. The strength of the method is the use of a set of identical up-to-date models and standards in unique software. The normal equation matrices obtained by the different groups are then stacked to derive weekly solutions of station coordinates and Earth Orientation Parameters (EOP). Results are made available at the IERS site (ftp iers1.bkg.bund.de) in the form of SINEX files.

The analyses we have performed show that for the accuracy and stability of the EOP solution is very sensitive to a number of critical parameters mostly linked to the terrestrial reference frame realization, i.e. minimum constraints application and localities. We present the recent analyses and the latest results obtained.

Station Positioning and the ITRF

Zuheir Altamimi[1]

1. Institut Geographique National, ENSG/LAREG, 6-8 Avenue Blaise Pascal, 77455 Champs-sur-Marne, FRANCE

Abstract

The International Terrestrial Reference Frame (ITRF) as a realization of the International Terrestrial Reference System is one of the scientific products of the International Earth Rotation and Reference Systems Service (IERS). The ITRF is the standard frame recommended for a variety of applications, from surveying to the very fine studies in Earth Sciences. In order to satisfy science requirements, the ITRF should be accurate, reliable and internally consistent over time with unambiguously specified datum definition (origin, scale, orientation and their respective time evolution). Starting with the ITRF2005, the input data requested for the ITRF construction are under the form of time series of station positions and Earth Orientation Parameters (EOPs). Such data do not only allow an appropriate evaluation of the frame accuracy and internal consistency, but also are adequately suited to measure the positioning performance of space geodesy techniques. This paper attempts to review the positioning performance of space techniques via the analysis of the submitted time series to ITRF2005. A special focus will also be given to address the current accuracy level of the ITRF datum definition.

Introduction

The concept of reference systems and frames is one of the fundamental mathematical foundations of modern geodesy with the advent of space techniques since the early eighties. We refer to the pioneering work by a certain number of geodesists and astronomers in (Kovalevsky et al., 1989) who established the foundation of the concept of reference systems and frames followed and used as a basis for the ITRF derivation. Indeed, it is fundamental to adopt that clearly defined concept which distinguish between the system as a theoretical inaccessible mathematical model and the frame as the numerical realization of the system. Moreover, the frame is not only accessible to the users but it is also by essence perfectible, being based on and derived from space geodesy observations.

Using the commonly accepted model of 7(14)-parameter euclidian similarity (also known as Helmert or Bursa-Wolf parameters), it becomes then straightforward to estimate discrepancies between solutions over the frame physical parameters. This is the case for instance where large translation components are often found between SLR on one hand and GPS or DORIS solutions on the other hand. Less scattered temporal behavior of the SLR translation components (as seen from time series analysis), compared to GPS or DORIS, leads to privilege SLR for the ITRF origin definition. Regarding the scale, it is of course admitted that from the theoretical and technology point of view, VLBI and SLR techniques should agree on the TRF scale. However, because we have the possibility to check for their scale consistency (or inconsistency), then when comparing their respective solutions, the possible inconsistency is obviously due to some systematic errors that should be investigated.

The ITRF Product Center hosted by the Institut Géographique National, France, together with the contribution of the ITRF combination centers (DGFI and NRCan) released the ITRF2005 solution in October 2006. Contrary to previous ITRF versions,

the ITRF2005 integrates time series of station positions and daily Earth Orientation Parameters (EOP's). The ITRF2005 input time-series solutions are provided in a weekly sampling by the IAG International Services of satellite techniques: the International GNSS Service-IGS (Dow et al. 2005), the International Laser Ranging Service-ILRS (Pearlman et al., 2002) and the International DORIS Service-IDS, (Tavernier et al., 2006), and in a daily (VLBI session-wise) basis by the International VLBI Service-IVS (Schlueter et al., 2002). Each per-technique time-series is already a combination, at a weekly basis, of the individual Analysis Center (AC) solutions of that technique, except for DORIS where two solutions are submitted by two ACs, namely the Institut Géographique National (IGN) in cooperation with Jet Propulsion Laboratory (JPL) and the Laboratoire d'Etudes en Geophysique et Oceanographie Spatiale (LEGOS) in cooperation with Collecte Localisation par Satellite (CLS), designated by (LCA).

Reasons for which it was decided to use time series of station positions and EOPs as input to ITRF2005 include:

- monitoring of non-linear station motions and all kinds of discontinuities in the time series: Earthquake related ruptures, site instability, seasonal loading effects, etc;
- rigorously and consistently including EOPs in the combination and ensuring their alignment to the combined frame;
- examining the temporal behavior of the frame physical parameters, namely the origin and the scale;
- assessing space geodesy positioning performance, through the estimation of the weekly (daily) Weighted Root Mean Scatter (WRMS) with respect to the long-term solution resulting from the stacking of the time series.

In the following sections we will primarily focus on two main issues: the positioning performance of space geodesy techniques and the temporal behavior of the SLR origin and the scale and the VLBI scale of the contributed solutions to the ITRF2005.

Combination Methodology

The approach that is currently adopted for the combination of various TRF solutions provided by a single or several space geodesy techniques is built on the construction of a unique (combined) TRF, making use of the mathematical (7)14-parameter euclidian similarity. It considers defining the combined TRF at a given (arbitrary) reference epoch and adopting a TRF time evolution law that is supposed to be linear (secular). Consequently, 14 degrees of freedom are always necessary to completely ensure the TRF datum definition: 6 for the TRF origin and its rate (time derivative), 2 for the scale and its rate and 6 for the orientation and its rate. The inclusion of EOPs into the combination requires additional equations where the link between the TRF and EOPs is ensured via the 6 orientation parameters. The combination model considered by the ITRF Product Center allows the estimation of station positions and velocities, transformation parameters of each individual TRF solution with respect to the combined TRF and, if included, consistent series of EOPs. The input solutions usually used in this kind of combination are either (1) time series of station positions and EOPs or (2) long-term solutions composed by station positions and velocities and EOPs. In the first case where the combination amounts to rigorously stacking the time series, the un-modeled non-linear part of geodetic parameters are implicitly embedded in the combination output: possible seasonal (e.g. annual or semi-annual) station or/and geocenter motions are respectively left in the output time series of

station residuals and the transformation parameters. For more details, regarding the combination methodology the reader may refer to (Altamimi et al. 2007a, 2007b).

Positioning Performance

When stacking station positions time series (weekly for satellite techniques and daily for VLBI), global WRMS per week (day) is computed, that is to characterize the internal precision and repeatability over time of each individual position time series. Figure 1 illustrates the WRMS per week (day) for each one of the 4 technique time series over the horizontal and vertical components and Table 1 summarizes the WRMS range. It is to be noted that the WRMS values do not qualify the techniques, but rather the solutions of the techniques which were submitted to the ITRF2005, and they are highly dependent on the quality of each station/instrument. Other factors are also important such as the number of the satellites available, e.g. in case of DORIS it was shown (Altamimi et al. 2006) that the quality (WRMS) improves when the number of satellites increases. However, from Figure 1 and Table 1, we can postulate that the current positioning performance for the best cases is around 2 mm for the horizontal component and around 5 mm for the vertical component.

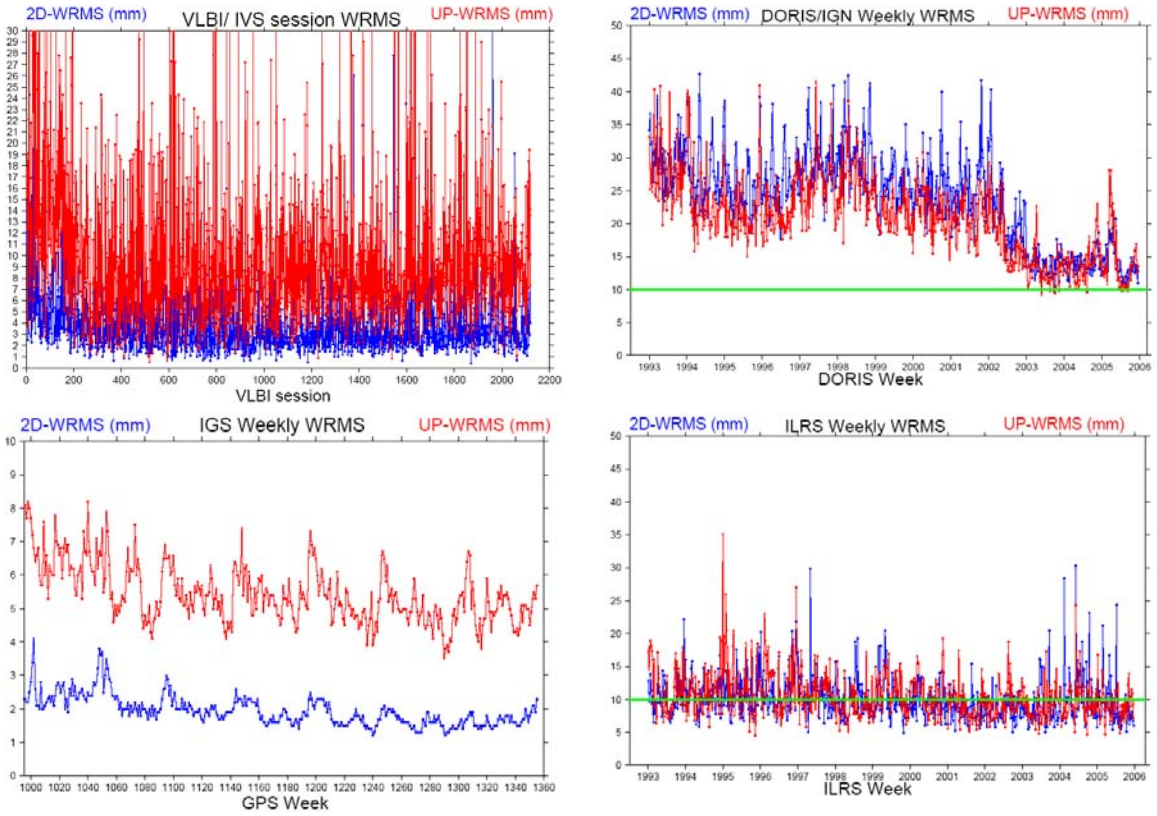

***Figure 1**. Weekly (daily) WRMS as results from the time series stacking.*

Accuracy of the ITRF Origin and Scale

The Origin

Although it is hard to assess the origin accuracy of the single ILRS solution that is submitted to ITRF2005, we attempt however to evaluate its consistency with respect to ITRF2000. Figure 2 shows the 3 translation time variations with respect to ITRF2000, using a reference set of 12 stations. Given their observation history and good performance, these are the only stations that are usable to link the combined

Table 1. *WRMS range per technique*

Solution	2-D WRMS mm	Up WRMS mm
VLBI	2-3	5-7
SLR	5-10	5-10
GPS	2-3	5-6
DORIS	12-25	10-25

SLR TRF resulting from the stacking of the time series to the ITRF2000 frame. Because the estimated transformation parameters are heavily sensitive to the network geometry, the distribution of the reference set of 12 stations is far from being optimal; only two of them are in the southern hemisphere (Yaragadee, Australia, and Arequipa, Peru). Apart from the seasonal variations that could be estimated over the translation parameters, the linear trends are of great importance to the ITRF origin stability over time. From Figure 2 we can easily see that the most significant trend is that of the Z-translation component, being of the order of 1.8 mm/yr. This bias will therefore exist between ITRF2000 and ITRF2005, and could be regarded as the current level of the origin accuracy as achieved by SLR. From that figure we can also distinguish a "piece-wise" behavior of the Z-translation: between respectively 1993-1996; 1996-2000 and 2000-2006. In our opinion, this is completely related to and correlated with the change of the ILRS network geometry over time. In order to illustrate that effect, we plotted on Figure 3 the number of SLR stations available in each weekly solution. From this plot, one can easily see the decreasing tendency of the number of stations, starting around 2000, which should be correlated with the Tz component that starts to significantly drifting at this same epoch (see Figure 2). In addition, among the approximately 80 SLR stations available in the ITRF2005, approximately 20 of them have sufficient time-span of observations to be considered as core stations for useful and comprehensive analysis.

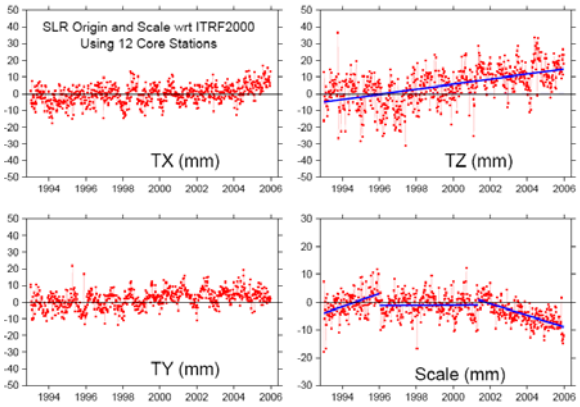

Figure 2*. Translations and scale variations with respect to ITRF2000 of the ILRS SLR time series submitted to ITRF2005.*

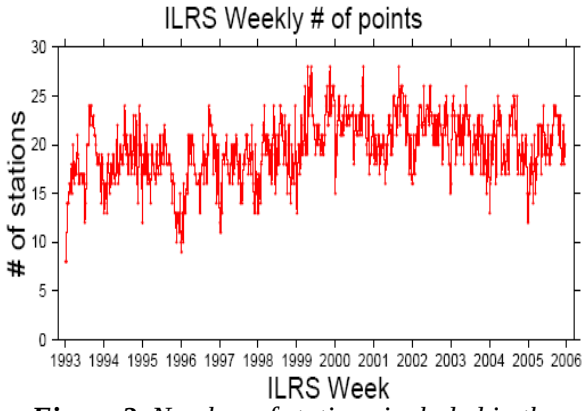

Figure 3*. Number of stations included in the weekly ILRS SLR time series submitted to the ITRF2005.*

The Scale

The ITRF2005 combination (making use of local ties in co-location sites) revealed a scale bias of 1 ppb between VLBI and SLR solutions at epoch 2000.0 and a scale drift of 0.08 ppb/yr. VLBI scale selected to define that of ITRF2005 is justified by (1) the availability of the full VLBI history of observations (26 years versus 13 for SLR)

embedded in the submitted time series and (2) the the non-linear behavior (discontinuities) observed in the ILRS scale (see Figures 3). In order to illustrate more the inconsistency between the two scales, Figure 4 displays both scales with respect to ITRF2005, showing a clear bias both in the offset and the linear trend.

The accuracy assessment of the ITRF scale is not easy to evaluate, being dependent on several factors, as for instance, the quality and distribution of the local ties, the SLR range bias effect, the tropospheric modeling in case of VLBI and other possible systematic errors of the two techniques. However, given the level of consistency mentioned above between VLBI and SLR scales and despite the optimistic accuracy estimate of the ITRF2000 datum definition as stated in (Altamimi et al., 2002), and to be more conservative, we can postulate that the current level of accuracy of ITRF scale is around 1 ppb and 0.1 ppb/yr.

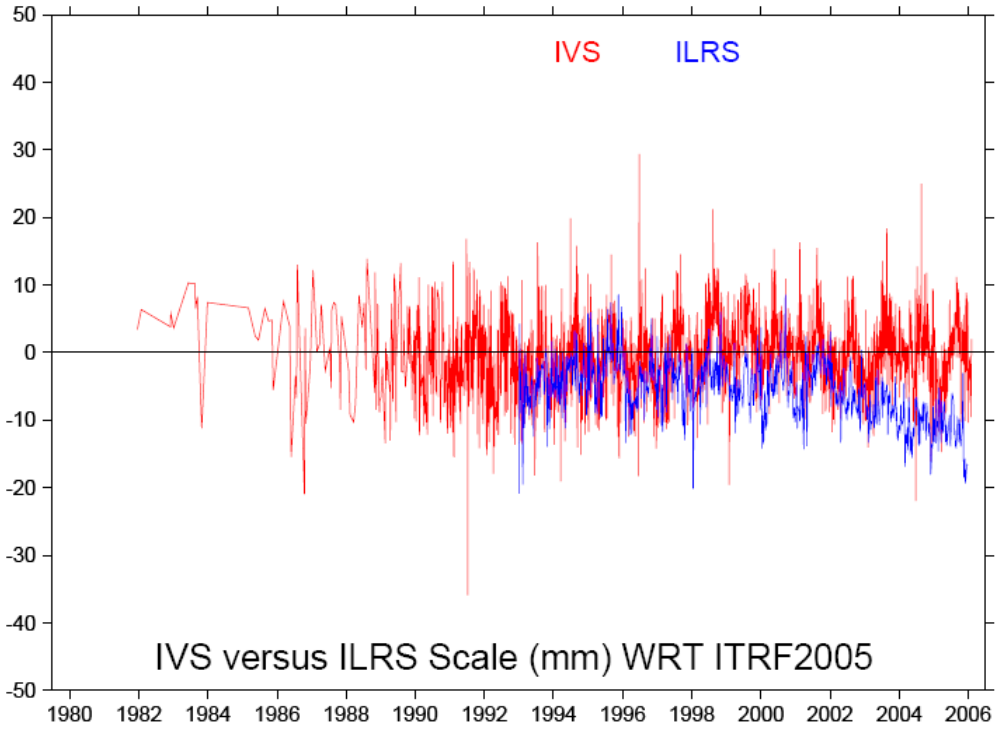

***Figure 4**. VLBI and SLR Scale factor variations with respect to ITRF2005.*

Conclusion

The ITRF2005 experience, using time series as input data, showed how sensitive the frame parameters are to the network geometry and in particular in case of SLR and VLBI and their co-locations. The scale bias between VLBI and SLR solutions revealed by the ITRF2005 combination is most probably due to multiple reasons that include poor VLBI and SLR co-locations, local tie uncertainties, systematic errors and possible differences in correction models (e.g. troposphere, SLR range bias, relativity) employed in the data analysis of both techniques. As results from the ITRF2005 analysis, the positioning performance at the weekly/daily basis, range between 2 to 25 mm, depending on the measurement technique, the instrument quality or station performance.

References

[1] Altamimi, Z., P. Sillard and C. Boucher (2002), ITRF2000: A New Release of the International Terrestrial Reference Frame for Earth Science Applications, Journal of Geophys. Res., 107(B10), 2214, doi:10.1029/2001JB000561.

[2] Altamimi, Z., X. Collilieux and C. Boucher, (2007a), Accuracy assessment of the ITRF datum definition, VI Hotine-Marussi Symposium of Theoretical and Computational Geodesy: Challenge and Role of Modern Geodesy, International Association of Geodesy, in press.

[3] Altamimi, Z., X. Collilieux J. Legrand, B. Garayt and C. Boucher, (2007b), ITRF2005: A new release of the International Terrestrial Reference Frame based on time series of station positions and Earth Orientation Parameters, Journal of Geophys. Res., in Press.

[4] Altamimi, Z., X. Collilieux, C. Boucher, 2006, DORIS Contribution to ITRF2005, Journal of Geodesy, doi: 10.1007/s00190-006-0065-5.

[5] Dow J.M, R.E. Neilan and G. Gendt, 2005, The International GPS Service (IGS): Celebrating the 10th Anniversary and Looking to the Next Decade, Adv. Space Res. 36 vol. 36, no. 3, pp. 320-326, doi:10.1016/j.asr.2005.05.125.

[6] Kovalevsky, J., Mueller, I. I., and B. Kolaczek (Eds.), 1989, {\it Reference Frames in Astronomy and Geophysics,} 474 pp., Kluwer Academic Publisher, Dordrecht.

[7] Pearlman, M.R., J.J. Degnan and J.M. Bosworth, 2002, The International Laser Ranging Service, Adv. Space Res., Vol. 30, No. 2, pp. 135-143.

[8] Schlueter W., E. Himwich, A. Nothnagel, N. Vandenberg, and A. Whitney, 2002, IVS and Its Important Role in the Maintenance of the Global Reference Systems, Adv. Space Res., Vol. 30, No. 2, pp. 145-150.

[9] Tavernier, G., H. Fagard M. Feissel-Vernier, K. Le Bail, F. Lemoine, C. Noll, R. Noomen, J.C. Ries, L. Soudarin, J.J Valette, and P. Willis, 2006, The International DORIS Service: genesis and early achievements, in DORIS Special Issue, P. Willis (Ed.), Journal of Geodesy, 80(8-11):403-417, doi: 10.1007/s00190-006-0082-4.

Station Coordinates, Earth Rotation Parameters, and Low Degree Harmonics from SLR within GGOS-D

R. Koenig[1], H. Mueller[2]

1. GeoForschungsZentrum Potsdam (GFZ)
2. Deutsches Geodaetisches Forschungsinstitut (DGFI), Alfons-Goppel-Str. 11, 80539 Muenchen.

Contact: koenigr@gfz-potsdam.de

Abstract

Time series of station coordinates, Earth rotation parameters, and low degree harmonics of the gravity field are generated in weekly batches from Satellite Laser Ranging (SLR) measurements by two independent German institutes, the Deutsches Geodaetisches Forschungsinstitut (DGFI) and the GeoForschungsZentrum Potsdam (GFZ) and their two software packages for parameter and orbit determination, DOGS (DGFI Orbit and Geodetic Parameter estimation Software) and EPOS (Earth Parameter and Orbit System) respectively.

The products are based on common standards laid down by a consortium of some more German institutes joined in the GGOS-D (Global Geodetic Observing System - Deutschland (Germany)) project. GGOS-D strives for a rigorous and proper combination of the various space-geodetic techniques. The details of the processing and model standards and the differences with the International Laser Ranging Service (ILRS) "pos&eop" products are presented. A first series covering the years 1993 to 2006 has recently been provided by DGFI and GFZ to the project, initial results are shown and compared.

Introduction

The overall objective of the GGOS-D project is the investigation of the technological, methodological and information-technological realization of a global geodetic-geophysical observing system. The main fields of research are the development and implementation of data collection and data management systems as well as the generation of consistent and integrated geodetic time series for the description and modelling of the geophysical processes in the Earth system. The time series have to be referred to a unique, extremely accurate reference frame, stable over decades, and should be generated in such a way that they can be made available in near real-time to all users in science and society. Methods for a careful internal and external validation shall guarantee a very high reliability.

The space-geodetic techniques, i.e. Global Positioning System (GPS), SLR, and Very Long Baseline Interferometry (VLBI) with the exception of Doppler Orbitography and Radiopositioning Integrated by Satellite (DORIS), contribute to the processing with the models and as far as possible with the same set of parameters being applied by all the participating institutions, the Forschungsgruppe Satelliten Geodaesie (FSG), the Geodetic Institute of the University of Bonn (GIUB), the GFZ, the Bundesamt fuer Kartografie und Geodaesie (BKG), and the DGFI. The SLR part is covered by two independent contributions from DGFI with its DOGS and from GFZ with its EPOS software packages. The analysis should span the period 1983 until present date. A first solution beginning in 1993 up to early 2007 has recently been provided.

Processing

Geometric and dynamic models mainly coincide with those recommended for the routine processing of the so-called “pos&eop” product, weekly station coordinates and Earth Orientation Parameters (EOPs) based on SLR, by the ILRS (see Pearlman et al., 2002) analysis centers (DGFI and GFZ being part there as well). In case of the dynamic models however, the ocean tide model FES2004 (Letellier et al., 2007), and the gravity field model EIGEN-GL04S1 (the satellite-only solution of the EIGEN-GL04C model, see Foerste et al., 2006) have been chosen. Also the ocean tide loading site displacements as provided by Bos and Scherneck (2007) corresponding to the FES2004 are applied.

In a first step we processed weekly arcs for the years 1993 to 2006 solving for weekly stations coordinates, daily EOPs, i.e. X-, Y- pole, and UT1 at 0:00 h UTC, all piecewise linear and continuous (in case of “pos&eop” instead X-, Y- pole, and, notably, LOD at 12:00 UTC, all piecewise constant, are solved for). The GFZ solution additionally incorporates the low degree coefficients of the spherical harmonic representation of the Earth's gravity field (shortly “low degree harmonics”) of degree 0 to 2 (in case of “pos&eop” the low degree harmonics are not solved for). In order to overcome the datum defect, the coordinates, the EOPs, and the low degree harmonics are endowed with an a priori sigma of 1 meter or its equivalent.

First Results

The overall orbital fit and statistics for the whole period are shown in Table 1. The intention was to include as many stations as possible in the solutions. As a minimum however, stations should contribute with more than 10 observations per weekly arc. Besides that, iterative editing has been performed according to some criteria chosen individually by both institutes. This becomes evident in the number of observations used for the processing and the resulting orbital fit, and could end up in some differences of the solved-for parameters. In a next step, DGFI and GFZ are going to compare their editing procedures and to analyse the effect on the solution.

Table 1*. Global orbital fit of the two solutions.*

	EPOS	**DOGS**
No. of Arcs	742	759
Period	25-Oct-1992 - 13-Jan-2007	11-Nov-1992 - 20-May-2007
Global Orbital Fit RMS (cm)	1.04	1.07
No. of Observations	1,749,965	1,997,569
No. of Observations per Arc	2,358	2,632

In Figure 1 the weekly orbital fits of the DGFI solution show that some weeks are determined with worse accuracy, especially prior to 1999 or GPS week 990. This is mainly induced by some poorly performing non-core stations, the orbital fit for the core stations remains stable mostly below 1 cm all over the analysis period. In general, Lageos-1 turns out slightly more accurate than Lageos-2. Once up-to-date corrections for the Stanford-counter range bias problems or for the station dependent centre of mass corrections become available, we expect improved orbits and hence an improved quality of the resulting parameters.

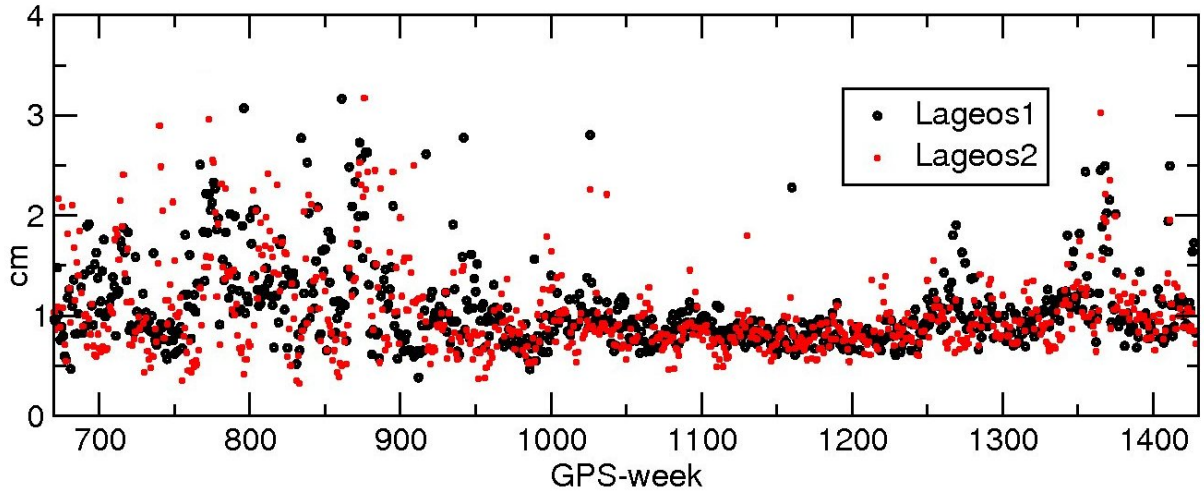

***Figure 1**: Weekly orbital fits of the DOGS solutions.*

Figure 2 shows a comparison of the GFZ C_{20} time series to the recently published series by Cheng and Tapley (2005). Obviously the GFZ series shows a larger scatter, being mainly an effect of the dense resolution of the parameters and of the multitude of solved-for parameters. A generalization of the coordinate and low degree harmonic parameters would presumably stabilize the solution. Underneath the scatter, the general agreement of the curves is visible.

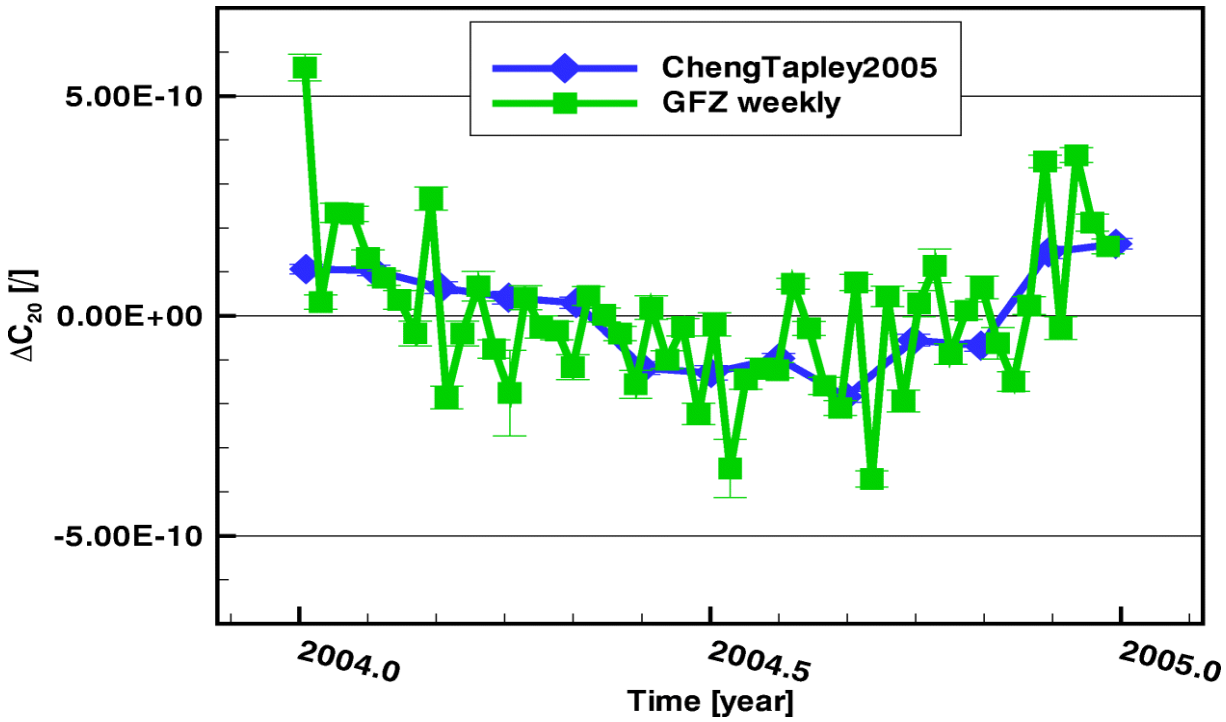

***Figure 2**: Comparison of the EPOS C_{20} time series to the Cheng and Tapley (2005) series.*

The scale differences between the DOGS and the EPOS coordinate solutions are shown in Fig. 3. A small offset of about 1 ppb is visible and may be related to the different editing and to the fact that the GFZ solution has solved in addition for the low degree harmonics including C_{00}, the dynamic scale parameter. The alignment of the editing criteria for DOGS and EPOS, and solving for the low degree harmonics in the DOGS solution as well, should improve the agreement. Also, Fig. 3 reveals a

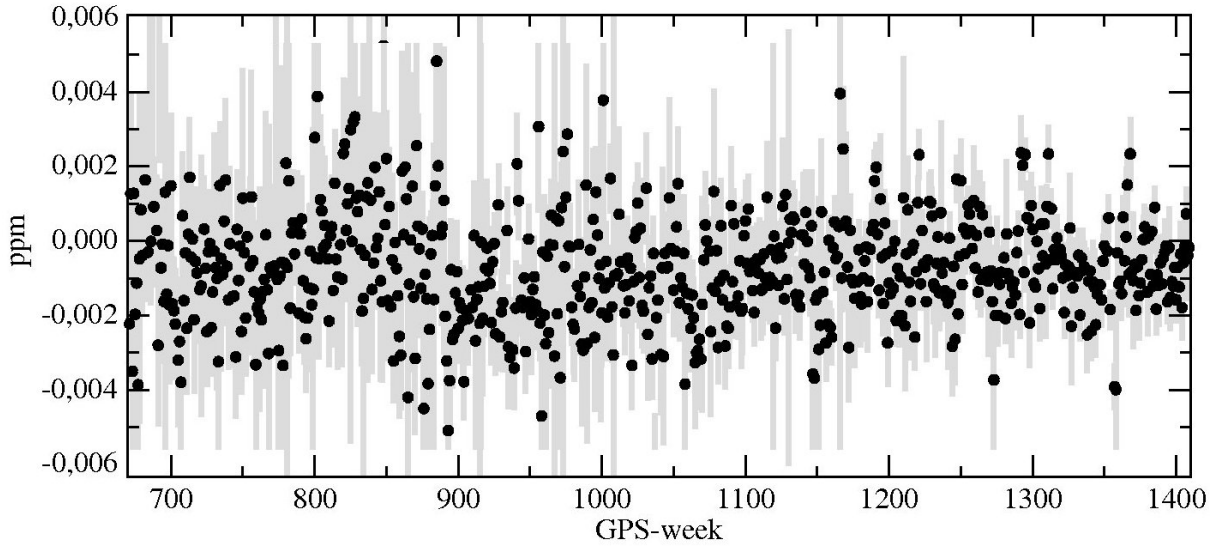

Figure 3*: Scale differences between the DOGS and EPOS coordinate solutions 1993-2007.*

decrease of the scatter in the course of time, demonstrating the improvement and stabilization of the SLR technique.

Conclusions

Within the GGOS-D project, DGFI and GFZ are processing SLR data with their independent software packages DOGS and EPOS based on common, modern standards. In a first iteration, a 14 year long time series of weekly solutions for coordinates, EOPs, and, in case of GFZ, for low degree harmonics, has been generated. The standards adopted here are different with respect to those of the routine ILRS analysis centre processing.

First results show an excellent quality of the two SLR solutions. Some efforts have to be undertaken to harmonize in particular the editing of the weekly arcs and to include the low degree harmonic parameters to the DGFI solution.

The combination of all space-geodetic techniques within GGOS-D is pending, but first preliminary combinations of GPS and VLBI results indicate an excellent agreement, better than that experienced earlier during the ITRF2005 combinations by DGFI (Meisel et al., 2005).

References

[1] Bos, M.S., Scherneck, H.-G.: *The free ocean tide loading provider website*. http://www.oso-.chalmers.se/~loading, modified 02/03/2007.

[2] Cheng, M., Tapley, B.D.: *Correction to „Variations in the Earth's oblateness during the past 28 years“*. Journal of Geophysical Research, 110, B03406, doi:10.1029/2005JB003700, 2005

[3] Förste, C., Flechtner, F., Schmidt, R., König, R., Meyer, U., Stubenvoll, R., Rothacher, M., Barthelmes, F., Neumayer, H., Biancale, R., Bruinsma, S., Lemoine, J.-M., Loyer, S., *A mean global gravity field model from the combination of satellite mission and altimetry/gravimetry surface data – EIGEN-GL04C*. Geophysical Research Abstracts, 8, 03462, 2006

[4] Letellier, T., Lyard, F., Lefebre, F.: *The new global tidal solution: FES 2004.* http://www.joss-.ucar.edu/joss_psg/meetings/Archived/TOPEX2004/abstracts/D/Letellier.htm, modified 06/-27/2007.

[5] Meisel B, Angermann D, Krügel M, Drewes H, Gerstl M, Kelm R, Müller H, Seemüller W, Tesmer V: *Refined approaches for terrestrial reference frame computations.* Advances in Space Research, Vol. 36, 350-357, Elsevier, 2005

[6] Pearlman, M.R., Degnan, J.J., Bosworth, J.M.: *The International Laser Ranging Service.* Advances in Space Research, 30, 135-143, doi:10.1016/S02731177-(02)00277-6, 2002

An original approach to compute Satellite Laser Range biases

D. Coulot[1], Ph. Berio[2], O. Laurain[2], D. Féraudy[2], P. Exertier[2]

1. IGN/LAREG - Marne-la-Vallée – France
2. CNRS/OCA/GEMINI - Grasse – France

Contact: David.Coulot@ensg.ign.fr / Fax: +33-1-64-15-32-53

Abstract

Although they are permanently calibrated, the Satellite Laser Ranging (SLR) stations can present residual systematic errors, the well-known "range biases". These biases must be considered in any SLR data processing. Indeed, they are strongly correlated with the Up component of the station positions. Thus, if they are not computed together with these positions, they can induce jumps in these latter and consequently damage the global scale factor of the underlying Terrestrial Reference Frame with respect to any given reference.

On the other hand, estimating range biases together with station positions is not so easy, due to the previously mentioned correlations. In this paper, we describe a new approach to derive range bias values together with station positions: the so-called "temporal de-correlation" approach. This method consists in computing station range biases per satellite over a "long" period of time (determined by instrumental changes) together with weekly station position time series in order to significantly reduce the correlations.

Introduction

This paper comprises four parts. First, we provide general considerations about the Satellite Laser Ranging (SLR) technique range biases. Second, we demonstrate the strength of our temporal de-correlation approach through numerical illustrations based on simulations. Then, we analyze the first results produced by this method which has already been used for CALVAL (CALibration/VALidation) experiments and for a SLR data analysis carried out over 12 years. Finally, we describe the recent method improvements, provide the results of this new approach, and produce some conclusions and prospects.

1. General considerations

Fig. 1 shows the Grasse SLR station (7835) Up component time series computed in ITRF2000 without considering any range bias. We can clearly detect a jump in these time series and the epoch of this jump (September 1997) corresponds to a modification of the detection system of the station. This detection system modification has certainly modified the station detection and, as a consequence, its associated systematic errors. As shown by this example, a great attention must be paid to the SLR biases.

As shown on Fig. 2, the International Laser Ranging Service (ILRS) monitors these range biases. Indeed, among all the quality criteria used to qualify the tracking stations, two are directly linked to these biases: the short and long-term bias stabilities.

- The short-term stability is computed as the standard deviation about the mean of the pass-by-pass range biases.

- The long-term stability is the standard deviation of the monthly range bias estimates.

Regarding the data analysis, the situation does not seem to be so clear. Indeed, there are various strategies used to take into account these range biases: not to take biases into account, to correct a priori data with estimated bias values, to compute weekly range biases, etc. This paper aims to describe a method close to the instrumental evolutions of the considered stations. This method allows us to derive range biases by taking into account the problems linked to the simultaneous computation of these latter and station positions.

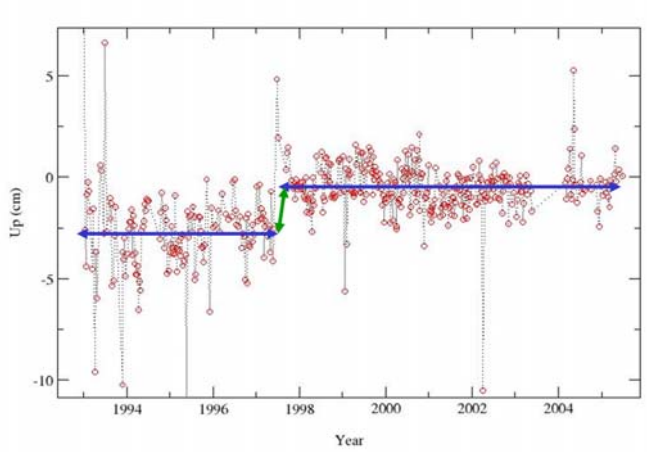

Figure 1. *Up component time series (in cm) of Grasse SLR station (7835) in ITRF2000. No range bias has been estimated nor applied during this computation.*

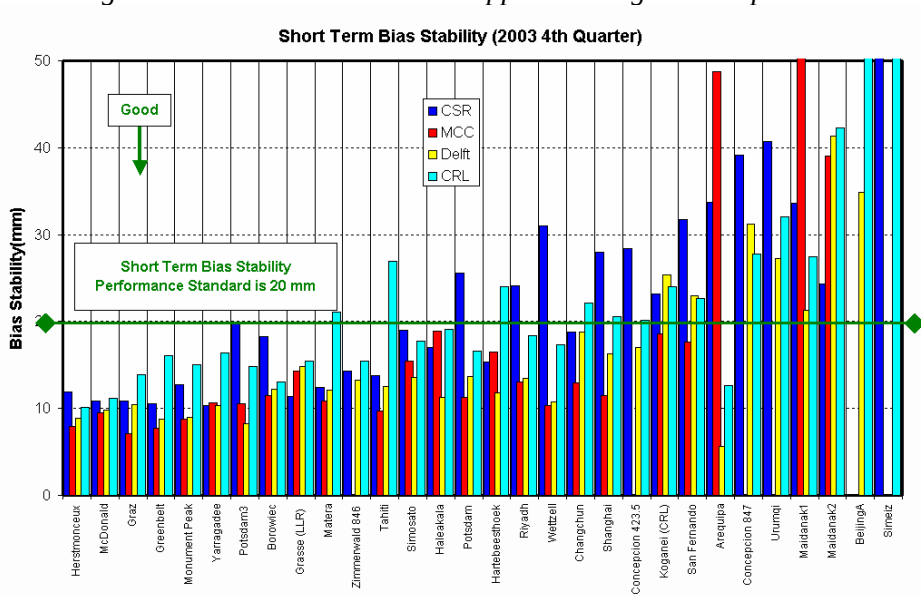

Figure 2. *Example of short-term range bias stabilities provided by ILRS for 2003.*
Source: http://ilrs.gsfc.nasa.gov.

2. Numerical illustrations

The simulations provided here aims to evidence the impact of range biases on any SLR data processing results. Fig. 3 shows the global simulation scheme. The first step consists in estimating the two LAGEOS satellite orbits. Then, these orbits are used with SLR measurements together with ITRF2000 [Altamimi et al., 2002], a model of atmospheric loading effects, and some range bias values to derive, on one hand, simulated range measurements and, on other hand, the partial derivatives of these simulated data with respect to station positions and, eventually, to range biases.

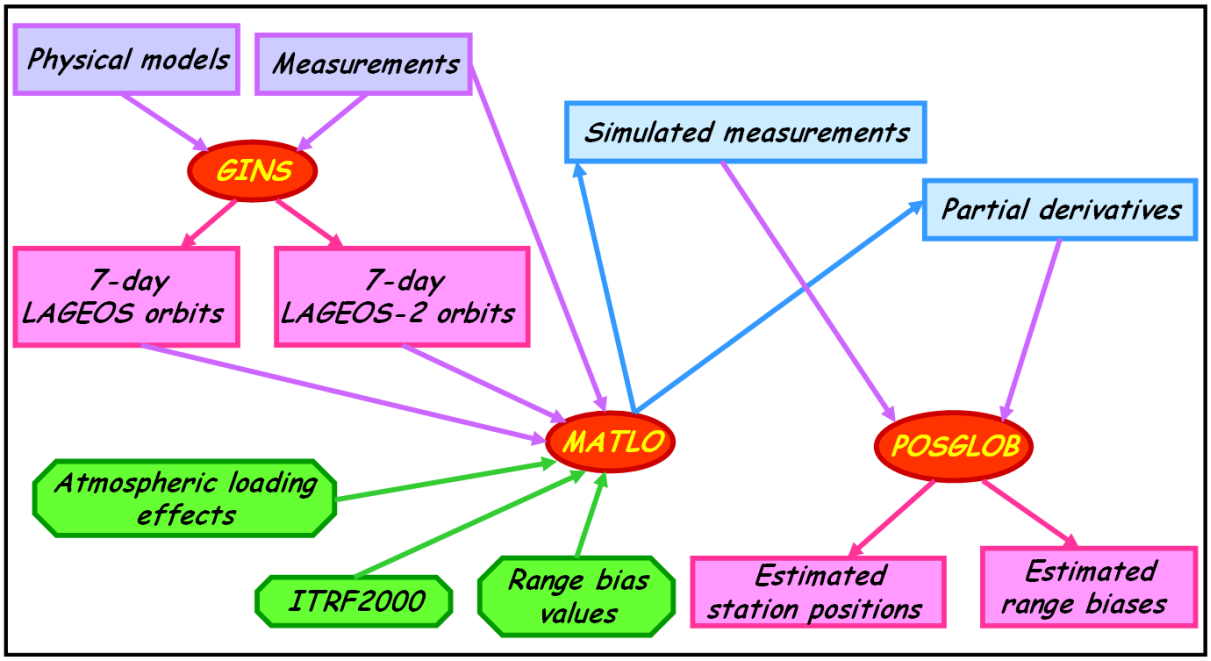

Figure 3. *Simulation method.*

Real orbital arcs and real SLR measurement epochs are used in order to get the most realistic simulations. Atmospheric loading effects are derived from the European Center for Medium-range Weather Forecasts (ECMWF, http://www.ecmwf.int/) pressure grids. As these loading signals are not modeled in the a priori values used, estimated station position time series must evidence them.

For the first simulation (cf. Fig. 4), range biases are applied in simulated measurements but they are not estimated with the Yarragadee SLR station (7090) position time series. The results clearly show that the range biases make a great impact on the Up component time series. Indeed, the time series is completely biased (the mean difference value almost reaches the centimeter level) and is no more stable (the RMS value of the differences is near 5 mm, while the horizontal component RMS values of differences are only at the millimeter level). Thus, range biases must be

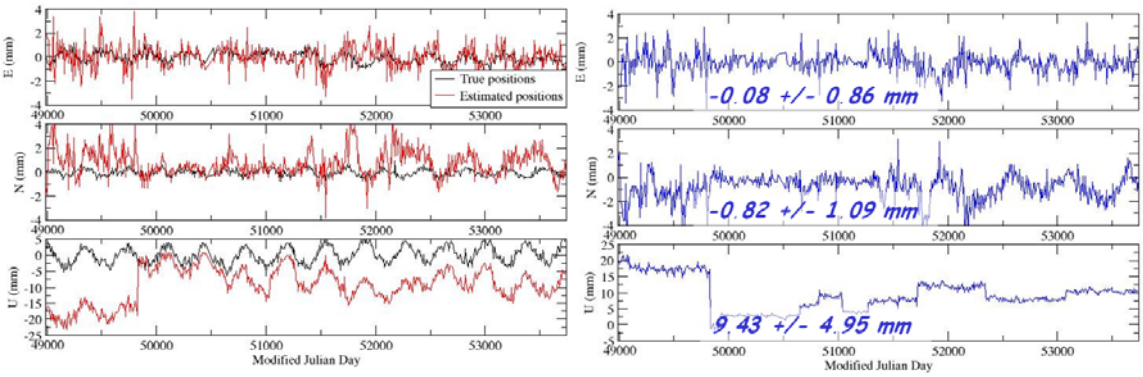

Figure 4. *Results of the first simulation carried out for the Yarragadee SLR station (7090). Values are provided in mm for the three positioning components East, North, and Up. Graphs on the left: black (resp. red) curves correspond to the position time series computed without any bias in simulated measurements (resp. the time series computed with biases applied in simulated measurements). Graphs on the right: differences between red and black curves. Numerical values correspond to the mean and the RMS values.*

estimated together with station positions.

In a second simulation, range biases are applied in simulated measurements and weekly range biases are estimated with the Yarragadee SLR station weekly position time series.

The results shown on Fig. 5 are clearly improved in comparison with those shown on Fig.4. Indeed, the mean value of the Up component differences is divided by 23 and the RMS value by 3.5. Furthermore, the values are also improved for the horizontal components (the difference RMS values are almost divided by 2), proof that range biases can also make an impact (of course lower than the one on the vertical component) on these components. But,

- we can notice large correlations between estimated bias and Up component values (96% on the average);
- spurious signals clearly appear in the weekly estimated biases, even if these latter have made the piece-wise behavior of the Up component time series disappearing.

Thus, range biases must be estimated over a longer period. For the third and last simulation (see the results on Fig. 6), range biases are still applied in simulated

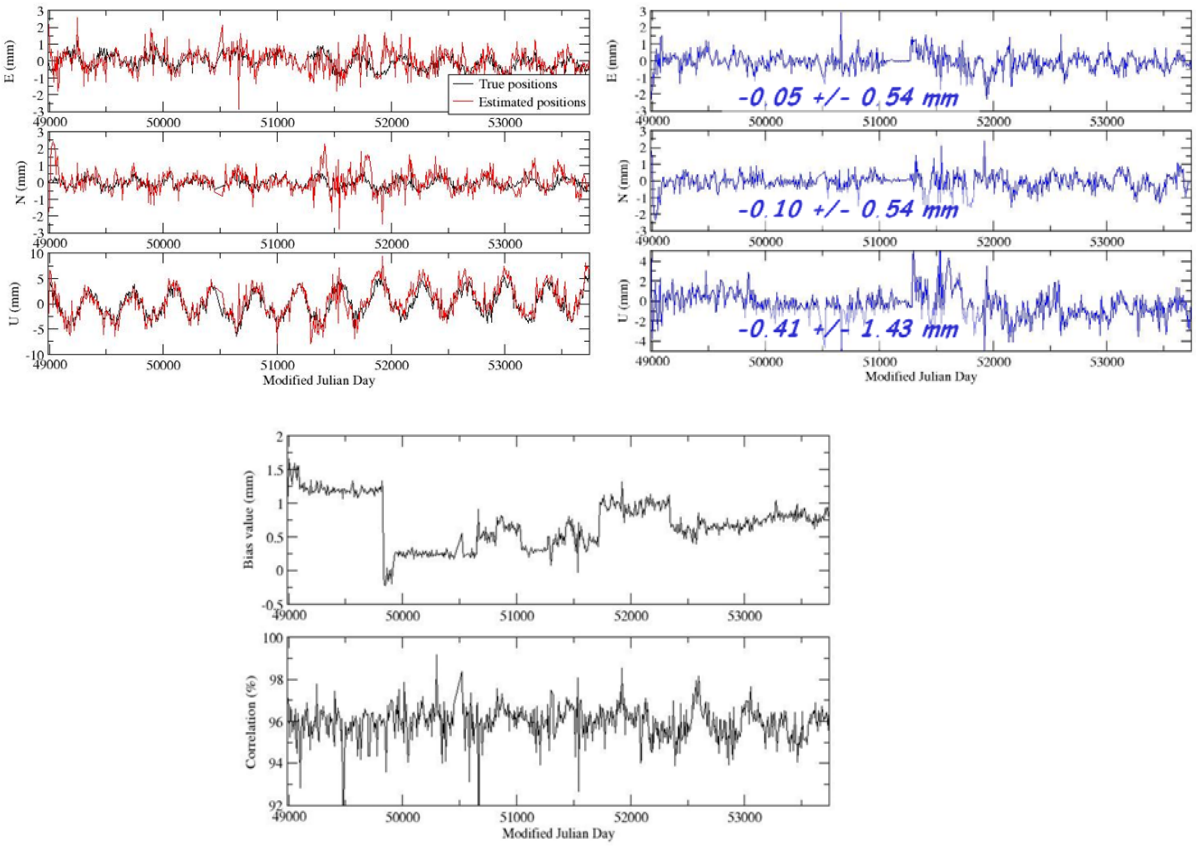

Figure 5. *Results of the second simulation carried out for the Yarragadee SLR station (7090). Values are provided in mm for the three positioning components East, North, and Up. Graphs on the top left: black (resp. red) curves correspond to the position time series computed without any bias in simulated measurements (resp. the time series computed together with weekly range biases with biases applied in simulated measurements). Graphs on the top right: differences between red and black curves. Numerical values correspond to the mean and the RMS values. Graphs below: weekly computed range biases and correlations between bias and Up component estimated values.*

measurements but range biases are now estimated over “long” periods together with the weekly Yarragadee SLR station position time series. The produced results are very satisfying. Indeed, the differences are quite negligible (the mean and the RMS values are below 0.5 mm). Moreover, estimating range biases per satellite allows us to take into account the possible constant signature effects. The correlations have decreased but they are still large (86% on the average).

This approach (that we have called the “temporal de-correlation method”) is the most satisfying one. Moreover, it is fully justified from an instrumental point of view. Indeed, the range biases are directly linked to the tracking instrumentation and we can suppose (at least for the most stable stations) that these instrumentations do not change all the time. As a result, the range biases can be supposed constant over given time intervals.

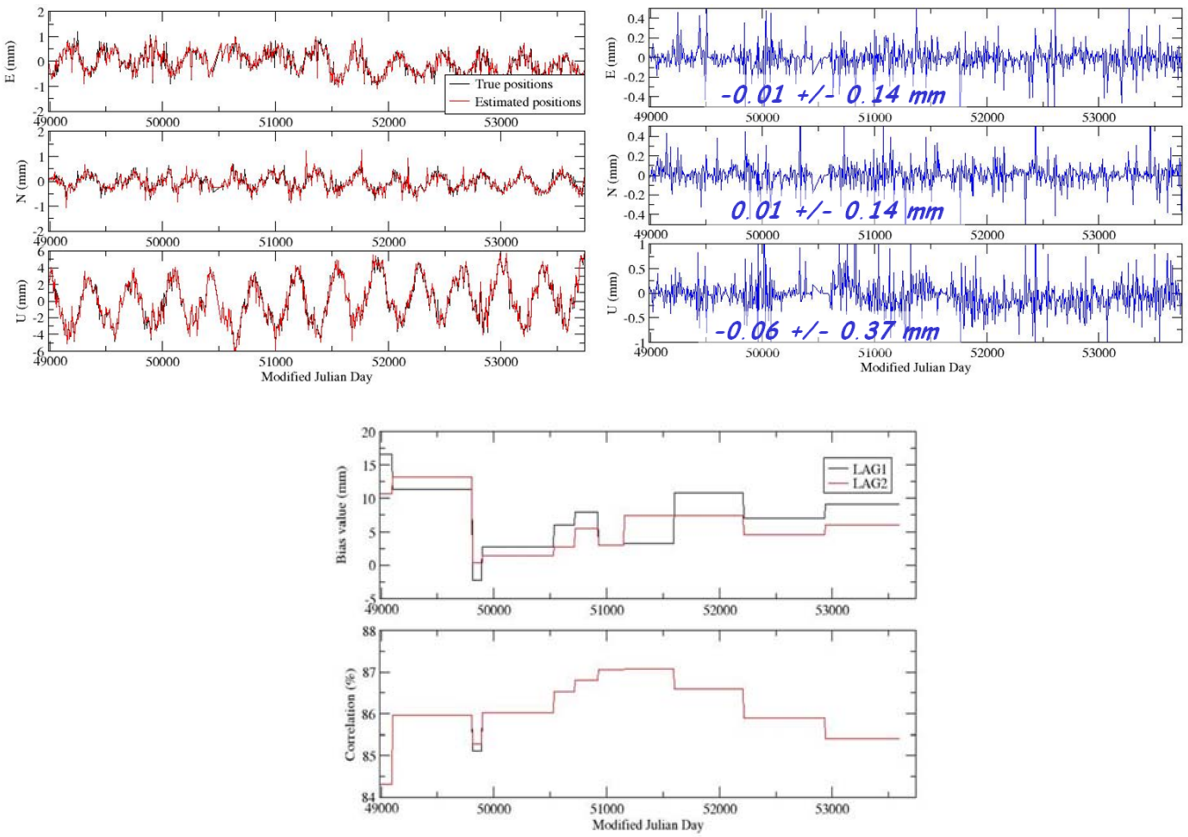

Figure 6. *Results of the third simulation carried out for the Yarragadee SLR station (7090). Values are provided in mm for the three positioning components East, North, and Up. Graphs on the top left: black (resp. red) curves correspond to the position time series computed without any bias in simulated measurements (resp. the time series computed together with the “long-period” range biases with biases applied in simulated measurements). Graphs on the top right: differences between red and black curves. Numerical values correspond to the mean and the RMS values. Graphs below: “long-period” computed range biases per satellite and correlations between bias and Up component estimated values.*

3. First results of the temporal de-correlation method

3.1. CALVAL experiment

These experiments were carried out with the French Transportable Laser Ranging System (FTLRS, see [Nicolas, 2000]) in Corsica in 2002 [Exertier et al., 2004] (and, more recently, in 2005) and in Crete in 2003 [Berio et al., 2004]. As an illustration of the use of our temporal de-correlation method, here is the example of the GAVDOS project, e.g. of the Crete campaign carried out in 2003. During such campaign, the FLTRS aims to calibrate the satellite altimeter (see Fig. 7) with the help of a short-arc technique [Bonnefond et al., 1995]. Thus, we need the most accurate positioning for this transportable station as well as an exhaustive knowledge of its error budget and, in particular, an accurate estimate of its range bias.

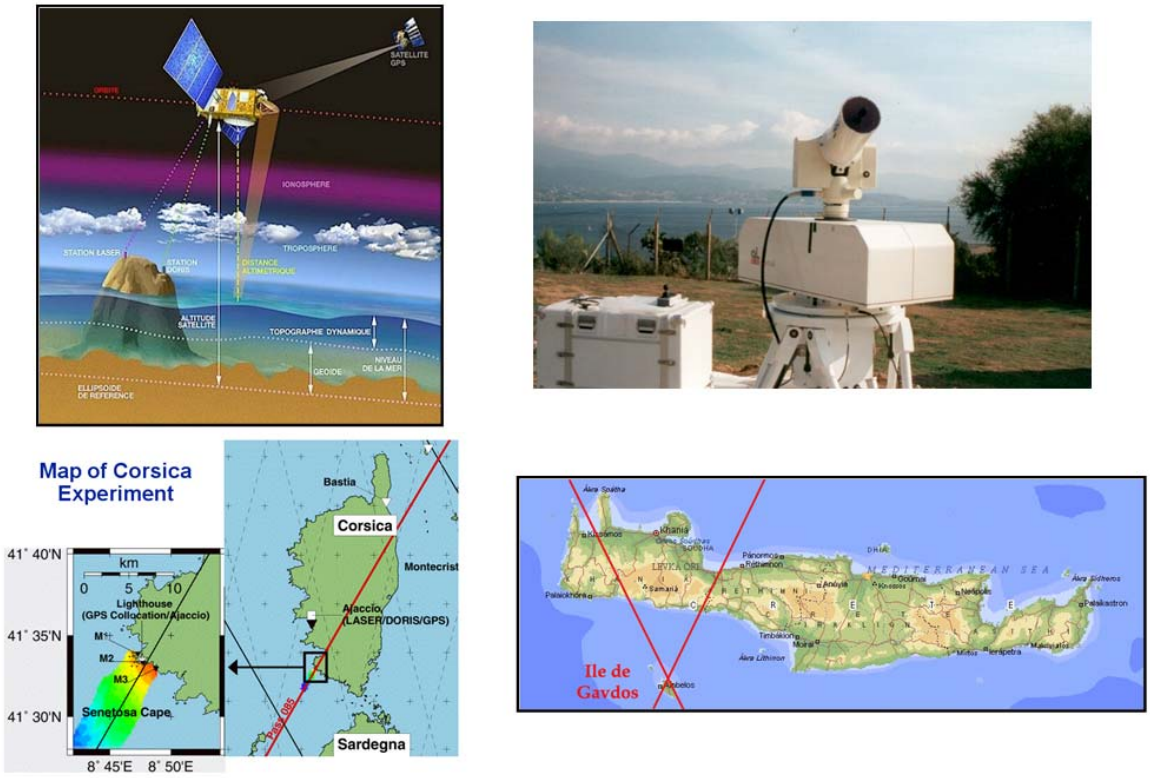

Figure 7. *CALVAL experiments with the FTLRS in Corsica and in Crete.*

Regarding the number of normal points collected on the two LAGEOS satellites by the FTRLS during this campaign (see Tab. 1), it is clear that we need to use the four satellite data to compute the FTLRS positioning. To do so, we have carried out two kinds of computations:

1. the FTLRS position and the range biases per satellite are computed over the whole period of time;
2. we compute weekly FTLRS positions together with range biases per satellite which are computed over the whole period of time (temporal de-correlation approach).

Satellite	Number of normal points
LAGEOS-1	108
LAGEOS-2	315
STARLETTE	2 902
STELLA	1 479

Table 1. *Number of normal points collected by the FTLRS during the Crete campaign carried out in 2003.*

In the both computations, the FTRLS positions are computed with respect to the ITRF2000 position [Altamimi et al., 2002] corrected for the solid Earth tides and the solid Earth pole tide in agreement with [McCarthy, 1996]. With the first method, the mean FTLRS position is directly computed, while, with the second approach, the mean FTLRS position is provided as the weighted mean value of the weekly estimated positions. The results produced by these two methods are summarized in Table 2.

The horizontal component estimated values are left unchanged between both approaches. And, the correlation is strongly decreased with the temporal de-correlation method. We can also notice a transfer between the biases and the Up components (the value is close to 1 cm) between both methods. Only the results of the second method are retained and, as a result, the mean FTLRS range bias value is -13,8 mm. [Nicolas et al. 2002] provides - 5 mm. This difference is explained. Indeed, during the whole campaign, the internal and external FTLRS calibrations exhibited a constant 1-cm difference.

Method	East	North	Up	BLAG1	BLAG2	BSTE	BSTA	Corr.
Method 1	2,5	-5,9	0,3	-19,7	-20,6	-28,3	-22,4	0,93
Method 2	1,6	-5,8	12,5	-9,6	-9,7	-20,2	-15,7	0,57
Absolute differences	0,9	0,1	12,2	10,1	10,9	8,1	6,7	.

Table 2*. Results (in mm) produced by the two methods studied to compute the FTLRS mean position and range bias during the Crete campaign carried out in 2003. The FTLRS mean positions are provided in the ENU local frame. BXXXX corresponds to the FTLRS bias computed for the satellite XXXX and corr. is the maximum value of the correlations between the estimated FTLRS range bias values per satellite and its Up component positioning values.*

Finally, we can see differences between the bias estimated values per satellite (both LAGEOS satellites versus STELLA and STARLETTE satellites). These differences could be explained by a radial constant error of 1 cm found for STELLA [Bonnefond, 2006] and by the fact that the signature effects depend on satellite and on detection system [Nicolas, 2000].

3.2. 12-year SLR data analysis

The temporal de-correlation method has also been applied over 5-month running windows in the framework of a 12-year SLR LAGEOS satellite data analysis (see [Coulot et al., 2005] and [Coulot, 2005] for more details).

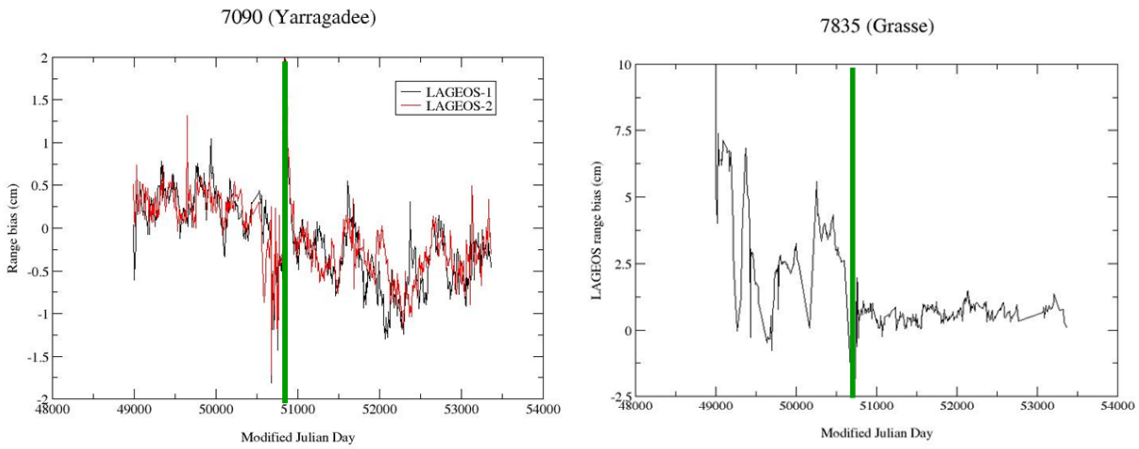

Figure 8. *Bias (in cm) time series with a 5-month sampling computed for the Yarragadee (on the left) and the Grasse (on the right) SLR stations during the 12-year SLR LAGEOS satellite data analysis.*

Fig. 8 provides two examples of bias time series computed during this study. Regarding the Yarragadee (7090) SLR station results, we can first notice that the bias values per satellite are very close: the RMS of the difference is 0.03 mm! A jump is clearly detected in the two time series. And, the epoch of this jump (January 1998) in fact corresponds to a detection system change.

Regarding the Grasse (7835) SLR station results, a jump is also detected in September 1997 and this jump corresponds to the detection system change previously mentioned in section 1 (cf. Fig. 1). We can finally notice the great stabilization of the range biases after this discontinuity. Indeed, the bias RMS value after this latter is 3.0 mm whereas this value is 20.5 mm before the jump!

4. Method improvement

4.1. New approach

Up to now, the limits of the time interval over which biases are supposed to be constant were not rigorously determined. As previously mentioned, range biases are directly linked to SLR instruments. Thus, biases are now supposed to be constant

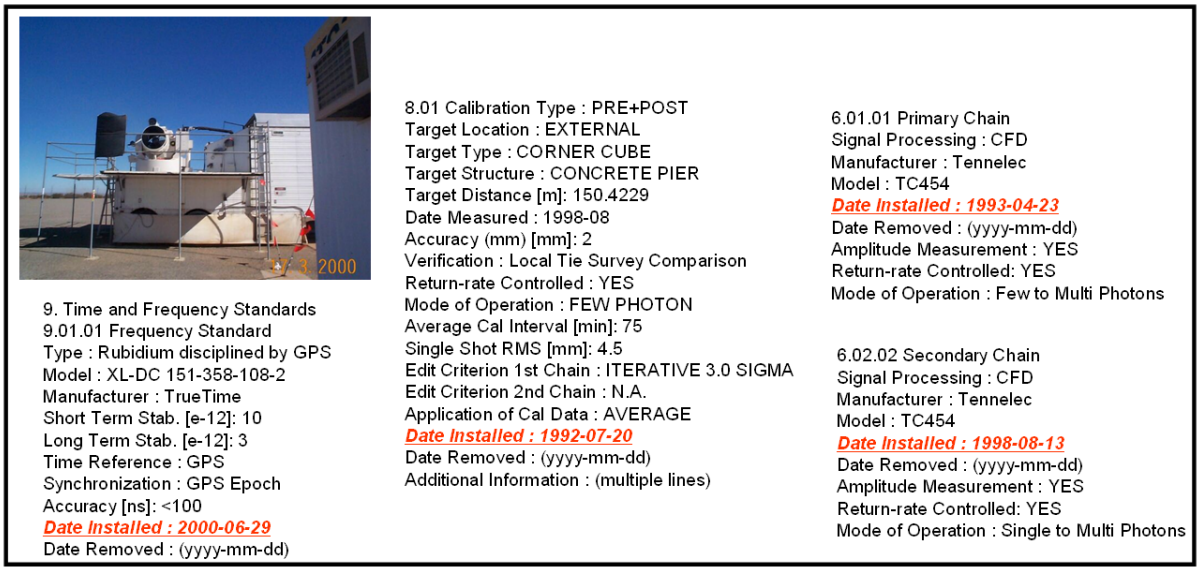

Figure 9. *Examples of instrumental change epochs found in the log file of the Yarragadee SLR station (7090).*

between two instrumental changes. We use station log files to determine these changes. Fig. 9 shows examples of instrumental change epochs used for the Yarragadee station (7090). Examples of so computed biases per satellite are provided in [Coulot et al., 2007].

4.2. Results

Fig. 10 compares the results produced with our improved temporal de-correlation method with those produced without considering any range bias during the data processing. Results are satisfying. Indeed, for instance, the scale factor time series is

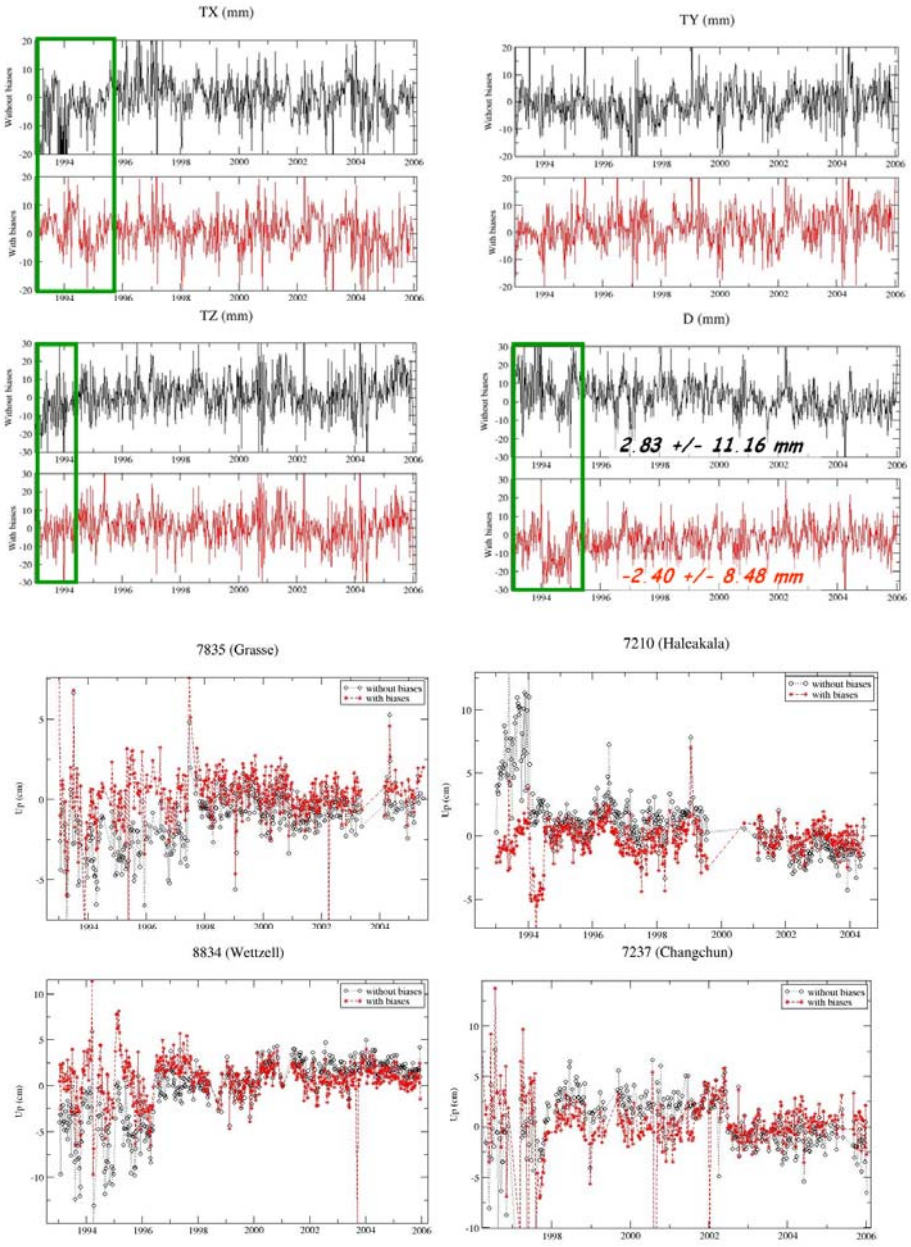

Figure 10. *Translation and scale factor parameters (in mm) computed between the weekly Terrestrial Reference Frames and ITRF2000 and four station Up component time series computed in ITRF2000 (in cm). Black (resp. red) curves correspond to the computation carried out without considering any bias (resp. the computation for which our improved temporal de-correlation method has been applied).*

more stable (RMS value of 8.5 mm to be compared with the 11.2 mm value provided by the computation carried out without bias). Moreover, the drift exhibited by the black scale factor time series disappears when our approach is used. Finally, the station time series are clearly more stable even if some discontinuities are still detected.

5. Conclusions and prospects

The two approaches ("running windows" or "instrumental change epochs") produce very satisfying results. They could be coupled to detect jumps which are not clearly linked to reported instrumental evolutions. Furthermore, it would allow us to rigorously apply the method to "poor quality stations", e.g.. stations for which biases are not stable.

Our method takes into account the correlation between station position Up components and range biases. We should also pay attention to the correlations with the possible radial orbital errors in the framework of a semi-dynamical approach (see [Coulot et al., 2007]). It would thus require a global estimation of all parameters for the whole network involved.

References

[1] Altamimi, Z., P. Sillard, and C. Boucher: "ITRF2000: a new release of the International Terrestrial Reference Frame for Earth science applications", J. Geophys. Res., 107(B10), 2214, doi: 10.1029/2001JB000561, 2002.

[2] Berio, P., P. Exertier, F. Pierron, J. Weick, D. Coulot, and O. Laurain: "FTLRS support to the Gavdos project: tracking and positioning", in Proceedings of the 14th International Laser Ranging Workshop, 2004.

[3] Bonnefond, P., P. Exertier, P. Shaeffer, S. Bruinsma, and F. Barlier: "Satellite Altimetry from a Short-Arc Technique: Application to the Mediterranean", J. Geophys. Res., 100(C12), p. 25 365-25 382, 1995.

[4] Bonnefond, P., personal communication, 2006.

[5] Coulot, D., P. Berio, O. Laurain, D. Féraudy, P. Exertier, and K. Le Bail: "Analysis of 12 years (1993-2004) of SLR data", poster presented at the 2nd European Geosciences Union General Assembly, Vienna, Austria, 2005.

[6] Coulot, D.: "Télémétrie laser sur satellites et combinaison de techniques géodésiques. Contributions aux Systèmes de Référence Terrestres et Applications", Ph. D. thesis, Observatoire de Paris, 2005.

[7] Coulot, D., P. Berio, O. Laurain, D. Féraudy, P. Exertier, and F. Deleflie: "Analysis of 13 years (1993-2005) of Satellite Laser Ranging data on the two LAGEOS satellites for Terrestrial Reference Frames and Earth Orientation Parameters", same issue, 2007.

[8] Exertier, P., J. Nicolas, P. Berio, D. Coulot, P. Bonnefond, and O. Laurain: "The role of Laser Ranging for calibrating Jason-1: the Corsica tracking campaign", Mar. Geod., 27, p. 1-8, 2004.

[9] McCarthy, D.D.: "IERS Conventions", IERS Technical Note 21, Observatoire de Paris, 1996.

[10] Nicolas, J.: "La Station Laser Ultra Mobile. De l'obtention d'une exactitude centimétrique des mesures à des applications en océanographie et géodésie spatiales", Ph. D. thesis, Université de Nice-Sophia-Antipolis, 2000.

[11] Nicolas, J., P. Bonnefond, O. Laurain, F. Pierron, P. Exertier, and F. Barlier: "Triple laser ranging collocation experiment at the Grasse Observatory, France - September - November 2001-", in Proceedings of the 13th International Laser Ranging Workshop, 2002.

Analysis of 13 years (1993-2005) of Satellite Laser Ranging data on the two LAGEOS satellites for Terrestrial Reference Frames and Earth Orientation Parameters

D. Coulot[1], Ph. Berio[2], O. Laurain[2], D. Féraudy[2], P. Exertier[2], F. Deleflie[2]

1. IGN/LAREG - Marne-la-Vallée – France
2. CNRS/OCA/GEMINI - Grasse - France

Contact: David.Coulot@ensg.ign.fr /Fax: +33-1-64-15-32-53

Abstract

The quality presently reached by space-geodetic techniques, regarding precision, accuracy such as spatial and temporal distributions of their measurements, allows us to compute time series of geodetic products.

In this context, we have developed a method to compute time series of Earth Orientation Parameters (EOPs) and terrestrial station positions through the analysis of Satellite Laser Ranging (SLR) data. This technique being an important basis for the computation of the International Terrestrial Reference Frame, it is crucial to derive accurate time series with a rigorous approach. Furthermore, this method will be used by the scientific department GEMINI of the Observatoire de la Côte d'Azur when it will become an official ILRS analysis center.

These times series are obtained with a good accuracy and a reasonable sampling (1 day for EOPs and 1 week for station positions). This good accuracy is ensured by i) a rigorous weighting of SLR measurements per satellite and per station; ii) a kinematic approach to compute orbital residual errors; iii) a rigorous control of range biases which is detailed in [Coulot et al.,2007].

In this paper, we first present the two aspects i) and ii) of our method. In a second part, we analyze 13 years (1993-2005) of SLR data on both LAGEOS satellites in order to study the Terrestrial Reference Frames and the EOPs so computed.

Introduction

This paper comprises four parts. First, we detail the two LAGEOS satellite orbit computation. Second, we provide general considerations about the Satellite Laser Ranging (SLR) data processing, regarding the data weighting, the orbital residual errors, and the range biases. Then, we describe the time series computation method and produce the results and, finally, we provide some conclusions and prospects.

1. Orbit computation

This section aims to briefly describe the two LAGEOS satellite orbit computation. Tables 1, 2, and 3 respectively show the physical models used for the orbit computations and for the Earth Orientation Parameters (EOPs) and the station positions during these computations.

Fig.1 shows the orbit residual WRMS and the numbers of data used and rejected for both satellites. Tab. 4 provides some statistics of these values. We can see that, on average, the residual WRMS are at the centimeter level for both LAGEOS satellites.

The sampling used for these computations is the GPS week but, in order to reduce the impact of the residual orbital errors, we in fact compute 9-day orbital arcs and only keep the 7-day central arcs. As a result, our orbital arcs provide 2-day overlaps. Fig. 2

shows the bias and the RMS values of the orbit differences so computed in RTN frame for both satellites. Table 5 provides the mean values of these difference bias and RMS values.

Table 1. *Physical models used for the orbit computations.*

Type	Description
Earth's gravity field	GRIM5_C1 [Gruber et al., 2000]
Atmospheric density	DTM94 [Berger et al., 1998]
Planetary ephemerides	DE403 [Standish et al., 1995]
Earth's time varying gravity field	
Solid Earth tides	Model in [McCarthy and Petit, 2004]
Solid Earth pole tide	Model in [McCarthy and Petit, 2004]
Oceanic tides	FES2002 [Le Provost, 2002]
Atmospheric pressure	ECMWF, http://www.ecmwf.int/

Table 2. *Physical models used for the EOPs during the orbit computations.*

Type	Description
Reference time series	EOPC04 [Gambis, 2004]
Quasi-diurnal Variations	Model in [McCarthy and Petit, 2004]
Precession	Model [Lieske et al., 1977]
Nutation	Model in [McCarthy, 1996]

Table 3. *Physical models used for the stations positions during the orbit computations.*

Type	Description
Terrestrial Reference Frame	ITRF2000 [Altamimi et al., 2002]
Celestial Reference Frame	ICRF [Arias et al., 1995]
Solid Earth tides	Model in [McCarthy and Petit, 2004]
Solid Earth pole tide	Model in [McCarthy and Petit, 2004]
Oceanic loading (only tidal components)	Computed with FES2002
Atmospheric loading (only non-tidal components)	Computed with ECMWF fields

Table 4. *Statistics of the values shown on Fig. 1.*

Satellite	Mean residual WRMS	Mean number of data used	Mean number of rejected data
LAGEOS	1.11 cm	1433	49
LAGEOS-2	0.95 cm	1320	35

Their interpretation is not easy, and yet these overlaps provide a way of controlling the orbit quality. From Table 5, we can see that the two LAGEOS satellite orbits provide differences with mean RMS values between 1 and 4.5 cm.

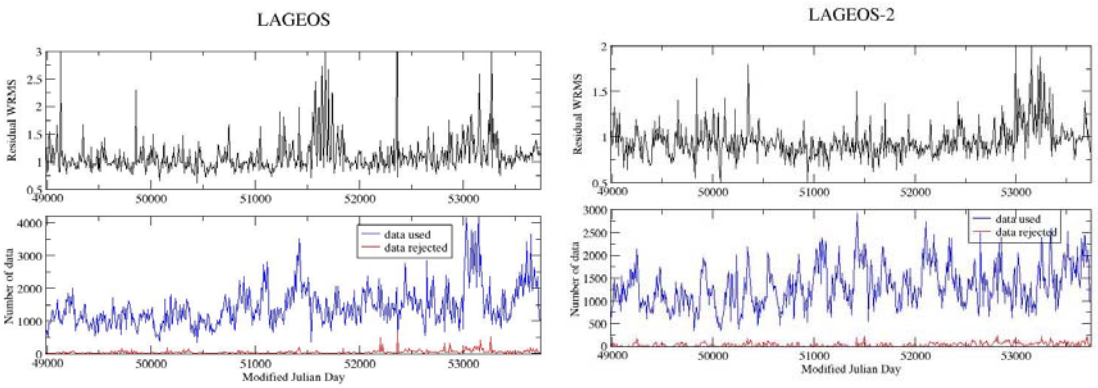

Figure 1.*Orbit residual WRMS (cm) (black curves) and numbers of data used (blue curves) and rejected (red curves) per orbital arc for both LAGEOS satellites (LAGEOS on the left and LAGEOS-2 on the right).*

Table 5. *Statistics of the values shown on Fig. 2.*

Satellite	R (cm)	T (cm)	N (cm)	.
LAGEOS	-0.02 2.57	-0.01 4.37	0.01 2.59	Mean bias Mean RMS
LAGEOS-2	0.01 1.32	-0.05 2.26	0.00 2.66	. .

2. General considerations

The SLR data processing method we have developed is divided in three steps. Fig. 3 shows the global computational scheme. First, GRGS (french Groupe de Recherche en Géodésie Spatiale, Spatial Geodesy Research Group, in English) GINS (Géodésie par Intégration Numérique Simultanée, Geodesy by Simultaneous Numerical Integration, in English) software provides the two LAGEOS satellite orbits with the help of physical models and SLR measurements (see previous section 1). Second, GRGS MATLO (MAThématiques pour la Localisation et l'Orbitographie, MAThematics for Localization and Orbitography, in English) software uses these orbital arcs and the SLR data to compute pseudo measurements as well as partial derivatives of these latter with respect to the parameters worthy of interest. Finally, an estimation software (POSGLOB for POSitionnement GLOBal or GLOBal POSitioning in English) produces parameter estimates from MATLO outputs.

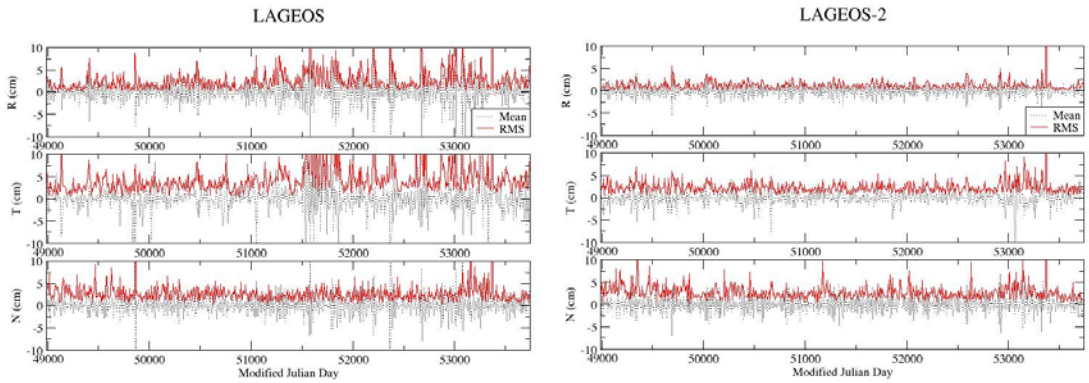

Figure 2. *Orbit differences (biases - in black - and RMS values - in red -, in cm) in the RTN frame computed over the two overlapping days for both LAGEOS satellites (LAGEOS on the left and LAGEOS-2 on the right).*

As shown in green boxes on Fig. 3, there are three critical issues in such computation: the range bias and residual orbital error handling and the data weighting. Thus, we try to build the optimal method to take these issues into account.

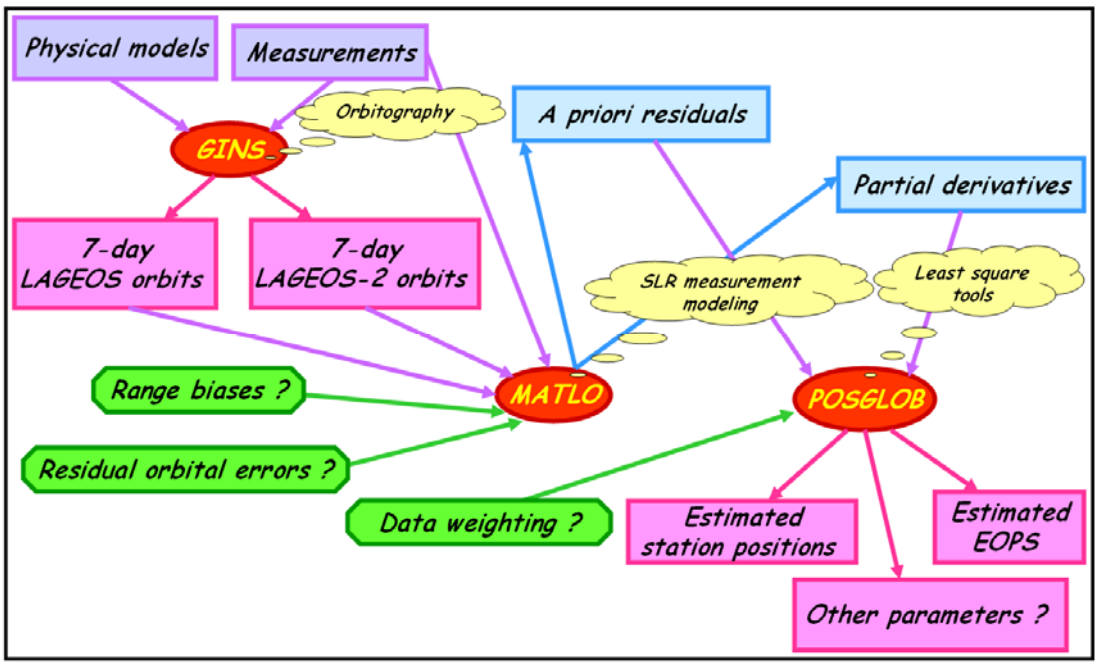

Figure 3. *SLR data processing scheme.*

2.1. Data weighting

SLR stations do not provide measurements of the same quality. As a consequence, we can not use the same weight for all SLR measurements but we have to find weights which really correspond to the quality of these measurements. To do so, we use an optimal variance component analysis method: the degree of freedom method inspired by [Persson, 1982]. The following scheme on Fig. 4 summarizes the method (see [Sillard, 1999] and [Coulot, 2005] for more details).

As shown on Fig.4, this method (as a great part of such variance component analysis method) is based on common parameters for all considered observation groups. In our case, the only real common parameters are EOPs as we consider that observation groups are measurements per station and per satellite. Thus, our variance component analysis approach only relies on these EOPs.

Fig. 5 shows the method used to derive the optimal weighting per station and per satellite. First of all, MATLO software is used to derive pseudo measurements and partial derivatives of these latter with respect to station positions and EOPs from the 7-day LAGEOS satellite orbits and the range biases computed with the temporal de-correlation method (see section 2.3 and [Coulot et al., 2007]. Then, a first computation is carried out with an empirical weighting derived from the mean orbit residual WRMS per station and per satellite.

For this computation, we apply weak constraints on station positions and EOPs. From this data processing results, we get estimated station positions which are used for the second computation. Indeed, for this latter, station positions are held fixed to the previous estimated values and, consequently, the only parameters to be computed are EOPs, the common parameters. From this computation, we then get the weekly

optimal weights per station and per satellite which can now be used for any SLR data processing.

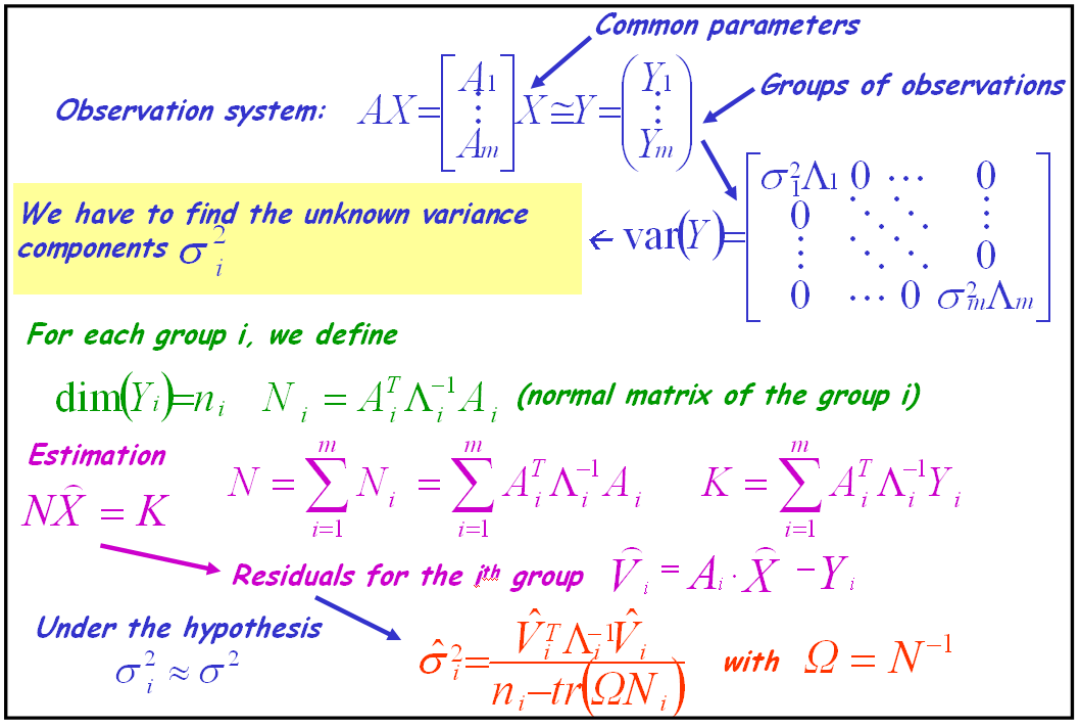

Figure 4. *Scheme of the degree of freedom method.*

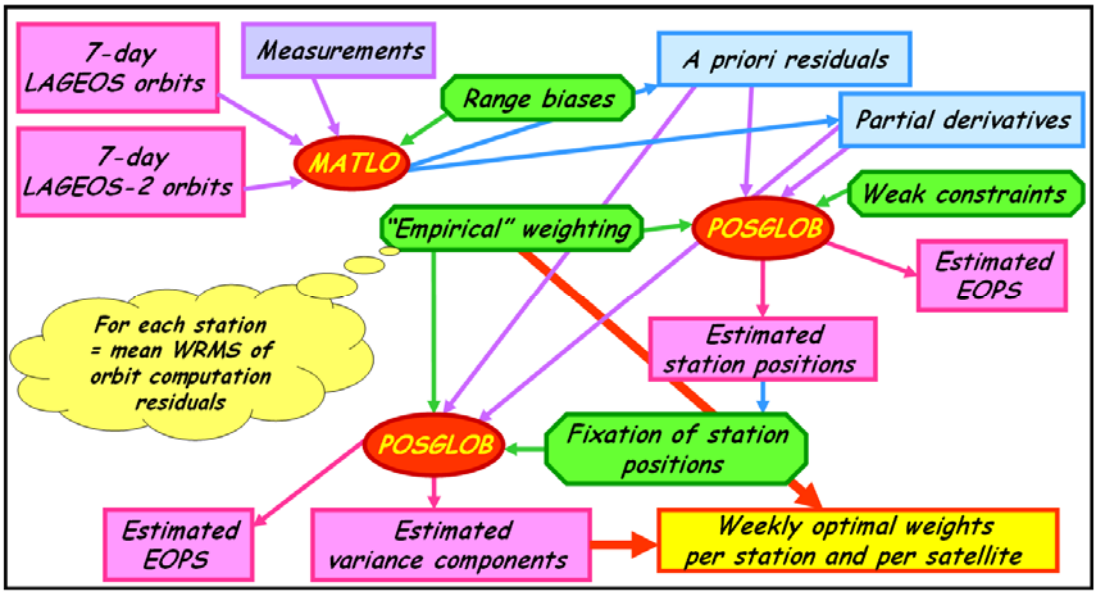

Figure 5. *Scheme of weekly optimal weight per station and per satellite computation.*

Table 6 provides the mean WRMS values of residuals per station and per satellite computed with the optimal weighting. On the whole, the values are consistent with the a priori knowledge one can have on the SLR network station quality but our approach should be more improved by the use of all the involved parameters to compute the optimal weighting. Indeed, orbital residual error parameters (see next section) are common parameters for measurements per station and we should study the impact of the non common parameters (namely, the station positions) on the results produced by variance component analysis methods. Moreover, these values

also evidence the fact that the model used to compute the optimal weighting does not explain the SLR measurements at the millimeter level (the best values are few millimeters). It is certainly mainly due to the fact that the residual orbital errors were not estimated.

Table 6. *Mean WRMS (in cm) values of residuals per station and per satellite computed with the weekly optimal weights derived from the method shown in Fig. 5. For each station, the first (resp. second) column corresponds to the mean WRMS for LAGEOS (resp. LAGEOS-2) satellite. Evidenced stations are present in less than 50 weeks over the 13-year time interval.*

1824	20.5	20.3	7210	1.0	0.9	***7502***	2.3	1.9	7840	0.9	0.9
1831	4.0	3.9	***7231***	5.1	6.2	***7505***	1.6	2.0	7841	1.1	1.1
1863	2.6	2.5	7236	11.4	10.4	7520	1.5	1.3	7843	1.8	1.6
1864	4.0	3.6	7237	2.0	1.9	7548	11.6	6.8	7845	1.0	0.9
1867	30.9	16.2	7249	5.1	4.5	***7597***	2.5	3.1	***7847***	9.9	12.9
1868	9.4	8.1	***7295***	0.9	0.9	***7805***	13.2	15.0	***7848***	2.3	1.9
1873	13.8	14.1	7308	2.0	1.9	***7806***	1.9	1.5	7849	2.3	1.1
1884	2.3	2.1	***7335***	1.0	0.9	7810	1.4	1.4	***7850***	0.7	0.8
1885	8.9	13.0	***7337***	1.0	2.2	7820	2.3	2.4	***7882***	0.5	0.6
1893	3.3	3.3	7339	1.2	0.8	***7821***	2.0	2.9	***7883***	0.5	0.6
1953	9.9	11.5	***7355***	4.3	3.7	7824	2.4	2.3	***7884***	1.2	0.6
7080	1.0	0.8	***7356***	2.8	2.8	7825	1.8	1.9	***7918***	0.9	1.1
7090	1.7	1.4	***7357***	4.9	6.0	***7830***	1.6	1.5	7939	6.9	6.8
7105	0.9	0.8	***7358***	5.0	6.9	***7831***	2.7	2.0	7941	0.9	0.8
7106	7.6	.	7403	1.5	1.1	7832	1.2	1.2	***8833***	2.8	2.7
7109	0.7	0.6	***7404***	4.9	1.8	7835	1.0	0.9	8834	1.4	1.4
7110	0.9	0.8	7405	2.7	2.7	7836	1.0	0.9	7811	1.8	1.6
7122	0.7	0.7	***7410***	0.7	0.6	7837	2.1	2.0			
7124	1.7	1.2	***7411***	0.5	0.6	7838	1.7	1.6			
7130	1.3	1.4	7501	2.2	2.1	7839	0.8	0.8			

2.2. Orbital residual errors

As previously shown in section 1, the LAGEOS satellite orbital arcs may be affected by some residual errors (cf. Fig. 2 and Tab. 5). The integration of Hill's satellite first-order motion differential equations ([Cretaux et al., 1994] and [Coulot, 2005]) provides the empirical form of such orbital residual errors in the RTN frame:

$$\delta R(t) = a_R t\cos(\bar{n}t) + b_R t\sin(\bar{n}t) + c_R\cos(\bar{n}t) + d_R\sin(\bar{n}t) + e_R + f_R t$$
$$\delta T(t) = a_T t\cos(\bar{n}t) + b_T t\sin(\bar{n}t) + c_T\cos(\bar{n}t) + d_T\sin(\bar{n}t) + e_T + f_T t + g_T t^2$$
$$\delta N(t) = a_N t\cos(\bar{n}t) + b_N t\sin(\bar{n}t) + c_N\cos(\bar{n}t) + d_N\sin(\bar{n}t) + e_N$$

The coefficients evidenced in yellow can be estimated. Thus, doing so, we can carry out a kinematic (or semi-dynamic) estimation of the orbital residual errors; see Fig. 6 for examples.

In order to avoid spurious transfers between the terrestrial and the orbital parameters, we should compute all the involved parameters (station positions, EOPs and orbital residual errors) in a same process. But, doing so gives rise to problems. Indeed, it creates supplementary reference system effects [Sillard and Boucher, 2001] on the third translation and on the scale factor of the underlying Terrestrial Reference Frame

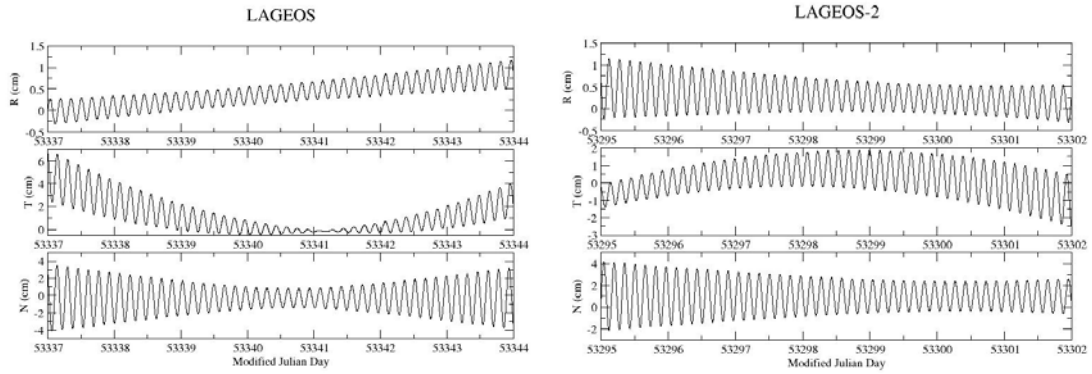

Figure 6. *Examples of orbital residual errors estimated, in cm, for both LAGEOS satellites in the RTN frame.*

(TRF). These parameters are thus damaged and the estimated orbital errors so computed are completely eccentric! Consequently, we have to find a rigorous balance between minimum constraints used to define the weekly TRFs and possible constraints applied on the orbital error coefficients. Furthermore, we have to take into account the physical coupling between the radial and tangential components [Coulot, 2005]. Finally, we have to carry out a sensitivity analysis to determine which coefficients can be optimally computed each week.

2.3. Range biases

Regarding range biases, we have developed a temporal de-correlation method in order to get the most accurate and consistent range bias values (see [Coulot et al., 2007] for more details). Fig. 7 provides an extract of the raw output file provided by this method. We can see that, when they are estimated over long periods, biases per satellite are very coherent. In other cases, the differences are at a few millimeter level.

Station	Validity (CNES J. Dates)		Values obtained for LAGEOS (m) Bias + precision		Values obtained for LAGEOS-2 (m) Bias + precision	
7835	15340	16544	1.395828547040809E-002	1.158416922784649E-003	1.234432517595224E-002	1.203503017002734E-003
7835	16544	16564	3.529396209728985E-002	1.475235139678072E-002	6.300895927387962E-002	1.990854928253546E-002
7835	16564	16679	3.320933374887905E-002	3.232515758791523E-003	2.891112857748582E-002	3.484324601453627E-003
7835	16679	17413	1.664937112299916E-002	1.430681097343033E-003	1.540554934193744E-002	1.520702451478579E-003
7835	17413	18143	-1.971404917293083E-003	3.328628424293636E-004	-6.434411963804878E-004	3.564485287931656E-004
7835	18143	18873	2.129710997299538E-003	3.360069389674007E-004	3.901844189266957E-003	3.633585927952743E-004
7835	18873	19603	9.131760532044128E-003	4.467022182450903E-004	5.700719983120365E-003	4.759540373836256E-004
7835	19603	20300	7.851262565453349E-003	9.554258819448195E-004	2.842151050185370E-003	1.004394426948261E-003
7845	17521	18305	-4.428851680859768E-003	6.223534556697570E-004	-1.201192209408536E-003	6.893149034575394E-004
7845	18305	19305	8.113087278820413E-003	4.018334706229168E-004	7.840983271450021E-003	4.356245988090018E-004
7845	19305	20035	1.285646431835049E-002	5.459565786674019E-004	1.654336641325428E-002	5.438026909611077E-004
7105	15317	16047	-3.746952854385001E-003	4.944474970946950E-004	-6.864306478378965E-003	5.264430332363305E-004
7105	16047	16777	-1.549706818118012E-002	6.921317933826075E-004	-1.064881791710468E-002	7.505764408214999E-004
7105	16777	16940	-1.105482201853714E-002	5.900205316694585E-004	-7.750502221599706E-003	6.391419698574262E-004
7105	16940	17670	-4.330403233925809E-003	3.766190351993729E-004	-2.921756834785135E-003	4.000337192808937E-004
7105	17670	17877	-8.797353166941418E-003	6.028898715788532E-004	-4.826611780213416E-003	6.371640591200326E-004
7105	17877	17959	-8.741490387424361E-003	1.310118230413150E-003	-1.019322123979381E-002	1.342775122007329E-003
7105	17959	18039	-4.648690714335582E-003	8.785822392202415E-004	-2.871015614103231E-003	9.488477693905651E-004
7105	18039	18666	-5.169111580414628E-003	3.867953242580351E-004	-4.312745700605802E-003	4.185257805300395E-004
7105	18666	18877	-3.472024871091189E-003	5.657230028905748E-004	-2.899406111483316E-003	6.018937033126987E-004
7105	18877	19607	-4.193980900330184E-003	3.817904507077791E-004	-5.491238818875488E-003	4.105820099047128E-004
7105	19607	20337	-6.548560807830205E-003	4.924245800410994E-004	-7.645452603994796E-003	5.332010012145024E-004
7105	20337	20500	-7.040431351813800E-003	9.396523059811853E-004	-6.322205532930170E-003	1.035964446496983E-003

Figure 7. *Examples of range bias values (m) per station and per satellite computed with the temporal de-correlation method [Coulot et al., 2007]. CNES JD=MJD-33 282.*

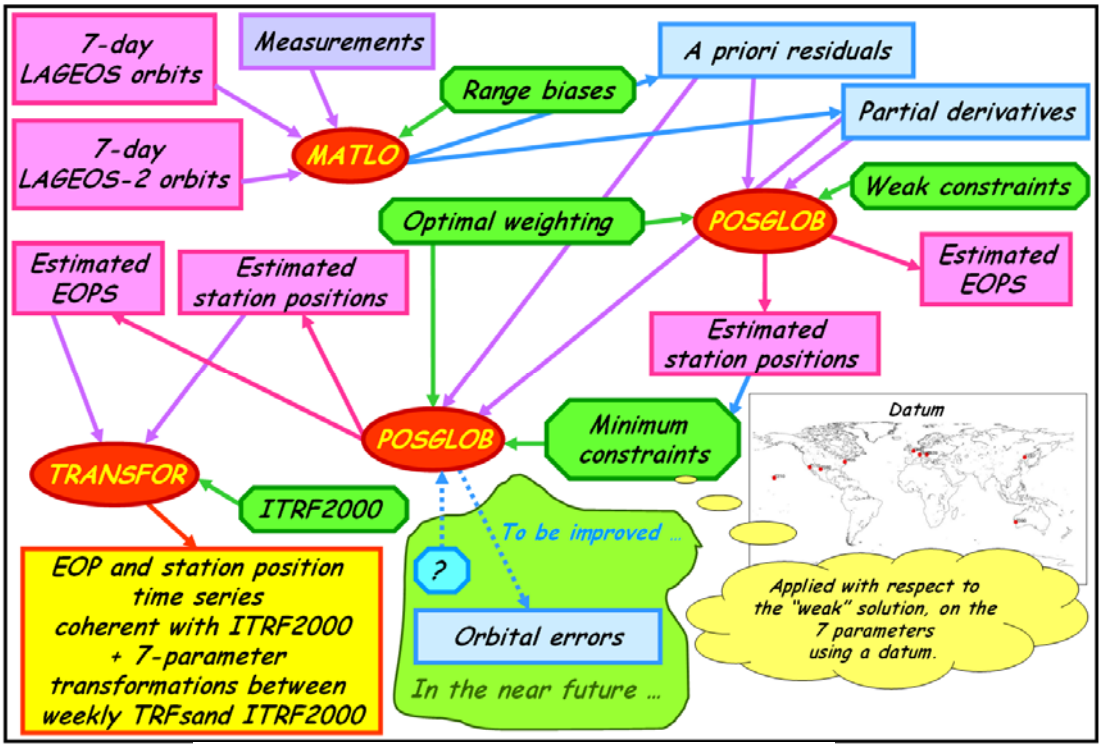

Figure 8. *Time series computation method scheme.*

3. Time series computation

3.1. Method

Fig. 8 shows the global method scheme. For the time series computation, the range bias values computed with our new method as well as our optimal weights are applied. For this first "long period" data processing carried out with MATLO/POSGLOB software, no orbital residual error is estimated nor applied.

3.2 Results

Fig. 9 shows the results produced with TRANSFOR software (cf. Fig. 8) for the three translation parameters. We have carried out frequency analyses of these time series. These analyses have been carried out with FAMOUS (Frequency Analysis Mapping On Unusual Sampling) software developed by F. Mignard (OCA, France) in the framework of the GAIA project [Mignard, 2004]. The TX (resp. TY) time series exhibit a 2.9 mm (resp. 3.2 mm)-amplitude annual signal and the TZ time series exhibit a 2.4 mm-amplitude annual signal as well as a 1.7 mm-amplitude semi-annual signal. Moreover, the scale factor time series are shown in [Coulot et al., 2007], Fig. 10. They exhibit a 2.6 mm-amplitude annual signal. This annual signal may be an artifact due to the SLR network geometry and the fact that the atmospheric loading effects have not been considered in the a priori modeling used for station positions (see next results for these station positions).

Regarding EOPs, the results are shown on Fig. 10. The weighted biases are respectively -119 and 7 µas for Xp and Yp and the WRMS are respectively 299 and 256 µas for Xp and Yp. Moreover, the opposite drifts detected between 2000.0 and 2006.0 certainly come from some network effects.

The station position time series are estimated with respect to the ITRF2000 mean position corrected for plate tectonics (ITRF2000 velocities), Earth solid tides, pole tide and oceanic loading effects in agreement with the IERS conventions [McCarthy

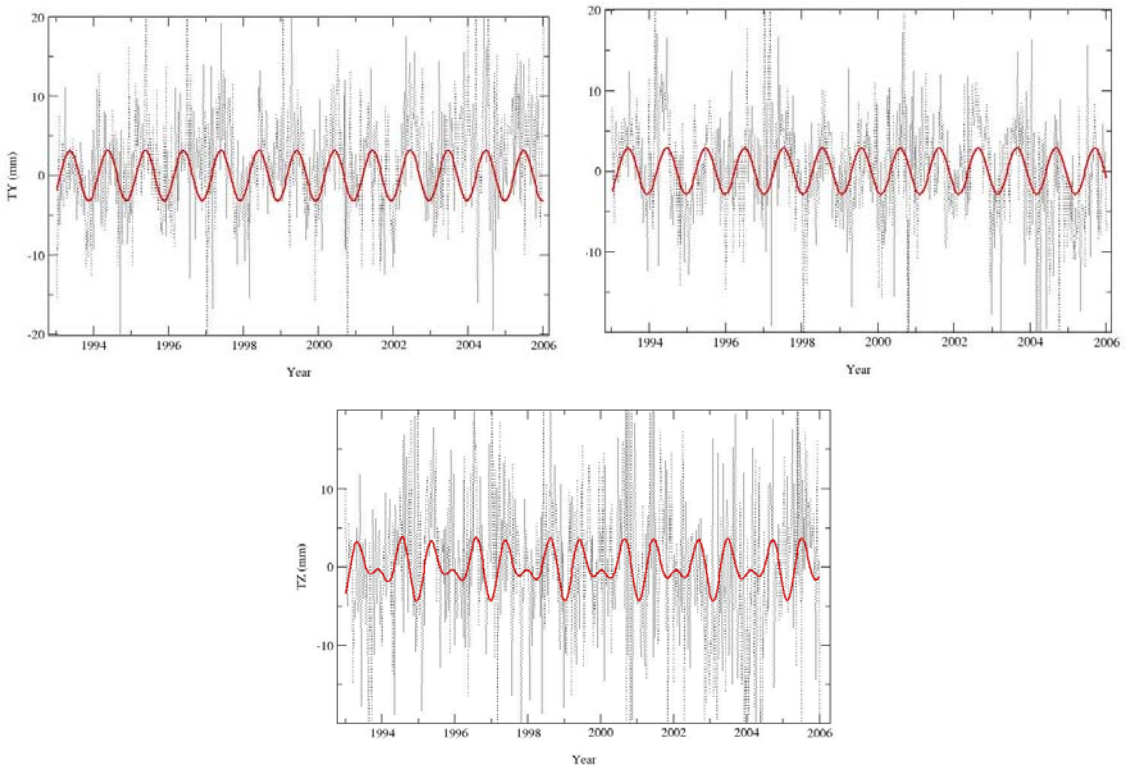

Figure 9. *Weekly translation parameter time series (mm) between weekly SLR TRFs and ITRF2000. Red curves correspond to the periodic signals detected and estimated with FAMOUS software.*

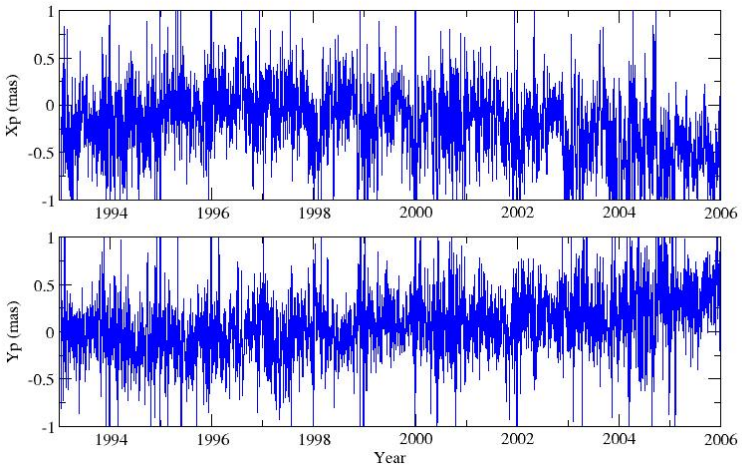

Figure 10. *Daily EOP time series (mas) computed with respect to the EOPC04 time series.*

and Petit, 2004]. These time series must consequently evidence the atmospheric and hydrologic loading effects.

Fig 11 shows 7839 and 7840 SLR station position time series in ITRF2000. Annual and semi-annual signals with amplitudes between 5 mm and 1 cm are detected by FAMOUS software in such Up component time series for some stations. These annual signals may be linked to the previously mentioned loading effects.

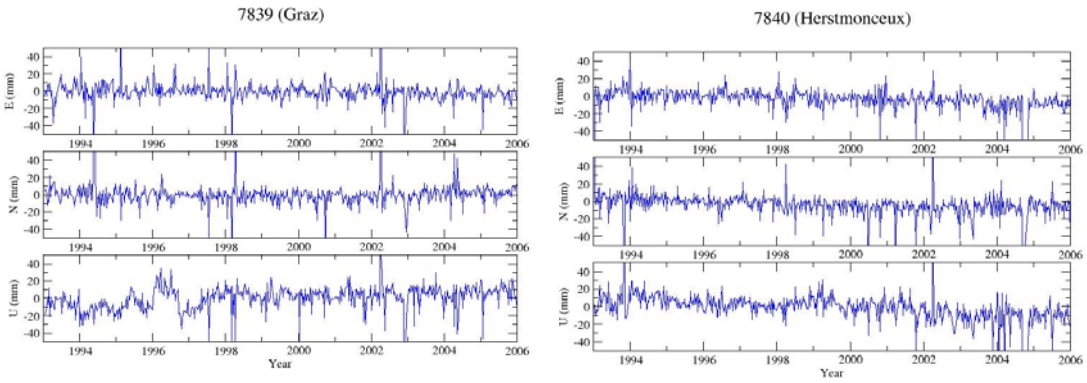

Figure 11. *Examples of station position time series computed (in mm) in the ENU local frame in ITRF2000. On the left: Graz, 7839. On the right: Herstmonceux, 7840.*

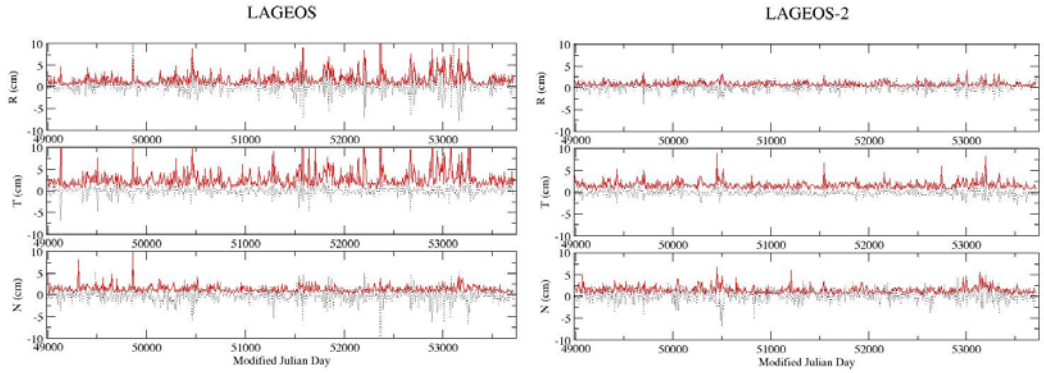

Figure 12. *Empirical orbital errors (biases - in black - and RMS values - in red -, in cm) in the RTN frame computed with our semi-dynamic approach for both LAGEOS satellites (LAGEOS on the left and LAGEOS-2 on the right).*

Table 7. *Statistics of the values shown on Fig. 12.*

Satellite	R (cm)	T (cm)	N (cm)	.
LAGEOS	0.38 1.71	0.06 2.73	-0.13 1.32	Mean of means Mean of RMS
LAGEOS-2	0.31 0.90	-0.11 1.65	0.20 1.46	. .

Finally, although our global method (cf. Fig. 8) does not provide any orbital error estimate, we have tested our semi-dynamic approach by keeping station positions and EOPs fixed. Almost all effects are included in the a priori modeling then used for station positions: plate tectonics, solid Earth tides, pole tide, and oceanic and atmospheric loading effects (European Center for Medium-range Weather Forecasts - ECMWF, http://www.ecmwf.int/- pressure fields were used to derive the atmospheric loading effect models) as well as the range biases provided by the temporal de-correlation method. Fig. 12 shows the bias and the RMS values of the empirical orbital errors so computed in RTN frame for both satellites. Tab. 7 provides the mean values of these error bias and RMS values. These values are coherent with the 2-day LAGEOS overlaps (cf. Fig. 2 and Tab. 5).

4. Conclusions and prospects

Our time series estimation method should be operational soon. To do so, we still have to:

- finalize our method regarding orbital errors;
- use all available common parameters to get optimal weekly weightings;
- go further with our temporal de-correlation approach for range biases [Coulot et al., 2007].

New computations should be carried out with ITRF2005 and the improved EOPC04 time series. And, in the near future, we plan to:

- carry out computations with atmospheric loading effect models in the a priori modeling for station positions to quantify their impact;
- use other satellites and study the impact on the involved TRFs.

References

[1] Altamimi, Z., P. Sillard, and C. Boucher: “ITRF2000: a new release of the International Terrestrial Reference Frame for Earth science applications”, J. Geophys. Res., 107(B10), 2214, doi: 10.1029/2001JB000561, 2002.

[2] Arias, E.F., P. Charlot, M. Feissel, and M.F. Lestrade: “The Extragalactic Reference System of the International Earth Rotation Service, ICRS”, Astron. Astrophys., 303, p. 604-608, 1995.

[3] Berger, C., R. Biancale, M. Ill, and F. Barlier: “Improvement of the empirical thermospheric model DTM: DTM94- a comparative review of various temporal variations and prospects in space geodesy applications”, J. Geod., 72(3), p. 161-178, 1998.

[4] Coulot, D.: “Télémétrie laser sur satellites et combinaison de techniques géodésiques. Contributions aux Systèmes de Référence Terrestres et Applications”, Ph. D. thesis, Observatoire de Paris, 2005.

[5] Coulot, D., P. Berio, O. Laurain, D. Féraudy, and P. Exertier: “An original approach to compute satellite laser range biases”, same issue, 2007.

[6] Cretaux, J.F., F. Nouel, C. Valorge, and P. Janniere: “Introduction of empirical parameters deduced from the Hill's equations for satellite orbit determination”, Manuscr. Geod., 19, p. 135-156, 1994.

[7] Gambis, D: “Monitoring Earth orientation using space-geodetic techniques: state-of-the-art and prospective”, J. Geod., 78, p. 295-305, 2004.

[8] Gruber, T., A. Bode, C. Reigber, P. Schwintzer, R. Biancale, and J.M. Lemoine: “GRIM5-C1: combination solution of the global gravity field to degree and order 120”, Geophys. Res. Lett., 27, p. 4005-4008, 2000.

[9] Le Provost, C.: “FES 2002 - A new version of the FES tidal solution series”, paper presented at Jason-1 Science Working Team Meeting, Biarritz, France, 2002.

[10] Lieske, J.H., T. Lederle, W. Fricke, and B. Morando: “Expressions for the precession quantities based upon the IAU (1976) System of Astronomical Constants”, Astron. Astrophys, 58, p. 1-16, 1977.

[11] McCarthy, D.D.: “IERS Conventions”, IERS Technical Note 21, Observatoire de Paris, 1996.

[12] McCarthy, D.D. and G. Petit: “IERS Conventions”, IERS Technical Note 32, Verlag des Bundesamts für Kartographie und Geodäsie, Frankfurt, 2004.

[13] Mignard, F.: “Overall science goals of the GAIA mission”, in Proceedings of the symposium "The Three-Dimensional Universe with GAIA", 2004.

[14] Persson, C.G.: “Adjustment, weight-testing and detection of outliers in mixed SFF-SFS models, Manuscr. Geod., 7, p. 299-323, 1982.

[15] Standish, E.M., X.X. Newhall, J.G. Williams, and W.M. Folkner: “JPL planetary and lunar ephemerides, DE403/LE403”, JPL IOM 314.10-127, 1995.

[16] Sillard, P. and C. Boucher: “Review of algebraic constraints in terrestrial reference frame datum definition”, J. Geod., 75, p. 63-73, 2001